APPLIED PHYSICS LETTERS VOLUME 85, NUMBER 19 8 NOVEMBER 2004
ISBN:978-84-691-1552-7 /DL:T.151-2008

# Growth, optical characterization, and laser operation of epitaxial $Yb:KY(WO_4)_2/KY(WO_4)_2$ composites with monoclinic structure

A. Aznar, R. Solé, M. Aguiló, and F. Diaz[a)]
*Grup de Fisica i Cristal lografia de Materials (FiCMA), Universitat Rovira i Virgili, Plaça Imperial Tarraco, 1, 43005 Tarragona, Spain*

U. Griebner,[b)] R. Grunwald, and V. Petrov
*Max-Born-Institute for Nonlinear Optics and Ultrafast Spectroscopy, 12489 Berlin, Germany*

(Received 29 December 2003; accepted 4 September 2004)

Epitaxial monoclinic double tungstate laser crystals were grown with high crystalline quality. Based on these Yb-doped composites, laser operation was demonstrated. Continuous-wave laser emission of a Yb:KYW/KYW crystal was achieved at 1030 nm. The 25-$\mu$m-thin Yb:KYW layer was pumped at wavelengths near 980 nm by a Ti:sapphire laser. A maximum output power of 40 mW was obtained at room temperature. © *2004 American Institute of Physics*. [DOI: 10.1063/1.1814426]

Yb-doped materials are well suited for building simple and robust diode-pumped lasers in the 1 $\mu$m spectral range[1] which have proved their potential in high power operation.[2] The attraction of Yb-doped materials are their small quantum defect and the absence of excited state absorption, upconversion processes, cross relaxation, and concentration quenching. Moreover, the broad absorption bands of these laser materials are covered by high-power InGaAs laser diodes that permit efficient pumping. The small Stokes shift ($\sim$600 $cm^{-1}$) between absorption and emission reduces the thermal load and increases the laser efficiency.

The magnitudes of the $Yb^{3+}$ absorption and emission cross-section peaks strongly depend on the chosen laser host material. The Yb-doped monoclinic low temperature phases of the double tungstates $KY(WO_4)_2$ (KYW) and $KGd(WO_4)_2$ (KGW) stand out because of their large absorption and emission cross sections.[3] Comparative studies based on the spectroscopic characteristics predicted that they are one of the most promising representatives of this class of materials.[4] KYW can incorporate higher concentrations of $Yb^{3+}$ ions than KGW approaching the stoichiometric composition $KYb(WO_4)_2$ (KYbW)[5] while maintaining the same structure. Yb:KYW, Yb:KGW, and KYbW are strongly anisotropic and all show an absorption maximum near 981 nm which, for light polarization parallel to the $N_m$-crystallo-optic axis, is about 15 times higher than that of Yb:YAG. In all three of them, efficient laser operation near 1 $\mu$m has already been demonstrated.[3,5,6]

The extremely high absorption and emission cross sections of Yb:KYW permit the use of very thin crystals. For such laser crystals even low beam quality pump sources (like most of the laser diodes) can be used, still achieving a good overlap of pump beam and resonator mode. As $Yb^{3+}$ is a quasi-three-level system, poor overlap would not only mean wasted pump power but also cause additional reabsorption of the stimulated emission. Thin disk Yb lasers have already proved their potential for high output powers,[2,6] but have required complicated pump optics to realize several pump passes through the active medium for efficient absorption. This problem can be overcome by using highly doped tungstate materials, but the handling of free-standing crystals is a great technological challenge, in particular for a thickness between 10 and 50 $\mu$m. Therefore thin epitaxial structures of highly Yb-doped KYW on KYW substrates seem to be ideal for face-cooled laser concepts including microchip lasers and thin disk laser designs. Our approach is to achieve cw lasing by the use of such epitaxial samples to minimize the reabsorption loss and to pump near the absorption maximum at 981 nm.

Liquid phase epitaxy (LPE) is a well-known technique to obtain homogeneous single crystal layers.[7] It is based on epitaxial growth from solution over a crystalline substrate and allows doping the layers during growth with optically active ions like ytterbium. Moreover it is possible to control the layer thickness by adjusting the temperature and the growth time. Some preliminary results on LPE of KYbW films on KYW substrates were reported only very recently.[8] In the present letter we describe the growth and the properties of an epitaxial Yb:KYW/KYW structure with improved crystal quality at the interface which permitted laser generation to be achieved with a strongly anisotropic (monoclinic) composite structure used as an active medium.

Single crystals of KYW to be used as substrates have been grown by the top seeded solution growth (TSSG) method. The experiments were performed in a vertical cylindrical furnace and the solvent chosen was $K_2W_2O_7$.[9] The solution composition was, in molar ratio, $K_2W_2O_7/KYW = 88/12$. We inserted the reagents, $K_2CO_3$, $Y_2O_3$, and $WO_3$, mixed in the appropriate ratios, weighting about 200 g, in a platinum crucible of an inner diameter of 50 mm. The solution was homogenized by maintaining the temperature at 50 K above the expected temperature of saturation, $T_{sat}$. The axial thermal gradient in the solution was about 1 K/cm, keeping the bottom hotter than the surface. After homogenization of the solution the $T_{sat}$ has been accurately determined in each run and it is, on average, 920 °C.

Then, the crystal growth process was initiated on seeds in contact with the surface of the solution, which was cooled at a rate of 0.05 K/h by 6 K. Finally, the crystals were removed from the solution and cooled down slowly to room temperature.

a)Author to whom correspondence should be addressed; electronic mail: diaz@quimica.urv.cs
b)Electronic mail: griebner@mbi-berlin.de

 

ISBN:978-84-691-1552-7 /DL:T.151-2008

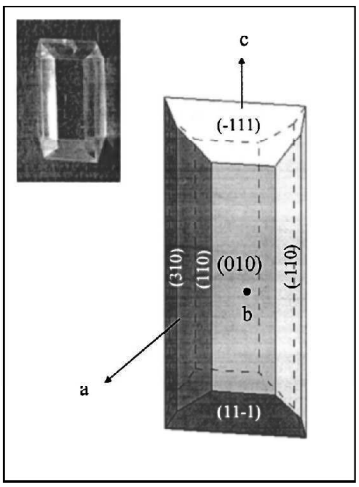


FIG. 1. KYW crystal grown and its morphological scheme.

The KYW substrates obtained were transparent and free from macroscopic defects. The typical dimensions ranged between $3\times3\times6$ and $5\times5\times8$ mm$^3$ in $a$, $b$, and $c$ crystallographic directions, respectively. The unit cell parameters of KYW in the $C2/c$ space group determined at room temperature are,[10] $a=10.6313(4)$ Å, $b=10.3452(6)$ Å, $c=7.5547(3)$ Å, and $\beta=130.752(2)°$ and the unit cell parameters of KYbW amount to $a=10.590(4)$ Å, $b=10.290(6)$ Å, $c=7.478(2)$ Å, and $\beta=130.70(2)°$.[5] It can be seen in Fig. 1 that the KYW morphology is mainly formed by {010}, {110}, {310} and {−111} faces.

The LPE experiments were performed in a vertical furnace with practically no axial gradient to obtain a homogeneous epitaxial layer thickness on every crystal face. The solution was prepared by mixing about 70 g of the reagents in a cylindrical platinum crucible with a 30 mm diameter. The ratio between the solvent, $K_2W_2O_7$, and the solute, $KY_{0.8}Yb_{0.2}(WO_4)_2$, was decreased by 7% as compared to the value in the substrate growth, to perform the epitaxial growth at lower temperatures. This permits a better control of the growth rate according to the solubility curve of KYW in $K_2W_2O_7$.[10]

Once the solution was homogeneous, we accurately determined $T_{sat}$ in each run being, on average, 820 °C, which means 100 °C less than $T_{sat}$ obtained in the substrate growth. Next we studied the kinetics of the growth and dissolution of a seed at different temperatures close to $T_{sat}$, before the epitaxial growth. This information was very useful for the choice of the temperature and time to perform the epitaxial growth. The substrate was introduced slowly into the furnace and maintained near the surface of the solution for about 30 min to reach a thermal equilibrium with the solution. At the beginning of the epitaxial growth, the temperature of the solution was kept 1 °C higher than $T_{sat}$ with the objective to dissolve the outer layer of the crystal. Thus, the substrate was dipped into the solution at this temperature for 5 min and then the temperature was decreased to 2 °C below $T_{sat}$ for 4 h to grow the epitaxial layer. The crystal rotation velocity during all these procedures (also for TSSG) was kept constant at 40 rpm. Finally we removed the crystal from the solution and took it out slowly from the furnace to avoid cracks due to thermal shocks and the differences of the thermal expansion coefficients between the layer and the substrate. It is important to note that the epitaxial growth takes place on all natural faces of the crystals used as substrates.

TABLE I. Epitaxial film thickness and rate of growth, $R$, for different crystallographic faces measured by SEM.

| Face | Thickness ($\mu$m) | $R$ ($\mu$m/h) |
|---|---|---|
| (010) | 48.1 | 12 |
| (110) | 29.9 | 7.5 |
| (310) | 8.0 | 2 |

The thickness of the epitaxial layers was measured by a scanning electron microscope (SEM) using backscattered electrons with the sample cut and polished perpendicular to the $c$ crystallographic direction. The results obtained are listed in Table I. The rate of layer growth was faster on the {010} faces followed by the {110} and {310} faces. From the images obtained by SEM a sharp interface between the substrate and the 48 $\mu$m thin doped layer, corresponding to a (010) face, can be detected visually (inset Fig. 2).

The substrate and layer composition was determined by electron probe microanalyses with a CAMECA SX-50 equipment. The results obtained show that the Yb content in the layer ($11.96\times10^{20}$ $Yb^{3+}$ ions/cm$^3$) is more or less the same as in the solution, while the Yb content in the substrate is zero, even close to the interface. Thus, the distribution coefficient of $Yb^{3+}$ in these layers is close to unity, which is very favorable for obtaining a homogeneous distribution of ytterbium in the epitaxy. Figure 2 represents the evolution of yttrium and ytterbium concentration at the substrate/layer interface. We observe that there is practically no diffusion of $Yb^{3+}$ into the substrate.

Using an optical microscope we could detect that the surface morphology of these layers was quite good and flat over large areas. There was no essential difference in surface morphology between the different natural faces of the crystal, although the face (010) seems to be the best. The typical defects that appeared were steps of growth in all faces. Furthermore, in {110} and {310} faces some cracks could be identified.

For the laser experiments the (010) faces of the epitaxial crystal were additionally polished with high optical quality. From the measured absorbed pump power we deduced a thickness of the 20% Yb/Y-site KYW layer of 25 $\mu$m. The

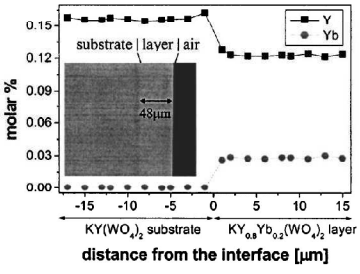


FIG. 2. Evolution of the yttrium (Y) and ytterbium (Yb) concentration at the substrate/layer interface. Inset: SEM micrograph of the epitaxial crystal with the Yb:KYW/KYW interface.

ISBN:978-84-691-1552-7 /DL:T.151-2008

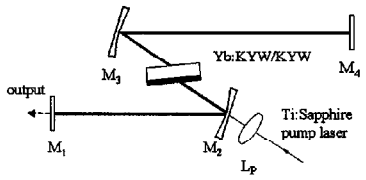


FIG. 3. Laser setup: $M_2$, $M_3$—folding mirrors (RC=100 mm); $M_1$—output coupler; Yb:KYW/KYW—1.6-mm-thick epitaxial crystal; $L_P$—focusing lens.

uncoated 1.6-mm-thick Yb:KYW/KYW epitaxial crystal with an aperture of $3 \times 5$ mm$^2$ was positioned in the laser resonator under Brewster angle to minimize the Fresnel losses. Pump light absorption was maximized by orienting the crystal for the $N_m$-crystallo-optic axis parallel to the pump light polarization. The experiments were performed with a cw Ti:sapphire laser as the pump source. It was optimized for emission in the range from 960 to 1025 nm with a linewidth $<1$ nm, delivering more than 2 W output power. We studied a Z-shaped resonator with two folding mirrors in the middle (Fig. 3) to form a 30 $\mu$m intracavity beam waist at the position of the epitaxial crystal. No special provision was made for cooling the sample. The Ti:sapphire beam was focused by an $f=62.8$ mm lens through the folding mirror $M_2$ giving an estimated 30 $\mu$m pump waist.

Laser operation could be obtained for pump wavelengths between 963 and 997 nm determined by the absorption characteristics of the Yb:KYW layer. Independent of the pump wavelength, the laser emission was centered at 1030 nm (inset Fig. 4). Because of the reduced reabsorption in the thin active layer, the spectral emission corresponds to the maximum of the gain curve. Continuous-wave laser operation was achieved for all pump wavelengths. Approaching the absorption peak near 981 nm, thermal problems occurred and resulted in decreasing the slope efficiency.

The cw laser performance of the Yb:KYW/KYW epitaxial crystal was studied at pump wavelengths $\lambda_p$ below and above the main absorption peak. Using the setup of Fig. 3, stable laser operation was observed for output coupler transmissions up to 3.5%. Best performance was achieved at $\lambda_p=984$ nm with a 2% transmission output coupler. The laser threshold of the 25-$\mu$m-thin Yb:KYW layer was reached at an absorbed pump power of about 275 mW. The maximum output power amounted to 40 mW resulting in a slope efficiency of 33% with respect to the absorbed pump power (Fig. 4). Applying a chopper with a duty cycle of 4% and comparing the output power for $\lambda_p=984$ nm and $\lambda_p=981$ nm, an increase of nearly a factor 4 could be obtained for pumping in the main absorption peak.

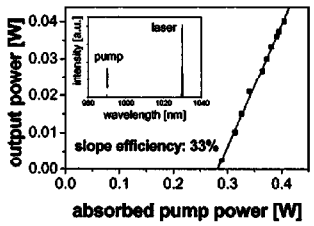


FIG. 4. Output power vs absorbed pump power of the continuous-wave Yb:KYW/KYW laser. Inset: Spectral record of the Yb:KYW/KYW and pump laser emission.

In conclusion, epitaxial monoclinic double tungstate crystals have been grown with high optical quality by the LPE method. A 48 $\mu$m thin KYW (010) layer doped with 20% $Yb^{3+}$ as the active ion was grown on a KYW substrate. Laser operation of a Yb:KYW/KYW epitaxial crystal was achieved. Continuous-wave lasing at 1030 nm with an output power of 40 mW was obtained at room temperature. There is great potential for applying such Yb-doped epitaxial KYW crystals in waveguide structures and microchip lasers which profit from the short absorption length.

The authors gratefully acknowledge financial support from CICyT under Project Nos. MAT2002-04603-C05-03, FIT-07000-2001-477, and FIT-07000-2002-461, from CIRIT under Project No. 2001SGR00317, and the EU Project DT-CRYS, STRP-505580-1, and the EU-LIMANS Programme No. mbi000367 for MBI.

[1]W. F. Krupke, IEEE J. Sel. Top. Quantum Electron. **6**, 1287 (2000).
[2]C. Stewen, K. Contag, M. Larionov, A. Giesen, and H. Hügel, IEEE J. Sel. Top. Quantum Electron. **6**, 650 (2000).
[3]N. V. Kuleshov, A. A. Lagatsky, A. V. Podlipensky, V. P. Mikhailov, and G. Huber, Opt. Lett. **22**, 1317 (1997).
[4]G. Boulon, A. Brenier, L. Laversenne, Y. Guyot, C. Goutaudier, M.-T. Cohen-Adad, G. Metrat, and N. Muhlstein, J. Alloys Compd. **341**, 2 (2002).
[5]M. C. Pujol, M. A. Bursukova, F. Güell, X. Mateos, R. Solé, J. Gavaldà, M. Aguiló, J. Massons, F. Díaz, P. Klopp, U. Griebner, and V. Petrov, Phys. Rev. B **65**, 165121 (2002).
[6]S. Erhard, J. Gao, A. Giesen, K. Contag, A. A. Lagatsky, A. Abdolvand, N. V. Kuleshov, J. Aus der Au, G. J. Spühler, F. Brunner, R. Paschotta, and U. Keller, in *Conference on Lasers and Electro-Optics*, OSA Trends in Optics and Photonics (TOPS), Vol. 56, Technical Digest, Postconference Edition (Optical Society of America, Washington, DC, 2001), p. 333.
[7]B. Ferrand, B. Chambaz, and M. Couchaud, Opt. Mater. (Amsterdam, Neth.) **11**, 101 (1999).
[8]A. Aznar, D. Ehrentraut, Y. E. Romanyuk, R. Solé, M. Aguiló, P. Gerner, H. U. Güdel, and M. Pollnau, in Fifth International Conference on f-elements, Geneve, Switzerland, 24–29 August 2003, Final Programme and Abstract Book, p. 111, paper PC-42.
[9]R. Solé, V. Nikolov, X. Ruiz, J. Gavaldà, X. Solans, M. Aguiló, and F. Díaz, J. Cryst. Growth **169**, 600 (1996).
[10]M. C. Pujol, X. Mateos, R. Solé, J. Massons, J. Gavaldà, F. Díaz, and M. Aguiló, Mater. Sci. Forum **378–381**, 710 (2001).

UNIVERSITAT ROVIRA I VIRGILI
CRECIMIENTO Y CARACTERIZACIÓN DE CAPAS EPITAXIALES DE KRE 1-X 4BX (WO4)2 / KRE (WO4)2 (RE=Y,LU) PARA APLICACIONES LÁSER
Ana Isabel Aznar Écija

ISBN:978-84-691-1552-7 /DL:T.151-2008

ISBN:978-84-691-1552-7 /DL:T.151-2008

# Laser Operation of Epitaxially Grown Yb : $KLu(WO_4)_2$–$KLu(WO_4)_2$ Composites With Monoclinic Crystalline Structure

Uwe Griebner, Junhai Liu, Simon Rivier, Ana Aznar, Rüdiger Grunwald, Rosa Maria Solé, Magdalena Aguiló, Francesc Díaz, and Valentin Petrov

***Abstract*—Epitaxial monoclinic double tungstate composites based on the strongly anisotropic $KLu(WO_4)_2$ (KLuW) were grown with high crystalline quality and laser operation of ytterbium was demonstrated for the first time. Highly efficient CW laser emission of an Yb:KLuW–KLuW crystal was achieved near 1030 nm. The 100-$\mu$m-thick Yb:KLuW layer was pumped at wavelengths near 980 nm by a tapered diode laser as well as by a Ti:sapphire laser. More than 500 mW of CW output power and slope efficiencies up to 66% were obtained at room temperature without cooling.**

***Index Terms*—Diode pumping, epitaxial layers, monoclinic double tungstates, Yb lasers.**

## I. Introduction

THE growing interest in Yb-doped lasers has been underlined by creating new active materials with $Yb^{3+}$ as a dopant [1]–[3]. Some of these materials have already proved their potential in high-power lasers in the wavelength region near 1 $\mu$m. The attractive features of Yb-doped laser crystals include their small quantum defect, the absence of excited state absorption, up-conversion, cross-relaxation and concentration quenching processes, and the broad absorption bands which are covered by high-power InGaAs laser diodes. The relatively small Stokes shift between absorption and emission in the quasi three level Yb ion reduces the thermal load and sets an increased quantum limit for the laser efficiency in comparison to the Nd-ion operating in the same wavelength region.

The magnitudes of the $Yb^{3+}$ absorption and emission cross-section peaks strongly depend on the chosen laser host material. Comparative studies based on the spectroscopic characteristics predicted that the Yb-doped monoclinic low-temperature phases of the double tungstates $KY(WO_4)_2$ (KYW) and $KGd(WO_4)_2$ (KGdW) belong to the most promising representatives of this class of materials [4]. They stand out because of their large absorption and emission cross sections and their capability to adopt higher dopant concentrations [5]. $KLu(WO_4)_2$ (KLuW) is isostructural to KYW and KGdW and many relevant properties like refractive index, optical transparency, and thermal conductivity are very similar [6]. The spectral characteristics of Yb:KLuW are also similar to those of Yb:KYW and Yb:KGdW, and the measured fluorescence lifetime of 375 $\mu$s for low doped Yb:KLuW is slightly longer than the 300-$\mu$s lifetime of Yb:KYW and Yb:KGdW [7]. In fact, we could already demonstrate excellent laser performance of Yb:KLuW in the 1-$\mu$m spectral range [7] which was comparable to that reported for Yb:KGdW and Yb:KYW [5]. The highly efficient CW laser operation with this novel Yb-doped monoclinic double tungstate was achieved with 2.2–2.8-mm-thick, 5 at% and 10 at% Yb-doped KLuW samples oriented for polarization $E//N_m$. Output powers of the order of 1 W with pump efficiencies as high as 50% were obtained at room temperature [7].

Due to the closer ionic radii, KYW and KLuW can incorporate higher concentrations of $Yb^{3+}$-ions than KGdW approaching the stoichiometric composition $KYb(WO_4)_2$ (KYbW) [8] while maintaining the same structure. Yb:KYW, Yb:KGdW, Yb:KLuW, and KYbW are all strongly anisotropic and exhibit an absorption maximum centered near 981 nm. The maximum absorption cross section $\sigma_a$ for light polarization parallel to the $N_m$-principal optical axis is about 15 times larger than that of Yb:YAG. For KYbW, the absorption length (1/e level) calculated from $\sigma_a$ (981 nm) $= 11.7 \times 10^{-20}$ cm$^2$ is only 13.3 $\mu$m. Such exceptionally short absorption lengths permit the use of very thin crystals which considerably reduces the beam quality requirements for the laser diodes used for pumping. To achieve a good overlap of pump beam and resonator mode is especially important in quasithree-level systems like the $Yb^{3+}$ ion because poor overlap would not only mean wasted pump power but will also cause additional reabsorption of the stimulated emission. Thin-disk Yb lasers have already shown their potential for high output powers [2], [9], but up to now require complex pump optics to realize several pump passes through the active medium for efficient absorption. It is this problem that can be overcome by using very thin and highly doped monoclinic double tungstate crystals. Thermo-mechanical limitations, however, set a great technological challenge, in particular for the manufacturing of free standing active elements with a thickness less than 100 $\mu$m corresponding to the absorption length. Using epitaxially grown Yb-doped/undoped

Manuscript received August 9, 2004; revised October 5, 2004. This work was supported by the European Union under Project DT-CRYS, CICyT under Projects MAT2002-04603-C05-03 and FIT-070000-2003-661, and CIRIT under Project 2001SGR00317.

U. Griebner, J. Liu, S. Rivier, R. Grunwald, and V. Petrov are with the Max-Born-Institute for Nonlinear Optics and Ultrafast Spectroscopy, D-12489 Berlin, Germany (e-mail: griebner@mbi-berlin.de; jhliu@mbi-berlin.de; rivier@mbi-berlin.de; grunwald@mbi-berlin.de; petrov@mbi-berlin.de).

A. Aznar, R. M. Solé, M. Aguiló, and F. Díaz are with Grup de Fisica i Cristal.lografia de Materials (FiCMA), Universitat Rovira i Virgili, E-43005 Tarragona, Spain (e-mail: aznar@quimica.urv.es; sole@quimica.urv.es; aguilo@quimica.urv.es; diaz@quimica.urv.es).

Digital Object Identifier 10.1109/JQE.2004.842313

ISBN:978-84-691-1552-7 /DL:T.151-2008

TABLE I
UNIT CELL PARAMETERS ($C2/c$ SPACE GROUP, ROOM TEMPERATURE) OF KLUW AND KYW IN COMPARISON TO THE STOICHIOMETRIC KYBW AS AN IDEAL EPITAXIAL LAYER. FOR COMPARISON THE VALUES FOR YAG AND THE OTHER KNOWN STOICHIOMETRIC YB-CRYSTAL YBAG ARE ALSO INCLUDED

| lattice parameters | $a$ [Å] | $b$ [Å] | $c$ [Å] | $\beta$ | average |
|---|---|---|---|---|---|
| KLuW (ref. [17]) | 10.576(7) | 10.214(7) | 7.487(2) | 130.68(4)° | |
| KYbW (ref. [18]) | 10.590(4) | 10.290(6) | 7.478(2) | 130.70(2)° | |
| Difference | 0.13% | 0.74% | 0.12% | 0.02% | 0.33% |
| | | | | | |
| YAG (ref. [19]) | 12.0116(3) | | | | |
| YbAG (ref. [19]) | 11.9380(5) | | | | |
| difference | 0.61% | | | | 0.61% |
| | | | | | |
| KYW (ref. [20]) | 10.6313(4) | 10.3452(6) | 7.5547(3) | 130.752(2)° | |
| KYbW (ref. [8]) | 10.590(4) | 10.290(6) | 7.478(2) | 130.70(2)° | |
| difference | 0.39% | 0.53% | 1.01% | 0.04% | 0.64% |
| | | | | | |

composites instead of bulk crystals as gain media for thin disk lasers might be prospective, because this technology allows the fabrication of homogeneous epitaxial crystalline layers with perfect structure and suitable composition having a thickness down to the 10-$\mu$m range.

Very recently, the first demonstration of a CW thin-disk Yb laser based on an epitaxial crystal as an active material was reported [10]. The authors used a 200-$\mu$m-thick Yb:YAG film on YAG as the thin disk. With the 20 at% Yb-doped film and 24 passes for sufficient absorption of the pump light at 940 nm, they achieved 60 W of output power with 30% pump efficiency. Successful fabrication of some thin double tungstate layers with different dopants has also been realized very recently, e.g., by ion implantation (Tm:NaYW) [11] and by laser ablation (Nd:KGdW) [12], but without demonstration of laser operation.

The liquid phase epitaxy (LPE) used in [10] is a well-known technique to obtain homogeneous single crystal layers [13]. The first reports on successful growth of LPE layers were in 1972 [14]. LPE is based on epitaxial growth from solution over a crystalline substrate and allows doping the layers with optically active ions like $Yb^{3+}$ during the growth. Moreover, it is possible to control the layer thickness by adjusting the temperature and the growth time. Some preliminary results on LPE of KYbW films on KYW substrates were reported only very recently [15]. We demonstrated for the first time, to the best of our knowledge, laser operation based on epitaxial double tungstate structures by using a 25-$\mu$m 20 at% Yb-doped KYW layer on a KYW substrate crystal [16]. CW lasing at 1030 nm with 40 mW of output power could be achieved.

Essential for laser applications of composite structures is the high optical quality of the epitaxial interface. One important issue is the minimization of the crystal lattice mismatch between the substrate crystal and the epitaxial layer, otherwise stress induced defects can occur. We established that further increase of the Yb-doping concentration in the KYW layer produces a nontolerable stress in the epitaxial structure resulting in cracks at the interface. Consequently we were looking for alternative double tungstate host materials where a reduced stress at the epitaxial interface can be expected. Therefore, KLuW became the focus of our investigations on highly Yb-doped epitaxial double tungstate crystals because of the lower crystal lattice mismatch relative to KYbW in comparison to KYW. The present paper is devoted to characterization and laser investigations of epitaxially grown Yb:KLuW–KLuW composites with optimized crystal quality at the interface. We report highly efficient CW laser operation at room temperature without cooling.

## II. EPITAXIAL GROWTH

The top-seeded solution growth (TSSG) slow-cooling method was applied to synthesize KLuW single crystals to be used as substrates [17]. The KLuW substrates obtained were transparent and free from macroscopic defects. The typical dimensions ranged between $3 \times 3 \times 6$ and $5 \times 5 \times 8$ $mm^3$ in $a$, $b$ and $c$ crystallographic directions, respectively. The unit cell parameters of KLuW and KYW in the $C2/c$ space group determined at room temperature are listed in Table I in comparison to KYbW. Note that for KYbW and KLuW single crystal diffraction measurements are available whereas for YAG, YbAG, and KYW we used powder diffraction data. The closer unit cell parameters of KYbW and KLuW with differences of $0.12 \ldots 0.74\%$ against $0.39 \ldots 1.01\%$ between KYbW and KYW can be seen as a prerequisite for the growth of high-quality epitaxial structures. From Table I, we can also expect a lower induced stress due to the lower lattice mismatch of an epitaxial structure of KLuW and KYbW compared to a composite of YAG and YbAG, the other known Yb-containing stoichiometric crystal with demonstrated laser operation [21].

The LPE experiments were performed in a vertical furnace with practically no axial gradient to obtain a homogeneous epitaxial layer thickness on every crystal face. It is important to note that the epitaxial growth takes place on all natural faces of the crystals used as substrates. From Fig. 1 it can be seen that the KLuW morphology is mainly formed by $\{010\}$, $\{110\}$, $\{310\}$ and $\{-111\}$ faces. The thickness of the Yb:KLuW layer, grown on the (010) face, amounted to 130 $\mu$m. For the laser experiments, the (010) faces of the epitaxial crystal were additionally polished with high optical quality, resulting in a layer thickness of 100 $\mu$m measured by translating the sample in a ZYGO$^{TM}$ interferometer. Using the ZYGO$^{TM}$, we could detect that the surface morphology of the layer of interest was quite good and flat over large areas. Fig. 2(a) shows the surface profile plot of the (010) epitaxial surface. The radius of curvature of the surface

ISBN:978-84-691-1552-7 /DL:T.151-2008

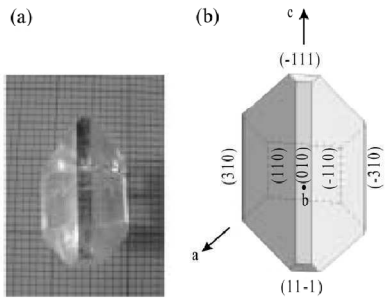


Fig. 1. (a) Photograph and (b) morphological scheme of the KLuW crystal.

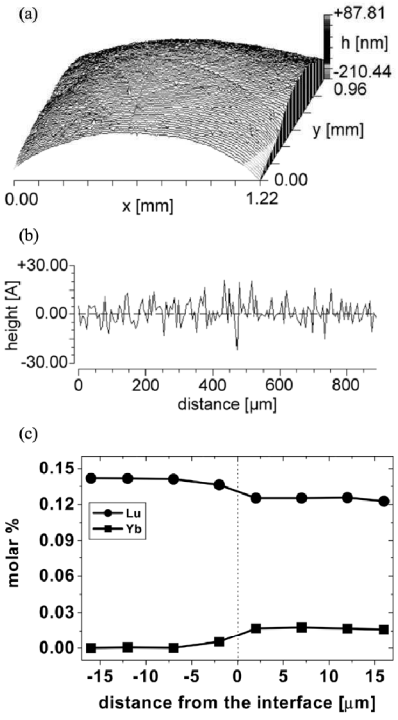


Fig. 2. Characterization of the epitaxial Yb:KLuW–KLuW crystal. (a) Surface profile plot of the (010) epitaxial layer. (b) Roughness of the (010) epitaxial surface. (c) Evolution of the lutetium (Lu) and ytterbium (Yb) concentration at the interface.

is 0.71 m. The surface roughness with an rms value of <0.8 nm presented in Fig. 2(b) emphasizes the excellent optical quality of the (010) epitaxial surface. No cracks at the epitaxial interface could be identified with the ZYGO™ interferometer.

The substrate and layer composition was determined by electron probe microanalysis with a CAMECA SX-50 equipment. The results obtained show that the Yb content in the layer ($7.888 \times 10^{20}$ $Yb^{3+}$ ions/$cm^3$) is more or less the same as in the solution, while the Yb content in the substrate is zero, even close to the interface. Thus, the distribution coefficient of $Yb^{3+}$ in these layers is close to unity, which is very favorable

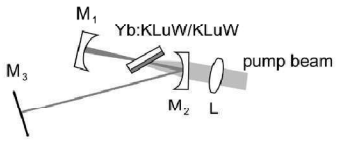


Fig. 3. Experimental setup. $M_1$: mirror with $ROC = -50$ mm or $-100$ mm, $M_2$: mirror with $ROC = -100$ mm; $M_3$: plane outcoupling mirror; $L$: $f = 6.28$ cm focusing lens; Yb:KLuW–KLuW—epitaxial crystal.

for obtaining a homogeneous distribution of ytterbium in the epitaxy. From Fig. 2(c), it can be seen that there is practically no diffusion of $Yb^{3+}$ into the substrate.

## III. Laser Setup

The laser experiments with Yb:KLuW–KLuW were performed in a V-type astigmatically compensated resonator as shown in Fig. 3. The 1.2-mm-thick epitaxial sample was positioned in the focal region between the two focusing mirrors which formed a 30-$\mu$m intracavity beam waist. It was uncoated and inclined under Brewster angle to minimize the Fresnel losses. The Yb:KLuW–KLuW crystal was oriented for propagation along the $\boldsymbol{b}(N_p)$ axis with faces parallel to the $N_m - N_g$ plane and polarization along the $N_m$ principal optical axis. Deviations from this orientation occurred only as a consequence of the Brewster geometry used but did not essentially modify the absorption and gain spectral profiles. The polarization choice plays a very important role for the optimization of the net amplification. The folding mirror $M_2$ (radius of curvature $ROC = -100$ mm) transmitted $\approx 99\%$ of the pump radiation near 980 nm and was highly reflective for the laser radiation. The end mirror $M_1$ with a $ROC = -50$ mm was highly reflective only for the laser wavelength, alternatively a mirror with $ROC = -100$ mm which was highly reflecting also for the pump radiation was applied in order to study double-pass pumping. The cavity length was about 67 and 72 cm, respectively. In both cases, the calculated mode size in the center of the stability range was about 40 $\mu$m for the Gaussian waist. The plane output coupler $M_3$ had a transmission between 1% and 10% near 1030 nm. No special care was taken for good thermal contact or cooling of the sample.

We used a diode laser or a Ti:sapphire laser as pumping sources but only in the latter case was it possible to realize a double pass pumping utilizing the residual radiation which was not absorbed in the first pass. The tunable Ti:sapphire laser was optimized for emission in the range from 960 to 1025 nm with a linewidth < 1 nm, delivering more than 2.5 W of output power. For the diode-pumped operation, a tapered diode laser (TDL) was used [22], delivering up to 2 W at an $M^2 < 3$ for the slow axis emission. Temperature tuning of this laser was possible between 975–982 nm. The emission of the TDL with a spectral bandwidth of only 1 nm was stabilized near 980 nm by feedback of a small amount of the radiation ($< 0.02\%$) using a reflection grating. Due to the excellent beam quality of the TDL, relatively simple beam shaping optics were required, and a good overlap of pump and cavity modes could be realized. The astigmatic emission of the TDL was formed by an aspherical ($f = 4.5$ mm) and a cylindrical ($f = 40$ mm) lens

ISBN:978-84-691-1552-7 /DL:T.151-2008

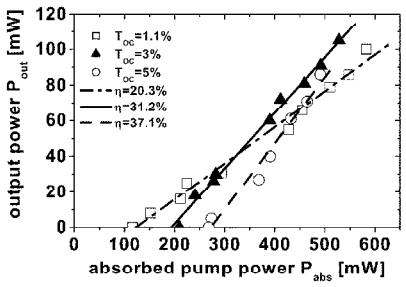


Fig. 4. Output power $P_{\rm out}$ versus absorbed pump power $P_{\rm abs}$ (symbols) of the TDL-pumped CW Yb:KLuW–KLuW laser obtained at the optimum $\lambda_P = 981.3$ nm, and linear fits (lines) for calculation of the slope efficiency $\eta$ for three different output couplers ($T_{\rm OC}$). In all cases $\lambda_L \approx 1030$ nm.

to achieve a nearly collimated pump beam. The pump beam was focused in both cases by an $f = 62.8$ mm AR-coated lens (Fig. 3) through the folding mirror $M_2$ onto the crystal giving an estimated 30-$\mu$m pump waist in the case of Ti:sapphire pumping and slightly larger for the TDL pump source.

The measured single pass low-signal absorption of the 10% Yb–Lu-site KLuW layer at 981.5 nm amounted to 64% in good agreement with the calculated value of 64.7% for a 100 $\mu$m thickness under Brewster angle ($\sigma_a = 11.8 \times 10^{-20}$ cm$^2$ at 981.5 nm [7]).

## IV. Results and Discussion

In the laser experiments with TDL pumping, the end mirror $M_1$ (Fig. 3, $ROC = -50$ mm) was highly transmittive for the pump radiation and the absorbed power in the single pass could be precisely measured. CW laser operation could be obtained for output coupler transmissions ($T_{\rm OC}$) between 1.1% and 10%. The output power ($P_{\rm out}$) versus the absorbed pump power ($P_{\rm abs}$) for three different $T_{\rm OC}$ is shown in Fig. 4. The laser threshold achieved with the 100-$\mu$m-thin Yb:KLuW layer was as low as $P_{\rm abs} \approx 120$ mW for the 1.1% output coupler. Note that the thresholds we measured with different outcouplers were three to five times lower than with the bulk Yb:KLuW samples [7] where reabsorption forced the laser to oscillate at longer wavelength $\lambda_L$. At the maximum applied pump power (1.25 W incident on the sample), the maximum output power amounted to 105 mW and the pump efficiency with respect to the absorbed power reached 20% ($T_{\rm OC} = 3\%$). The highest slope efficiency with respect to the absorbed power, $\eta = 37.1\%$, was achieved with the $T_{\rm OC} = 5\%$ output coupler.

The actual absorption depends on the depletion effect and can be substantially lower than the small-signal value. It depends, however, also on the output coupler transmission since the different intracavity power produces a different recycling effect which counteracts the depletion [23]. Fig. 5(a) shows the absorption dependence on the incident pump power $P_{\rm inc}$ for three output couplers and also without lasing. The incident pump intensity is comparable to or exceeding the saturation intensity and since the active layer thickness is smaller than the absorption length the absorption depletion effect can be clearly observed [Fig. 5(a)]. Note that this was not the case when pumping thick bulk samples of Yb:KLuW with the same

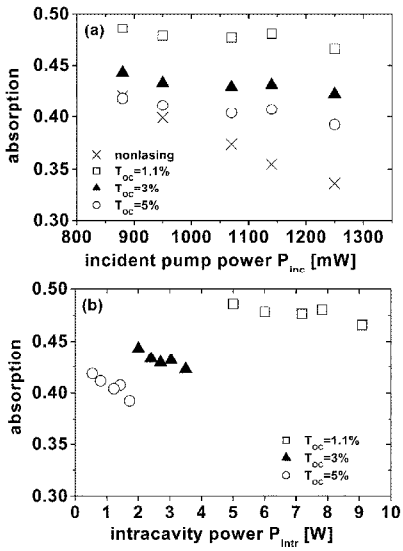


Fig. 5. Estimated single-pass absorption in the case of TDL pumping versus (a) the incident pump power $P_{\rm inc}$ on the epitaxial crystal and (b) the intracavity laser power $P_{\rm intr}$.

TDL [7]. It can be seen from Fig. 5(a) that the depletion effect is strongest when lasing is interrupted (in the $M_2-M_3$ arm in Fig. 3). Lower $T_{OC}$ corresponds to increased intracavity power $P_{\rm intr}$ and consequently the absorption increases [Fig. 5(b)]. But for a given $T_{OC}$ the dependence on $P_{\rm inc}$ is not strong because $P_{\rm intr}$ also increases with $P_{\rm inc}$ [Fig. 5(a) and (b)].

With the Ti:sapphire laser used as a pump source in the same single-pump-pass cavity configuration, a much better performance was achieved which was due to its nearly diffraction limited beam quality and the improved mode matching between the pump and laser modes as compared to the TDL pumping. The CW output characteristics are presented in Fig. 6. We limited the incident pump power applied to 1.85 W. The maximum measured output power of 415 mW corresponds to a maximum efficiency of 55% with respect to the absorbed pump power ($T_{\rm OC} = 3\%$). The slope efficiency with respect to the absorbed power increases with $T_{\rm OC}$ reaching a maximum value of $\eta = 66\%$ ($T_{\rm OC} = 10\%$, Fig. 6). Both the pump and slope efficiencies exceed those we recently reported for a 2.2-mm-thick 10 at% Yb-doped bulk KLuW in a similar pump and laser configuration [7]. This is attributed to the strongly reduced reabsorption which leads to about 4 times lower thresholds in the case of the epitaxial sample (about 70 mW in Fig. 6) and to shorter laser wavelengths $\lambda_L$. Note that the dependence of $\lambda_L$ on $T_{\rm OC}$ in Fig. 6 can be explained by stronger absorption depletion and more homogeneous pumping along the beam path when increasing $T_{\rm OC}$.

The dependence of the actual absorption on the intracavity intensity is more pronounced in the case of Ti:sapphire laser pumping because of the stronger pump induced absorption depletion (Fig. 7). The stronger saturation due to the smaller pump spot size can be seen by comparison of the absorption with

ISBN:978-84-691-1552-7 /DL:T.151-2008

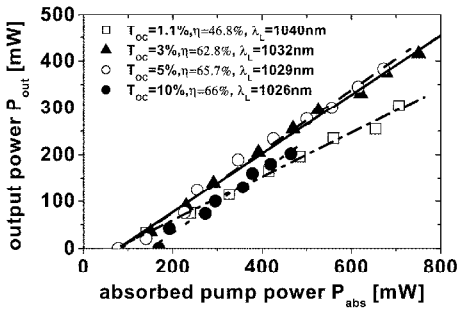


Fig. 6. Output power $P_{\text{out}}$ versus absorbed pump power $P_{\text{abs}}$ (symbols) of the Ti:sapphire laser pumped CW Yb:KLuW–KLuW laser obtained at the optimum $\lambda_P = 981.5$ nm, and linear fits (lines) for calculation of the slope efficiency $\eta$ for four different output couplers $T_{\text{OC}}$.

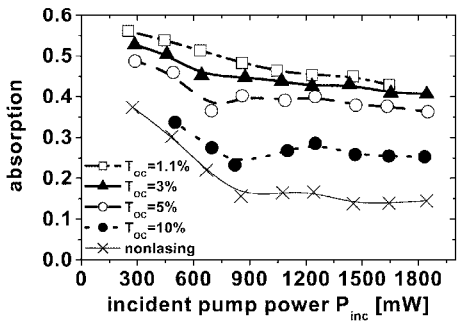


Fig. 7. Estimated single-pass absorption in the case of Ti:sapphire laser pumping versus the incident pump power $P_{\text{inc}}$ on the epitaxial crystal.

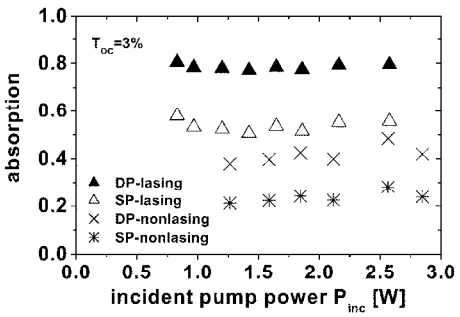


Fig. 8. Estimated single-pass (SP) and double-pass (DP) absorption with lasing and without lasing in the case of Ti:sapphire laser pumping with feedback versus the calculated incident pump power $P_{\text{inc}}$ on the epitaxial crystal.

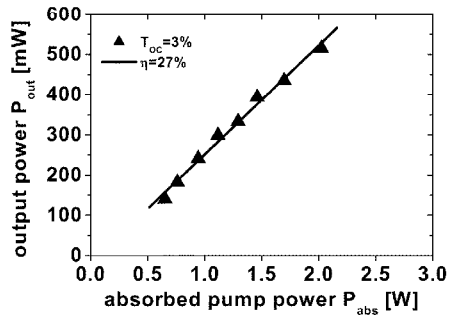


Fig. 9. Output power $P_{\text{out}}$ in the case of Ti:sapphire laser pumping with feedback versus the calculated absorbed pump power in double pass $P_{\text{abs}}$.

lasing interrupted in the cases of diode and Ti:sapphire laser pumping. In the case of Ti:sapphire laser pumping, the absorption is depleted at relatively low incident powers and the further dependence on $P_{\text{inc}}$ is saturated.

We examined the influence of thermal effects by employing a chopper with a 1:10 duty cycle. We observed only a weak effect of about 10% at the maximum applied pump powers (see Fig. 6), i.e., the maximum average output power achieved with the chopper was 45 mW.

The Ti:sapphire laser beam quality and the close pump and laser wavelengths allow in principle simple double pass pumping by using a retroreflector for the pump radiation. In general the second pass can help to suppress the reabsorption effect. In the present case, we were motivated to try this on one hand by the reduced single-pass absorption in comparison to the small-signal case (Fig. 7) and on the other hand by the observation that feedback effects caused by mirror $M_1$ (Fig. 3) could increase the pump power leading to coupled cavities or equivalently the Yb:KLuW–KLuW laser could be considered as being partially intracavity pumped. To investigate this possibility we employed another mirror $M_1$ with $ROC = -100$ mm which was highly reflective both for the pump and laser radiation. The feedback effect on the Ti:sapphire pump laser strongly depended on its output power and decreased at higher powers.

In the CW regime, we applied a maximum pump power of 950 mW measured at the output of the Ti:sapphire laser. The actual incident pump power was calculated by monitoring a weak retroreflection from the lens (Fig. 3). As can be seen from Fig. 8, the absorption without lasing was strongly saturated but increased with the second pass. Lasing not only increased the actual absorption but as a consequence of this decreased the feedback and the maximum incident pump power was lower ($P_{\text{inc}} - 2.85$ W without lasing and $P_{\text{inc}} - 2.58$ W with lasing, respectively).

The maximum output power $P_{\text{out}}$ obtained from the Yb:KLuW–KLuW laser with pump feedback reached 515 mW with $T_{\text{OC}} = 3\%(\lambda_L = 1030$ nm) (see Fig. 9). This corresponds to a maximum pump efficiency of 25.5%. The maximum $P_{\text{out}}$ slightly dropped with $T_{\text{OC}} = 5\%$ to 480 mW and amounted to 400 mW with the 1.1% output coupler.

Using the same chopper with 1:10 duty cycle, we increased then the Ti:sapphire laser pump power measured directly at its output to 2 W. The feedback increased this value to $P_{\text{inc}} = 3$ W. With the 3% output coupler, the average output power of the epitaxial laser was 100 mW and the wavelength remained unchanged, $\lambda_L = 1030$ nm. The estimated double-pass absorption leads in this case to a pump efficiency of 40% which means a substantial increase in comparison with Fig. 9. Notwithstanding the fact that the results in terms of efficiency are worse in comparison to the case of pumping without feedback (presumably because of poor mode matching and overestimation of the absorption in the second pass), the feedback provides higher

ISBN:978-84-691-1552-7 /DL:T.151-2008

output powers. While this type of quasi-intracavity pumping is of practical interest because it increases the overall (relative to the Ar laser) pump efficiency about two times, the feedback mechanism is expected to play a minor role at increased dopant concentrations. From the maximum output power obtained with the chopper, it can be concluded that CW output powers in excess of 1 W can be expected from this epitaxial laser once a proper cooling is provided.

It is interesting to note that, even without cooling, no damage of the epitaxial crystal occurred regardless of the high power levels (intracavity intensity exceeding 1 MW/cm$^2$ with the $T_{OC} = 1.1\%$ outcoupler).

In conclusion, we studied for the first time, to the best of our knowledge, CW lasing in the 1-$\mu$m range of $Yb^{3+}$-doped epitaxial layers using the monoclinic host KLuW as a substrate. Pump efficiencies as high as 55% and CW output powers exceeding 500 mW were achieved without active cooling the crystal. This is an improvement of about one order of magnitude in comparison to our initial results obtained with Yb:KYW–KYW epitaxies [16]. In the present work we also demonstrated diode pumping of the epitaxial laser near 980 nm. Work is in progress to increase the doping level of the epitaxial layer toward the stoichiometric composition KYbW.

## REFERENCES

[1] W. F. Krupke, "Ytterbium solid-state lasers—The first decade," *IEEE J. Select. Topics Quantum Electron.*, vol. 6, no. 6, pp. 1287–1296, Nov./Dec. 2000.

[2] C. Stewen, K. Contag, M. Larionov, A. Giesen, and H. Hügel, "A 1-kW CW thin disc laser," *IEEE J. Sel. Topics Quantum Electron.*, vol. 6, no. 4, pp. 650–657, Jul.–Aug. 2000.

[3] V. Petit, J. L. Doualan, P. Camy, V. Menard, and R. Moncorge, "CW and tunable laser operation of $Yb^{3+}$ doped $CaF_2$," *Appl. Phys. B*, vol. 78, pp. 681–684, 2004.

[4] G. Boulon, A. Brenier, L. Laversenne, Y. Guyot, C. Goutaudier, M.-T. Cohen-Adad, G. Metrat, and N. Muhlstein, "Search of optimized trivalent ytterbium doped-inorganic crystals for laser applications," *J. Alloys Compounds*, vol. 341, pp. 2–7, 2002.

[5] N. V. Kuleshov, A. A. Lagatsky, V. G. Shcherbitsky, V. P. Mikhailov, E. Heumann, T. Jensen, A. Diening, and G. Huber, "CW laser performance of Yb and Er, Yb doped tungstates," *Appl. Phys. B*, vol. 64, pp. 409–413, 1997.

[6] A. A. Kaminskii, K. Ueda, H. E. Eichler, J. Findeisen, S. N. Bagaev, F. A. Kuznetsov, A. A. Pavlyuk, G. Boulon, and F. Bourgeois, "Monoclinic tungstates $KDy(WO_4)_2$ and $KLu(WO_4)_2$—New $\chi^{(3)}$ -active crystals for laser Raman shifters," *Jpn. J. Appl. Phys.*, vol. 37, pp. L923–L926, 1998.

[7] X. Mateos, V. Petrov, M. Aguiló, R. M. Solé, J. Gavaldà, J. Massons, F. Díaz, and U. Griebner, "Continuous-wave laser oscillation of $Yb^{3+}$ in monoclinic $KLu(WO_4)_2$," *IEEE J. Quantum Electron.*, vol. 40, no. 8, pp. 1056–1059, Aug. 2004.

[8] M. C. Pujol, M. A. Bursukova, F. Güell, X. Mateos, R. Solé, J. Gavaldà, M. Aguiló, J. Massons, F. Díaz, P. Klopp, U. Griebner, and V. Petrov, "Growth, optical characterization, and laser operation of a stoichiometric crystal $KYb(WO_4)_2$," *Phys. Rev. B, Condens. Matter*, vol. 65, no. 165 121, 2002.

[9] S. Erhard, J. Gao, A. Giesen, K. Contag, A. A. Lagatsky, A. Abdolvand, N. V. Kuleshov, J. Aus der Au, G. J. Spühler, R. Brunner, R. Paschotta, and U. Keller, "High power Yb:KGW and Yb:KYW thin disk laser operation," in *OSA Trends in Optics and Photonics (TOPS), Conf. Lasers and Electro-Optics, Tech. Dig., Postconference Edition*, Washington, DC, 2001, p. 333.

[10] S. B. Ubizskii, A. O. Matkovskii, S. S. Melnyk, I. M. Syvorotka, V. Müller, V. Peters, K. Petermann, A. Beyertt, and A. Giesen, "Optical properties of epitaxial YAG:Yb films," *Phys. Stat. Sol. (a)*, vol. 201, pp. 791–797, 2004.

[11] F. Chen, H. Hu, K.-M. Wang, F. Lu, B.-R. Shi, F.-X. Wang, Z.-X. Cheng, H.-C. Chen, and D.-Y. Shen, "Refractive index profiles of ion implanted waveguides in thulium sodium yttrium tungstate," *Opt. Commun.*, vol. 200, pp. 179–185, 2001.

[12] P. A. Atanasov, A. Perea, M. Jimenez de Castro, J. A. Chaos, J. Gonzalo, C. N. Afonso, and J. Perriere, "Luminescence properties of thin films prepared by laser ablation of Nd-doped potassium gadolinium tungstate," *Appl. Phys. A*, vol. 74, pp. 109–113, 2002.

[13] B. Ferrand, B. Chambaz, and M. Couchaud, "Liquid phase epitaxy: A versatile technique for the development of miniature optical components in single crystal dielectric media," *Opt. Mat.*, vol. 11, pp. 101–114, 1999.

[14] J. P. Van der Ziel, W. A. Bonner, L. Kopf, and L. G. Van Uitert, "Coherent emission from $Ho^{3+}$ ions in epitaxially grown thin aluminum garnet films," *Phys. Lett.*, vol. 42A, pp. 105–106, 1972.

[15] A. Aznar, D. Ehrentraut, Y. E. Romanyuk, R. Solé, M. Aguiló, P. Gerner, H. U. Güdel, and M. Pollnau, "Liquid-phase epitaxy and optical investigation of stoichiometric $KYb(WO_4)_2$ thin layers," in *5th Int. Conf. f-Elements*, Geneve, Switzerland, Aug. 24–29, 2003, Final Programme and Abstract Book, paper PC-42, p. 111.

[16] A. Aznar, R. Solé, M. Aguiló, F. Díaz, U. Griebner, R. Grunwald, and V. Petrov, "Growth, optical characterization and laser operation of epitaxial Yb : $KY(WO_4)_2/KY(WO_4)_2$ composites with monoclinic structure," *Appl. Phys. Lett.*, vol. 85, no. 19, pp. 4313–4315, 2004.

[17] X. Mateos, A. Aznar, M. C. Pujol, R. Solé, X. Solans, J. Massons, F. Díaz, and M. Aguiló, "Crystal growth and structural characterization of undoped and Yb-doped $KLu(WO_4)_2$," J. Appl. Cryst., 2004, submitted for publication.

[18] M. C. Pujol, X. Mateos, R. Solé, J. Massons, J. Gavaldà, X. Solans, F. Díaz, and M. Aguiló, "Structure, crystal growth and physical anisotropy of $KYb(WO_4)_2$, a new laser matrix," *J. Appl. Cryst.*, vol. 35, pp. 108–12, 2002.

[19] X. Xu, Z. Zhao, P. Song, G. Zhou, J. Xu, and P. Deng, "Structural, thermal, and luminescent properties of Yb-doped $Y_3Al_5O_{12}$ crystals," *J. Opt. Soc. Amer. B*, vol. 21, pp. 543–547, 2004.

[20] M. C. Pujol, X. Mateos, R. Solé, J. Massons, J. Gavaldà, F. Díaz, and M. Aguiló, "Linear thermal expansion tensor in $KRE(WO_4)_2$ (RE = Gd, Y, Er, Yb) monoclinic crystals," *Mat. Sci. Forum*, vol. 378–381, pp. 710–717, 2001.

[21] F. D. Patel, E. C. Honea, J. Speth, S. A. Payne, R. Hutcheson, and R. Equall, "Laser demonstration of $Yb_3Al_5O_{12}$ (YbAG) and materials properties of highly doped Yb:YAG," *IEEE J. Quantum Electron.*, vol. 37, no. 1, pp. 135–144, Jan. 2001.

[22] P. Klopp, V. Petrov, U. Griebner, and G. Erbert, "Passively mode-locked Yb:KYW laser pumped by a tapered diode laser," *Opt. Exp.*, vol. 10, pp. 108–113, 2002.

[23] C. Lim and Y. Izawa, "Modeling of end-pumped CW quasi-three-level lasers," *IEEE J. Quantum Electron.*, vol. 38, no. 3, pp. 306–311, Mar. 2002.

**Uwe Griebner** received the Ph.D. degree in physics from the Technical University of Berlin, Berlin, Germany in 1996. His Ph.D. research was on fiber bundle lasers with high average power.

Since 1992, he has been with the Max-Born-Institute, Berlin, Germany, working on diode pumped solid-state lasers, fiber lasers, waveguide lasers, microoptics, microoptics for special resonators, and ultrafast lasers. He is currently focused on ultrafast diode-pumped solid-state lasers and amplifiers applying new active materials and the use of micro-optical components for femtosecond beam-shaping.

**Junhai Liu** was born in Shandong Province, China, in 1964. He received the B.S., M.S., and Ph.D. degrees in physics from Shandong University, Shandong, China, in 1984, 1990, and 1999, respectively.

His current research interest is within the field of diode-pumped solid-state lasers based on newly developed laser crystals.

**Simon Rivier** was born in Bristol, U.K., in 1978. He received the M.T.Sc. degree from the Swiss Polytechnical School, Lausanne, Switzerland, in 2003. Currently, he is working toward the Ph.D. degree at the Max-Born-Institute, Berlin, Germany. His doctoral work focuses on diode-pumped solid-state lasers with new active materials.

ISBN:978-84-691-1552-7 /DL:T.151-2008

**Ana Aznar** was born in Tarragona, Spain, in 1975. She received the B.Sc. degree in chemistry from Rovira i Virgili University (URV), Tarragona, Spain, in 1999, where she is currently working toward the Ph.D. degree. Her doctoral work focuses on crystal growth of $KRE(WO_4)_2$ layers doped with Yb and their characterization.

**Rüdiger Grunwald** studied physics at Humboldt University Berlin until 1982 and prepared a doctoral thesis on multiphoton dissociation and spectroscopy in 1986.

He worked in the development of gas and solid-state lasers and frequency conversion. Since 1998, he has been with Max-Born-Institute, Berlin, Germany, where his interest is concentrated on shaping and characterization of ultrashort-pulse lasers by thin-film microoptics and nonlinear nanooptics.

**Rosa Maria Solé** was born in Tarragona, Spain, in 1965. She received the Ph.D. degree in physics from Barcelona University, Barcelona, Spain, in 1994.

She is currently a Lecturer of applied physics at the Rovira i Virgili University (URV), Tarragona, Spain. Her research interests include phase diagrams, crystal growth, and physical properties of the solutions and crystals.

**Magdalena Aguiló** was born in Sa Pobla, Mallorca, Spain. She received the Ph.D. degree in physics from Barcelona University, Barcelona, Spain, in 1983.

Currently, she is Professor of Crystallography at the Rovira i Virgili University (URV), Tarragona, Spain. Her research interests include growth of bulk crystals, epitaxies and nanoparticles, X-ray diffraction, X-ray texture analysis, and physical properties in relation with the crystalline structure.

**Francesc Díaz** was born in Mondoñedo (Lugo), Spain, in 1953. He received the Ph.D. degree in physics from Barcelona University, Barcelona, Spain, in 1982.

Currently, he is Professor of Applied Physics at the Rovira i Virgili University (URV), Tarragona, Spain. His research interests include growth of bulk crystals, epitaxies and nanoparticles, optical spectroscopy (absorption and emission) of rare-earth ions for laser applications and nonlinear optical processes. He has published approximately 150 papers in scientific journals.

**Valentin Petrov** was born in Plovdiv, Bulgaria, in 1959. He received the M.Sc. degree in nuclear physics from the University of Sofia, Sofia, Bulgaria, in 1983 and the Ph.D. degree in optical physics from the Friedrich-Schiller-University, Jena, Germany, in 1988.

He joined the Max-Born-Institute for Nonlinear Optics and Ultrafast Spectroscopy, Berlin, Germany, in 1992. His research interests include ultrashort light pulses, laser physics, and nonlinear optics, and he has coauthored about 130 papers in scientific journals.

UNIVERSITAT ROVIRA I VIRGILI
CRECIMIENTO Y CARACTERIZACIÓN DE CAPAS EPITAXIALES DE KRE 1-X 4BX (WO4)2 / KRE (WO4)2 (RE=Y,LU) PARA APLICACIONES LÁSER
Ana Isabel Aznar Écija

ISBN:978-84-691-1552-7 /DL:T.151-2008

 OPTICS LETTERS / Vol. 30, No. 18 / September 15, 2005
ISBN:978-84-691-1552-7 /DL:T.151-2008

# Mode-locked laser operation of epitaxially grown Yb:KLu$(WO_4)_2$ composites

**Simon Rivier, Xavier Mateos, Valentin Petrov, and Uwe Griebner**
*Max-Born-Institute, Max-Born-Strasse 2A, D-12489 Berlin, Germany*

**Ana Aznar, Oscar Silvestre, Rosa Sole, Magdalena Aguilo, and Francesc Diaz**
*Física i Cristal·lografia de Materials (FiCMA), Universitat Rovira i Virgili, Marcel·lí Domingo, E-43007 Tarragona, Spain*

**Martin Zorn and Markus Weyers**
*Ferdinand-Braun-Institute, Gustav-Kirchhoff-Strasse 4, D-12489 Berlin, Germany*

Received February 24, 2005; revised manuscript received April 4, 2005; accepted April 22, 2005

Mode locking based on an epitaxial composite of the monoclinic double tungstate crystal Yb:KLu$(WO_4)_2$ is realized. A 100 $\mu$m thin Yb:KLu$(WO_4)_2$ layer grown on a KLu$(WO_4)_2$ substrate is used as an active medium in a laser passively mode locked by a semiconductor saturable absorber. Pulse durations of 114 fs have been achieved for an average power of 31 mW at 1030 nm. Results in the femtosecond and picosecond regimes of the Yb:KLu$(WO_4)_2$/KLu$(WO_4)_2$ laser are presented. The great potential of Yb-doped tungstate composite structures as active elements for mode-locked laser systems is demonstrated. © 2005 Optical Society of America

*OCIS codes:* 140.5680, 140.4050, 160.5690.

There is a strong trend toward simplification and miniaturization of Yb-based ultrashort-pulse solid-state lasers operating in the 1 $\mu$m spectral region. Yb-doped monoclinic $KRE^{3+}(WO_4)_2$ ($RE$=Y, Gd, Lu) single crystals are host–dopant combinations that are interesting for highly efficient laser operation.[1] The doping level can reach the stoichiometric structure[2] KYb$(WO_4)_2$ (KYbW), but thermomechanical limitations do not allow the fabrication and use of active elements with a thickness less than 100 $\mu$m. The absorption length, for operation in the absorption maximum at 981 nm and with polarization parallel to the $N_m$ dielectric axis, reaches 13.3 $\mu$m for KYbW. Epitaxial growth of highly Yb-doped layers on passive substrates is especially interesting for such strongly anisotropic hosts, where the extremely large cross sections would permit the utilization of the thin disk laser concept.[3] Furthermore, for operation at higher power levels, the undoped part of the epitaxial structure can act as a heat sink to reduce the temperature in the crystal. Recently, we demonstrated for the first time laser operation based on epitaxial double tungstate structures by using a 25 $\mu$m thin, 20 at. % Yb-doped KY$(WO_4)_2$ (KYW) layer on a KYW substrate crystal.[4] However, the crystal lattice mismatch seems to be the inherent limitation on the achievable interface quality in the case of KYW and KYbW, and the mismatch relative to KGd$(WO_4)_2$ (KGdW) is even larger. The closer ionic radii of Lu and Yb make potassium lutetium tungstate, KLu$(WO_4)_2$ (KLuW), potentially interesting as a passive host because of the possibility not only of doping with very high concentrations of $Yb^{3+}$ but also of the growth of KYbW/KLuW epitaxial structures. The maximum absorption $\sigma_a$ and emission cross sections $\sigma_e$ of Yb:KLuW and many other relevant laser properties are very close to those reported for Yb-doped KGdW and KYW.[1] The better match of the unit cell parameters of KYbW and KLuW with an average mismatch of 0.33% compared with 0.64% between KYbW and KYW can be seen as a prerequisite for the growth of high-quality epitaxial structures. Highly efficient cw[5] and mode-locked laser operation[6] with this novel Yb-doped monoclinic double tungstate was achieved by using a 2.8 mm thick, 5 at. % Yb-doped KLuW bulk sample. Output powers of the order of 1 W with pump efficiencies as high as 50% and pulse durations down to 81 fs with a saturable absorber mirror (SAM) used for mode locking were obtained at room temperature. The pulse durations achieved with bulk Yb:KLuW are slightly longer than the 71 fs once obtained with a Kerr-lens mode-locked Yb:KYW laser[7] but consistently shorter than the ≈100 fs limit reported for SAM mode-locked Yb:KGdW and Yb:KYW lasers.[8,9]

In this Letter we report for the first time to our knowledge mode-locked operation of Yb:KLuW/KLuW epitaxially grown composite crystal, and we compare its performance to the bulk Yb:KLuW laser.

Yb-doped KLuW layers have been grown with high crystalline quality by the liquid-phase epitaxy method. The thickness of the Yb:KLuW layer with an Yb-doping concentration of 10%, grown on the (010) face of a 1.1 mm thick KLuW substrate, amounted to 100 $\mu$m. The maximum $\sigma_a$ and $\sigma_e$ of Yb:KLuW for $E \| N_m$ amount to $\sigma_a = 1.18 \times 10^{-19}$ cm$^2$ and $\sigma_e = 1.47$

0146-9592/05/182484-3/$15.00 

ISBN:978-84-691-1552-7 /DL:T.151-2008

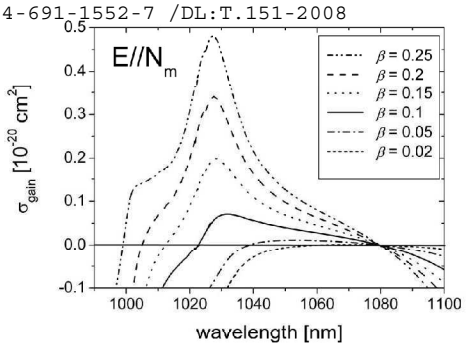


Fig. 1. Calculated gain cross section $\sigma_{\text{gain}}=\beta\sigma_e-(1-\beta)\sigma_a$ for polarization along the $N_m$ principal optical axis of Yb:KLuW and various population inversions $\beta$.

$\times 10^{-19}$ cm$^2$ at 981 nm.[5] In order to estimate the potential gain bandwidth for mode-locked operation, the gain cross section for various population inversions $\beta$ is calculated and presented in Fig. 1. $\beta$ is the ratio of the excited ion density to the total Yb-ion density.

We studied a $Z$-shaped astigmatically compensated resonator similar to that used in Ref. 6. The polished (010) faces of the epitaxial crystal were normal to the $N_p$ principal optical axis, and the sample was oriented for polarization parallel to $N_m$. The Yb:KLuW/KLuW crystal was positioned between two folding mirrors at the Brewster angle. The laser was pumped by a cw Ti:sapphire laser, delivering more than 3 W at the pump wavelength of 981 nm, focused to a beam waist of about 30 $\mu$m. The used semiconductor SAM was grown by metal organic vapor-phase epitaxy and consisted of a bottom Bragg mirror. The absorber was a 10 nm thick InGaAs surface quantum well structure[10] with a saturable absorption of $\approx$1%. Its relaxation time was measured by the pump–probe technique to be less than 5 ps.

The measured single-pass low-signal absorption of the 10% Yb:KLuW layer at 981 nm was 64%. Initially the cw laser performance without SAM and prisms in a three-mirror cavity was investigated. The maximum output power of 415 mW corresponds to a maximum optical conversion efficiency of 55% with respect to the absorbed pump power. Note that even without cooling the Yb:KLuW/KLuW composite, no thermal problems and no damage occurred. The pump and slope (up to 66%) efficiencies achieved both exceed those obtained with a 2.2 mm thick bulk KLuW doped with 10 at. % Yb in a similar pump and laser configuration.[5] This is attributed to the strongly reduced reabsorption.

Without intracavity prisms the SAM mode-locked laser operated in the picosecond regime at a pulse repetition frequency $f_{\text{rep}}=100$ MHz. In Fig. 2(a) the autocorrelation function is shown together with the emission spectrum centered at 1030 nm. Assuming a sech$^2$ pulse shape, the deconvolved FWHM of the pulse is 1.8 ps. The output power versus the absorbed pump power $P_{\text{abs}}$ in the picosecond configuration, below and above the mode-locking threshold, is shown in Fig. 2(b). Mode-locked operation was obtained with a maximum output power of 119 mW, applying an output coupler transmission $T_{\text{OC}}=3\%$. From these experimental data the measured slope efficiency amounted to 27%, and the optical conversion efficiency reached 17%. We attribute the overall reduction of the efficiency caused by the presence of the SAM to the cavity realignment connected with the additional focusing mirror. The femtosecond regime was realized by inserting two SF10 Brewster prisms with a separation of 31 cm into the arm containing $T_{\text{OC}}=1.1\%$, which resulted in an $f_{\text{rep}}=101$ MHz. The measured autocorrelation traces are well fitted, assuming a sech$^2$ pulse shape. Pulses as short as 114 fs [Fig. 3(a)] at a central wavelength of 1030 nm were generated with an average output power of 31 mW for $P_{\text{abs}}=632$ mW. The time–bandwidth product $\tau\Delta\nu=0.43$ is slightly above the Fourier limit [spectrum, inset Fig. 3(a)]. We believe that the lower limit for the pulse duration and the observed deviation from the transform-limited pulse performance are related to the reflection characteristics of the folding mirrors, which are restricted by the close separation between the pump and the lasing wavelengths. This entails a high transmission <980 nm and a high reflection >1020 nm. The output power could be increased by using $T_{\text{OC}}=3\%$, and 94 mW were obtained, again at 1030 nm, for $P_{\text{abs}}=671$ mW. The generated pulses

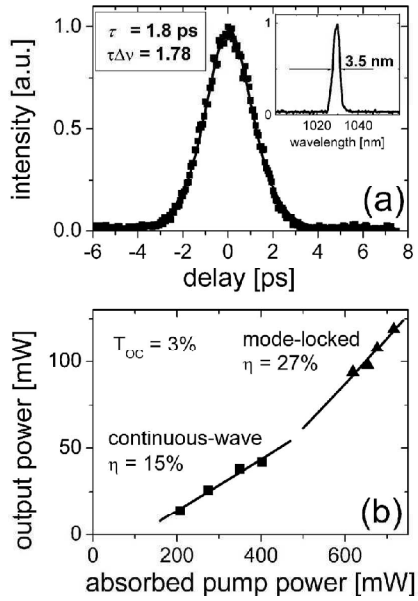


Fig. 2. Mode-locked laser performance of the Yb:KLuW/KLuW epitaxial composite in the picosecond regime; $T_{\text{OC}}$, output coupler transmission. (a) Autocorrelation trace and (inset) spectrum; $\tau$, pulse duration; $\tau\Delta\nu$, time–bandwidth product. (b) Output power versus absorbed pump power above and below the mode-locking threshold (cw); $\eta$, slope efficiency.

ISBN:978-84-691-1552-7 /DL:T.151-2008

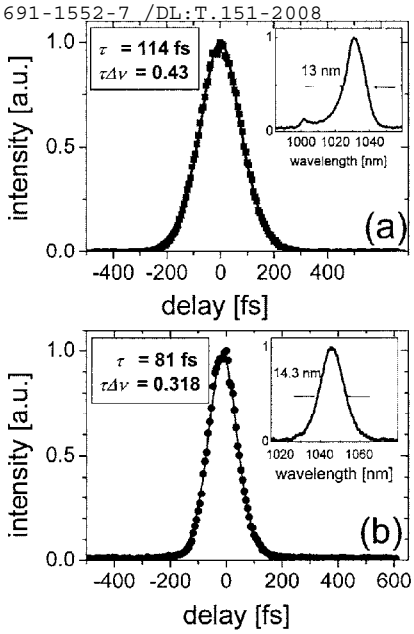


Fig. 3. Autocorrelation traces and (inset) spectra in the femtosecond regime. (a) Epitaxial composite, 100 $\mu$m thin Yb(10%):KLuW layer on a 1.1 mm thick KLuW substrate. (b) 2.8 mm thick Yb(5%):KLuW bulk single crystal; $\tau$, pulse duration; $\tau\Delta\nu$, time–bandwidth product.

had a FWHM of 200 fs in this case and were almost bandwidth limited ($\tau\Delta\nu$=0.32).

To illustrate that the 114 fs pulse duration is not the limit, we compare the femtosecond laser performance of the epitaxial Yb:KLuW with that of the bulk Yb(5%):KLuW (2.8 mm thick) single crystal [Fig. 3(b)] under the same experimental conditions. We expect a larger gain bandwidth for the epitaxial structure due to the reduced reabsorption, leading to a higher average population inversion $\beta$. Such behavior can be clearly observed in Fig. 1, visualizing the estimated gain bandwidth for various $\beta$. From the central wavelength of 1045 nm for spectrum of the bulk Yb:KLuW laser [inset Fig. 3(b)], $\beta \approx 0.08$ can be deduced. The pulse spectrum of the epitaxial composite is centered at 1030 nm with a broadened shape of the short-wavelength wing extending beyond 1000 nm. Both the central wavelength and the spectral shape can be associated with larger population inversion in Fig. 1 ($\beta > 0.2$), corresponding to broader gain bandwidths. Thus the strongly reduced reabsorption of the epitaxial Yb:KLuW, resulting in potentially broader gain bandwidths, is expected in the future to allow pulse lengths below 80 fs to be produced, by use of specially designed dichroic coatings for the folding mirrors.

For the development of composite-based femtosecond oscillators the use of epitaxial structures, where the layer and the substrate consist of the same crystal host, have essential advantages compared with heterocomposite structures like bonded crystals of Yb:YAG on sapphire.[11] They can reduce the problem of parasitic reflections and birefringence effects,[12] which could strongly affect the femtosecond regime and have to be taken into consideration. Neither in the emitted spectrum nor in the field distribution of the Yb:KLuW/KLuW laser could we detect any indications of modulations.

This work has been supported through the project DT-CRYS, NMP3-CT-2003-505580 (EU). X. Mateos acknowledges financial support from Secretaria de Estado de Educacion y Universidades of Spain and Fondo Social Europeo. U. Griebner's e-mail address is griebner@mbi-berlin.de.

## References

1. A. A. Lagatsky, N. V. Kuleshov, and V. P. Mikhailov, Opt. Commun. **165**, 71 (1999).
2. M. C. Pujol, M. A. Bursukova, F. Güell, X. Mateos, R. Sole, J. Gavalda, M. Aguilo, J. Massons, F. Diaz, P. Klopp, U. Griebner, and V. Petrov, Phys. Rev. B **65**, 165121 (2002).
3. F. Brunner, T. Südmeyer, E. Innerhofer, F. Morier-Genoud, R. Paschotta, V. E. Kisel, V. G. Shcherbitsky, N. V. Kuleshov, J. Gao, K. Contag, A. Giesen, and U. Keller, Opt. Lett. **27**, 1162 (2002).
4. A. Aznar, R. Solé, M. Aguiló, F. Díaz, U. Griebner, R. Grunwald, and V. Petrov, Appl. Phys. Lett. **85**, 4313 (2004).
5. X. Mateos, V. Petrov, M. Aguiló, R. M. Solé, J. Gavaldà, J. Massons, F. Díaz, and U. Griebner, IEEE J. Quantum Electron. **40**, 1056 (2004).
6. U. Griebner, S. Rivier, V. Petrov, M. Zorn, G. Erbert, M. Weyers, X. Mateos, M. Aguiló, J. Massons, and F. Díaz, Opt. Express **13**, 3465 (2005).
7. H. Liu, J. Nees, and G. Mourou, Opt. Lett. **26**, 1723 (2001).
8. G. Paunescu, J. Hein, and R. Sauerbrey, Appl. Phys. B **79**, 555 (2004).
9. P. Klopp, V. Petrov, U. Griebner, and G. Erbert, Opt. Express **10**, 108 (2002).
10. A. Garnache, S. Hoogland, A. C. Tropper, I. Sagnes, G. Saint-Girons, and J. S. Roberts, Appl. Phys. Lett. **80**, 3892 (2002).
11. C. L. Bonner, T. Bhutta, D. P. Shephard, and A. C. Tropper, IEEE J. Quantum Electron. **36**, 236 (2000).
12. F. Krausz, M. E. Fermann, T. Brabec, P. F. Curley, M. Hofer, M. H. Ober, C. Spielmann, E. Wintner, and A. J. Schmidt, IEEE J. Quantum Electron. **28**, 2097 (1992).

UNIVERSITAT ROVIRA I VIRGILI
CRECIMIENTO Y CARACTERIZACIÓN DE CAPAS EPITAXIALES DE KRE 1-X 4BX (WO4)2 / KRE (WO4)2 (RE=Y,LU) PARA APLICACIONES LÁSER
Ana Isabel Aznar Écija

ISBN:978-84-691-1552-7 /DL:T.151-2008

electronic reprint

Journal of
**Applied**
**Crystallography**
ISSN 0021-8898
Editor: **Gernot Kostorz**

# Structural redetermination, thermal expansion and refractive indices of $KLu(WO_4)_2$

**M. C. Pujol, X. Mateos, A. Aznar, X. Solans, S. Suriñach, J. Massons, F. Díaz and M. Aguiló**

ISBN:978-84-691-1552-7 /DL:T.151-2008

## research papers

Journal of
**Applied Crystallography**
ISSN 0021-8898

Received 12 August 2005
Accepted 3 February 2006

# Structural redetermination, thermal expansion and refractive indices of $KLu(WO_4)_2$

**M. C. Pujol,[a] X. Mateos,[a] A. Aznar,[a] X. Solans,[b] S. Suriñach,[c] J. Massons,[a] F. Díaz[a] and M. Aguiló[a]***

[a]Física i Cristal·lografia de Materials (FiCMA), Universitat Rovira i Virgili, Campus Sescelades c/ Marcel.lí Domingo, s/n, 43007-Tarragona, Spain, [b]Departament de Cristal·lografia, Mineralogia i Diposits Minerals, Universitat de Barcelona, 08028-Barcelona, Spain, and [c]Departament de Física, Universitat Autònoma de Barcelona, 08193-Bellaterra, Spain. Correspondence e-mail: magdalena.aguilo@urv.net

The crystal structure of monoclinic $KLu(WO_4)_2$ (KLuW) crystals was determined at room temperature by using single-crystal X-ray diffraction data. The unit-cell parameters were $a$ = 10.576 (7), $b$ = 10.214 (7), $c$ = 7.487 (2) Å, $\beta$ = 130.68 (4)°, with $Z$ = 4, in space group $C2/c$. The unit-cell parameters of $KLu_{1-x}Yb_x(WO_4)_2$ were determined in relation to Yb concentration. Vickers micro-indentations were used to study the microhardness of KLuW. The linear thermal expansion tensor was determined and the principal axis with maximum thermal expansion ($\alpha'_{33} = 16.72 \times 10^{-6}\,K^{-1}$), $X'_3$, was located 13.51° from the $c$ axis. The room-temperature optical tensor was studied in the near-infrared (NIR) and visible range. The principal optical axis with maximum refractive index ($n_g = 2.113$), $N_g$, was located 18.5° from the $c$ axis at 632.8 nm. Undoped and ytterbium-doped KLuW crystals were grown by the TSSG (top-seeded-solution growth) slow-cooling method. The crystals show {110}, {$\bar{1}$11}, {010} and {310} faces that basically constitue the habit of the KLuW crystals.



## 1. Introduction

The monoclinic phases of potassium and rare earth double tungstates $KRE(WO_4)_2$ (RE = Gd, Y and Yb) are an interesting family of materials that can be used as laser host media for lanthanide doping ($Ln^{3+}$ = Pr, Nd, Ho, Er, Tm and Yb) (Kaminskii, 1996). Ytterbium-doped potassium rare earth double tungstates (KREWs) provide broad bandwidths which can make some degree of tunability possible. They can also be efficiently and directly pumped with a diode laser at 940 or 980 nm. All this makes it possible to generate simplified femtosecond lasers and high-power amplifiers based on ytterbium KREW crystals (Brenier, 2001; Boulon, 2003; Krueger & Féru, 2004). These materials are also SRS (simulated Raman scattering) active hosts, so the number of possible laser emissions increases (Grabtchikov, 2000; Narkhova & Ustimenko, 1998; Ustimenko & Gulin, 1998, 2002). $KLu(WO_4)_2$ is isostructural with these materials and is expected to have similar promising optical/physical properties, characterized by a high anisotropy.

The KLuW structure has been studied in the past. Klevtsov & Kozeva (1969) measured the unit-cell parameters of KLuW with X-ray powder patterns: the parameters were $a$ = 7.99, $b$ = 10.21, $c$ = 7.49 Å. However, they did not mention the space group. Later, the same authors published the unit-cell parameters of one of the high-temperature phases of this compound, a trigonal phase, with $a$ = 5.91, $b$ = 8.04, $c$ = 7.31 Å (Klevtsov *et al.*, 1974). In another paper, Klevtsov *et al.* (1975) again used X-ray diffraction powder patterns to obtain the unit-cell parameters of the monoclinic phase: $a$ = 10.51, $b$ = 10.21, $c$ = 7.45 Å, $\beta$ = 130.5°, in space group $C2/c$. Later, Yudanova *et al.* (1986) used X-ray diffraction patterns to determine the unit-cell parameters $a$ = 10.592 (3), $b$ = 10.236 (6), $c$ = 7.498 (1) Å, $\beta$ = 130.75 (2)°, in the space group $I2/c$. As we have reported in a previous article (Pujol, Solé *et al.*, 2001), and in agreement with Kaminskii *et al.* (2002), unit-cell parameters of KREW can be expressed in three equivalent correct crystallographic settings: $C2/c$, $I2/c$ and $I2/a$, with the appropriate cell dimensions in each case. Kaminskii *et al.* (1998) reported the crystallographic data as $a$ = 7.99, $b$ = 10.21, $c$ = 7.45 Å, $\beta$ = 94°, expressed in $I2/c$ for KLuW material. According to the recommendations of the International Union of Crystallography regarding the standard setting, we have redetermined the structure of KLuW and expressed it in the $C2/c$ crystallographic setting. In the present paper, unit-cell parameters and fractional atomic coordinates are presented and interatomic distances are described in detail. Because of the monoclinic structure of this material, its physical properties are thought to be considerably anisotropic. Further applications of this material as a host laser single

crystal make it necessary to determine this anisotropy in the thermal and mechanical properties in detail, such as the linear thermal expansion and microhardness.

The $Yb^{3+}$ ion is recognized as a potentially interesting dopant for InGaAs diode-pumped solid-state lasers in the 1 μm region (Deloach *et al.*, 1993; Zou & Toratani, 1995; Krupke, 2000). The similar ionic radii (coordination number 8) of $Yb^{3+}$ (0.985 Å) and $Lu^{3+}$ (0.977 Å) ions and, consequently, the foreseen similarity between the cell parameters of KLuW and KYbW, make it possible to obtain highly Yb-doped KLuW layers on KLuW substrates with high quality (Griebner, Liu *et al.*, 2005). Highly doped materials with active ions are potentially interesting for thin-disc laser design; these materials have demonstrated their potential for high-output powers (Stewen *et al.*, 2005). KLuW can also incorporate high doping ytterbium concentrations with no important changes in the structure, as is reported in the present paper. Continuous wave (CW) highly efficient and mode-locked laser emission has been achieved very recently in ytterbium KLuW material both in bulk and epitaxic configuration (Mateos *et al.*, 2004; Griebner, Rivier *et al.*, 2005; Rivier *et al.*, 2005).

We present our structural studies of KLuW as a competitive host for ytterbium laser ions. The change in the unit-cell parameters due to the partial substitution of Lu by Yb is also reported. These results complement the laser performance in the system Yb:KLuW.

## 2. Structure of $KLu(WO_4)_2$

The single crystals used for the structural studies were obtained from high-temperature solutions, with $K_2W_2O_7$ as a solvent, and a solution composition of 12 mol% solute and 88 mol% solvent. The crystals nucleated on a platinum disc, 12 mm in diameter, rotating at 40 r.p.m. in the homogeneous solution. The crystals grew because of the supersaturation created by decreasing the temperature to about 10 K from the saturation temperature with a cooling rate of around 0.5–1 K $h^{-1}$.

Single-crystal X-ray diffraction data of KLuW were collected and then the structure was solved by Patterson synthesis using the *SHELXS97* computer program (Sheldrick, 1997), followed by refinement by the full-matrix least-squares method using *SHELXL97* (Sheldrick, 1997). The space group was *C*2/*c* of the monoclinic system and the unit-cell parameters were $a = 10.576$ (7), $b = 10.214$ (7), $c = 7.487$ (2) Å, $\beta = 130.68$ (4)°. Table 1 shows this information as well as the crystal data, data collection and refinement details. The atomic positions and interatomic distances are summarized in Tables 2 and 3, respectively.[1]

The structure is close to that of other KREW structures (Pujol, Solé *et al.*, 2001; Pujol *et al.*, 2002; Klevtsov *et al.*, 1968; Borowiec *et al.*, 2003; Kaminskii *et al.*, 1998). As in the other potassium double tungstates, the coordination figure of the tungstate anion is a distorted octahedron, $WO_6$ [W—O distances range from 1.767 (7) to 2.265 (8) Å]. The units, which are formed by two distorted octahedra that share the edges O2—$O2^i$ [2.341 (9) Å; symmetry code: (i) $-x, -y, 1-z$], make up the characteristic double chain in the crystallographic **c** direction by sharing vertex O4. Observing the distances W—O along the series KREW (RE = Gd, Yb and Lu), in KLuW there is an increase of the regularity of the coordination figure. We calculated the degree of distortion, $\Delta_d$, of the coordination polyhedra with

$$\Delta_d = (1/n)\sum_{i=1}^{n}\left\{\frac{[d(M-O)_n - \langle d(M-O)\rangle]}{\langle d(M-O)\rangle}\right\}^2$$

(Carvajal *et al.*, 2003). The results are summarized in Table 4. The average W—O distance decreases along KREW (RE = Gd, Yb and Lu) so we can expect the $WO_6$ groups in the KLuW host to be more compact and more covalent.

**Table 1**
Crystal data, data collection and refinement parameters of monoclinic $KLu(WO_4)_2$.

| | |
|---|---|
| Crystal data | |
| $KLu(WO_4)_2$ | Mo $K\alpha$ radiation |
| $M_r = 709.77$ | $\lambda = 0.71069$ Å |
| Monoclinic, *C*2/*c* | Cell parameters from 25 reflections |
| $a = 10.576$ (7) Å | $\theta = 12$–$21°$ |
| $b = 10.214$ (7) Å | $\mu = 54.071$ mm$^{-1}$ |
| $c = 7.487$ (2) Å | $T = 293$ (2) K |
| $\beta = 130.68$ (4)° | Sphere |
| $V = 613.3$ (6) Å$^3$ | 0.2 mm diameter |
| $Z = 4$ | Colourless |
| $D_x = 7.686$ Mg m$^{-3}$ | |
| Data collection | |
| Enraf–Nonius CAD-4 diffractometer | $R_{int} = 0.0343$ |
| $\omega$–$2\theta$ scans | $\theta_{max} = 29.97°$ |
| Absorption correction: spherical | $h = -14 \rightarrow 11$ |
| 1875 measured reflections | $k = 0 \rightarrow 14$ |
| 899 independent reflections | $l = 0 \rightarrow 10$ |
| 664 reflections with $I > 2\sigma(I)$ | 3 standard reflections every 120 min |
| | Intensity decay: none |
| Refinement | |
| Refinement on $F^2$ | $(\Delta/\sigma)_{max} = 0.002$ |
| $R[F^2 > 2\sigma(F^2)] = 0.0356$ | $\Delta\rho_{max} = 0.766$ e Å$^{-3}$ |
| $wR(F^2) = 0.0824$ | $\Delta\rho_{min} = -0.673$ e Å$^{-3}$ |
| $S = 1.209$ | Extinction correction: none |
| 899 reflections | Scattering factors from *International Tables for Crystallography* (Vol. C) |
| 56 parameters | |
| $w = 1/[\sigma^2(F_o^2) + (0.0275P)^2]$ where $P = (F_o^2 + 2 - F_c^2)/3$ | |

**Table 2**
Fractional atomic coordinates and equivalent isotropic displacement parameters (Å$^2$) of $KLu(WO_4)_2$.

| | Wyckoff position | *x* | *y* | *z* | $U_{eq}$ |
|---|---|---|---|---|---|
| Lu | 4*e* | 0 | 0.72841 (3) | 1/4 | 0.01989 (19) |
| W | 8*f* | 0.19691 (3) | 0.00005 (2) | 0.73532 (5) | 0.01801 (16) |
| K | 4*e* | 1/2 | 0.2027 (3) | 3/4 | 0.0249 (6) |
| O1 | 8*f* | 0.3768 (7) | −0.0828 (7) | 0.8121 (13) | 0.0462 (16) |
| O2 | 8*f* | 0.0239 (7) | −0.1070 (6) | 0.4722 (11) | 0.0334 (12) |
| O3 | 8*f* | 0.2835 (7) | 0.1522 (6) | 0.8784 (13) | 0.0418 (16) |
| O4 | 8*f* | 0.2003 (6) | −0.0749 (8) | 0.9536 (12) | 0.0402 (14) |

[1] Full crystallographic data (CIF and structure factors) are available from the IUCr electronic archives (Reference: KS5080). Services for accessing these data are described at the back of the journal.

ISBN:978-84-691-1552-7 /DL:T.151-2008



**Table 3**
Selected interatomic distances (Å) of monoclinic $KLu(WO_4)_2$.

| | | | | | | | |
|---|---|---|---|---|---|---|---|
| W—O3 | 1.767 (7) | Lu—O2$^{iii}$ | 2.260 (7) | K—O4$^{vii}$ | 2.786 (8) | W—W$^{i}$ | 3.261 (2) |
| W—O4 | 1.784 (8) | Lu—O1$^{iv}$ | 2.217 (9) | K—O4$^{ii}$ | 2.739 (6) | W—W$^{ii}$ | 3.743 (3) |
| W—O1 | 1.801 (6) | Lu—O3$^{v}$ | 2.299 (7) | K—O1$^{ii}$ | 2.894 (8) | W—W$^{ix}$ | 3.744 (3) |
| W—O2 | 1.930 (6) | Lu—O3$^{vi}$ | 2.765 (6) | K—O2$^{viii}$ | 2.976 (7) | | |
| W—O2$^{i}$ | 2.081 (6) | | | K—O3 | 3.050 (8) | W—Lu$^{x}$ | 3.513 (2) |
| W—O4$^{iii}$ | 2.265 (8) | | | K—O1 | 3.348 (7) | W—Lu$^{xi}$ | 3.803 (3) |
| | | | | | | W—Lu$^{xii}$ | 3.908 (3) |
| | | | | | | W—Lu$^{xiii}$ | 3.921 (3) |
| | | | | | | W—K$^{ix}$ | 3.648 (3) |
| | | | | | | W—K$^{xiv}$ | 3.803 (3) |
| | | | | | | W—K | 3.757 (3) |
| | | | | | | Lu—K$^{v}$ | 3.753 (3) |
| | | | | | | Lu—K$^{xv}$ | 3.753 (3) |
| | | | | | | Lu—Lu$^{xvi}$ | 4.045 (3) |
| | | | | | | Lu—Lu$^{vi}$ | 5.982 (3) |
| | | | | | | Lu—Lu$^{xvii}$ | 6.693 (3) |

Symmetry codes: (i) $-x, -y, 1-z$; (ii) $x, -y, z-\frac{1}{2}$; (iii) $x, 1+y, z$; (iv) $\frac{1}{2}-x, \frac{1}{2}-y, 1-z$; (v) $x-\frac{1}{2}, \frac{1}{2}+y, z-1$; (vi) $x, 1-y, z-\frac{1}{2}$; (vii) $\frac{1}{2}+x, \frac{1}{2}+y, z$; (viii) $\frac{1}{2}-x, \frac{1}{2}+y, \frac{3}{2}-z$; (ix) $x, -y, \frac{1}{2}+z$; (x) $x, 1-y, \frac{1}{2}+z$; (xi) $\frac{1}{2}+x, y-\frac{1}{2}, 1+z$; (xii) $\frac{1}{2}+x, \frac{1}{2}-y, \frac{1}{2}+z$; (xiii) $x, y-1, z$; (xiv) $x-\frac{1}{2}, y-\frac{1}{2}, z$; (xv) $x-\frac{1}{2}, \frac{1}{2}+y, z$; (xvi) $\frac{1}{2}-x, \frac{3}{2}-y, 1-z$; (xvii) $x, 2-y, z-\frac{1}{2}$.

**Table 4**
Structural and optical parameters for KREW (RE = Gd, Yb and Lu).

| | KGdW | KYbW | KLuW |
|---|---|---|---|
| IR (RE) (Å) | 1.053 | 0.985 | 0.977 |
| $a$ (Å) | 10.652 (4) | 10.590 (4) | 10.576 (7) |
| $b$ (Å) | 10.374 (6) | 10.290 (6) | 10.214 (7) |
| $c$ (Å) | 7.582 (2) | 7.478 (2) | 7.487 (2) |
| $\beta$ (°) | 130.80 (2) | 130.70 (2) | 130.68 (4) |
| $V$ (Å$^3$) | 634.2 (5) | 617.8 (5) | 613.3 (6) |
| $\Delta_{W-O}$ ($n$ = 6) | 12.4 (7) | 10.7 (4) | 8.8 (4) |
| $\Delta_{RE-O}$ ($n$ = 8) | 1.8 (5) | 3.8 (4) | 4.3 (5) |
| $\Delta_{K-O}$ ($n$ = 12) | 1.8 (1) | 3.0 (1) | 2.3 (1) |
| $H_V$ (100) | – | – | 440 |
| $H_V$ (010) | – | – | 410 |
| $H_V$ (001) | – | – | 560 |
| Hardness (Moh's scale) | 4.5–5 | – | 4–5.5 |
| $\alpha'_{11}$ | 10.64 | 8.72 | 8.98 |
| $\alpha'_{22}$ | 2.83 | 2.57 | 3.35 |
| $\alpha'_{33}$ | 23.44 | 16.68 | 16.72 |
| $\alpha'_{33}/\alpha'_{11}$ | 2.21 | 1.91 | 1.86 |
| $\kappa$ | 21.5 (5) | 19 (5) | 18.5 (5) |
| $2V_g$ ($\lambda$ – 1064 nm, RT) | 94.57 | 88.14 | 82.03 |
| $\sigma_{OA}$ (cm$^2$) for $E\|\|N_m$ at 981.1 nm | $1.2 \times 10^{-19}$† | $1.17 \times 10^{-19}$‡ | $1.18 \times 10^{-19}$ |
| $\sigma_{OE}$ (cm$^2$) for $E\|\|N_m$ at 981.1 nm | $1.46 \times 10^{-19}$† | $1.47 \times 10^{-19}$ | $1.47 \times 10^{-19}$ |

† Brenier & Boulon (2001), Bourdet (2001). ‡ Pujol, Bursukova *et al.* (2001).

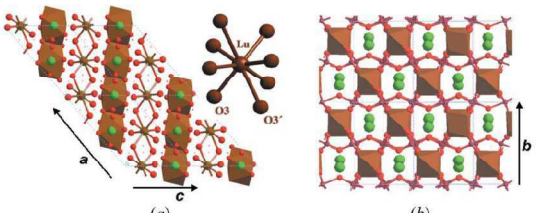


**Figure 1**
Projections of the crystalline structure of $KLu(WO_4)_2$. (*a*) Parallel to the **b** direction; the chain formed by lutetium polyhedra is along the [101] direction. Inset: the coordination figure of the lutetium ion. (*b*) Parallel to the [101] direction; the lutetium zigzag chain polyhedra are perpendicular to the observer.

The lutetium is eightfold coordinated by oxygen atoms to form a distorted square antiprism. These polyhedra form a single chain in the [101] direction by sharing the O3—O3$^{xvii}$ edges [3.081 (11) Å; symmetry code: (xviii) $\frac{1}{2}-x, \frac{1}{2}-y, 2-z$]. This shared edge, O3—O3$^{xviii}$ [3.081 (11) Å], increases in length along the KREW series RE = Gd, Yb and Lu (Pujol, Solé *et al.*, 2001; Pujol *et al.*, 2002) (see Fig. 1*a*). This is because the positive charge in the nucleus of the lanthanide element increases, so there is a corresponding increase in the strength of one of the Lu—O bonds, Lu—O3$^{v}$ [2.299 (7) Å; symmetry code: (v) $x-\frac{1}{2}, \frac{1}{2}+y, z-1$], which means that one oxygen from this edge is getting closer to a lutetium anion. As a consequence of this elongation in the shared edge O3—O3$^{xviii}$, the distortion of the coordination figure in the KREW increases. Table 4 summarizes these values.

The values of the Lu—Lu distances should also be mentioned, because of their importance in further substitutions by active lanthanide ions and energy-transfer phenomena between lanthanide ions (Kushida, 1973; Inokuti & Hirayama, 1965; Huber *et al.*, 1977). Each $LuO_8$ chain is parallel to the [101] direction and forms a zigzag, where the Lu—Lu$^{xvi}$ distances within a chain are 4.045 (3) Å [symmetry code: (xvi) $\frac{1}{2}-x, \frac{3}{2}-y, 1-z$]. Furthermore, each lutetium polyhedra chain is surrounded by four other equivalent chains (Fig. 1*b*) at Lu—Lu$^{vi}$ distances of 5.982 (3) Å [symmetry code: (vi) $x, 1-y, z-\frac{1}{2}$] and Lu—Lu$^{xvii}$ distances of 6.693 (3) Å [symmetry code: (xvii) $x, 2-y, z-\frac{1}{2}$].

This environment is similar to the other KREW compounds, with corresponding distances of 4.070 (2), 6.057 (2) and 6.804 (2) Å in KGdW, and 4.049 (2), 6.009 (2) and 6.721 (2) Å in KYbW.

### 2.1. Effects of doping: unit-cell parameter changes with ytterbium doping

The change in the unit-cell parameters can be measured to predict the structural changes related to doping. The unit-cell parameters of Yb:KLuW were obtained by X-ray powder diffraction analysis, using a Siemens D-5000 diffractometer (Bragg–Brentano parafocusing geometry and vertical $\theta$–$\theta$ goniometer). The X-ray powder diffraction patterns were recorded at $2\theta$ = 10–70°, step size = 0.02°, step time = 16 s. The samples were obtained with [$Yb^{3+}$] concentrations of 10, 20 and 50 (% solute in moles). The real composition in the crystal was calculated taking into account the distribution coefficient of ytterbium in KLuW from our growth experiences, which was obtained by electron microprobe analysis, as we shall describe below. As expected, the structure remains monoclinic in all cases [the isostructural material KYbW with 100 mol% ytterbium is also monoclinic (Pujol *et al.*, 2002)]. In order to obtain the cell parameters, the X-ray patterns were fitted using

the *FullProf* program (Rodriguez-Carvajal, 2000) and the structural model obtained for KLuW was fitted by single-crystal diffraction. Fig. 2 shows how the unit-cell parameters of KLuW increase with the ytterbium doping. The unit-cell parameters $a$, $b$ and $c$ increase and $\beta$ remains basically constant when ytterbium concentrations increase. This increase is expected because the ionic radius of ytterbium (0.985 Å) increases in relation to that of lutetium (0.977 Å) (Shannon, 1976).

## 3. Crystal growth of KLuW and Yb:KLuW

We synthesized undoped KLuW and Yb-doped KLuW bulk single crystals at several dopant concentrations by means of the top-seeded solution growth (TSSG) slow-cooling method as described by Solé *et al.* (1996), with a composition of 12/88 mol% solute/solvent ($K_2W_2O_7$). The dopant concentration ranged from 0.5 mol% to 25 mol% in solution. The temperature gradient in the solution was 0.1 K mm$^{-1}$ and the saturation temperature was between 1146 and 1162 K. The crystals grew by a seed parallel to the **b** crystallographic direction, with no inclusions or macroscopic defects. A cooling interval of 20 K with a cooling rate of 0.1–0.3 K h$^{-1}$ was used. Inclusion-free crystals of around 4 g and dimensions of 11 × 7 × 13 mm along the **a*** × **b** × **c** crystallographic directions were obtained in these conditions.

By way of example, Fig. 3 shows a photograph and a morphological scheme of a KLuW single crystal. The morphology obtained is basically similar to that of the other KREW tungstates, which we obtained with a similar methodology (Solé *et al.*, 1996; Pujol, Solé *et al.*, 2001; Pujol *et al.*, 2002). The present faces are: {110}, {$\bar{1}$11}, {010} and {310}. It is worth pointing out how important the external appearance of face (010) is in these KREW materials for their laser applications, and also as a structural reference so that samples can be prepared for further optical applications.

It has been observed that when similar growth methodologies are used, the area of face (010) tends to decreases along the series KREW (RE = Gd, Yb and Lu). This means that the rate of growth of this face increases along the series.

**Table 5**
Summary of the EPMA results of the analysis of $Yb^{3+}$:KLuW.

| | $K_{Yb^{3+}}$ | $[Yb^{3+}]$ (cm$^{-3}$) | Stoichiometric formula |
|---|---|---|---|
| 0.5% | 1.39 | $4.52 \times 10^{19}$ | $KLu_{0.993}Yb_{0.007}(WO_4)_2$ |
| 3% | 1.45 | $2.83 \times 10^{20}$ | $KLu_{0.986}Yb_{0.043}(WO_4)_2$ |
| 5% | 1.37 | $4.30 \times 10^{20}$ | $KLu_{0.931}Yb_{0.069}(WO_4)_2$ |
| 10% | 1.30 | $8.26 \times 10^{20}$ | $KLu_{0.870}Yb_{0.130}(WO_4)_2$ |
| 25% | 1.24 | $2.02 \times 10^{21}$ | $KLu_{0.690}Yb_{0.310}(WO_4)_2$ |
| 50% | 1.22 | $3.99 \times 10^{21}$ | $KLu_{0.390}Yb_{0.610}(WO_4)_2$ |

Electron probe microanalysis (EPMA) was used to determine the concentration of $Yb^{3+}$ in the crystals. The line $M\alpha$, the detector crystal TAP and a homemade KYbW standard were used to minimize the error caused by the different compositions of the sample and standard. The distribution coefficient of the doping element, $K_{Yb^{3+}}$, was calculated by

$$K_{Yb^{3+}} = \frac{[\text{moles } Yb^{3+}/(\text{moles } Yb^{3+} + \text{moles } Lu^{3+})]_{\text{crystal}}}{[\text{moles } Yb^{3+}/(\text{moles } Yb^{3+} + \text{moles } Lu^{3+})]_{\text{solution}}}$$

for the composition 12 mol% Yb:KLuW/88 mol% $K_2W_2O_7$. The results, presented in Table 5, show a very high distribution coefficient of $Yb^{3+}$ inside the host, which suggests the feasibility of doping this compound with ytterbium. However, values larger than 1 may create a gradient of ytterbium distribution inside the crystal during the growth process. For further industrial crystal growth of large single crystals of Yb:KLuW, this handicap can be overcome by using an ytterbium feeder in the solution during the crystal growth.

## 4. Microhardness measurements

For solid-state laser (SSL) and optical applications in general, samples must be previously cut and polished if results are to be good. The quality of the polishing of a given sample is directly related to the mechanical properties of the material, and significantly high hardness values can assure a better polish and quality of the laser surfaces.

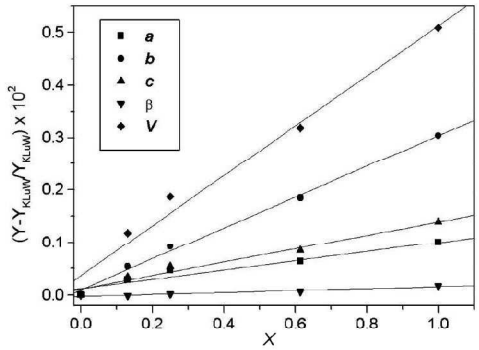


**Figure 2**
Change in cell parameters (%) of KLuW when the level of substitution of lutetium by ytterbium is increased in the crystal.

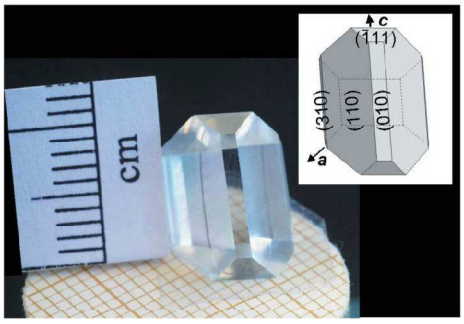


**Figure 3**
Monoclinic KLuW crystal grown in the **b** direction. Inset: morphological scheme.

Vickers microhardness measurements were made on three different faces of the KLuW single crystals. The measured faces were cut perpendicular to the three crystallographic directions **a***, **b** and **c**, respectively. The indenter used was a Vickers diamond square based pyramid (Vander Voort, 1989). The strengths used were 0.03 N, 0.05 N and 0.1 N. For each load, different indentations were made and the average diagonal imprints were used for the calculation. Scanning electron microscope (Jeol JSM 6400 equipment) images were used to quantify the diagonal imprint of the residual indentation impression.

The measured microhardness values, $H_V$, were 440, 410 and 560 (see Table 4) on the planes perpendicular to **a***, **b** and **c**, respectively. It is important to point out the expected anisotropy in the different crystallographic directions of our materials. Furthermore, the Vickers value ($H_V$) of the (010) face is 410, which is around 4 on Moh's scale. This means that the polishing procedure on face (010) would not be any better than on any other faces of our crystal.

**Table 6**
Evolution of the unit-cell parameters of KLuW at different temperatures.

| Temperature (K) | $a$ (Å) | $b$ (Å) | $c$ (Å) | $\beta$ (°) | $V$ (Å$^3$) |
|---|---|---|---|---|---|
| 298 | 10.5898 (5) | 10.2362(5) | 7.4962 (3) | 130.7445 (2) | 615.64 (5) |
| 323 | 10.5945 (4) | 10.2375 (3) | 7.5004 (2) | 130.7487 (2) | 616.29 (4) |
| 373 | 10.6000 (4) | 10.2406 (4) | 7.5059 (3) | 130.7508 (2) | 617.23 (5) |
| 473 | 10.6114 (4) | 10.2425 (4) | 7.5176 (3) | 130.7587 (3) | 618.91 (4) |
| 573 | 10.6214 (5) | 10.2470 (5) | 7.5298 (3) | 130.7624 (3) | 620.73 (5) |
| 673 | 10.6332 (5) | 10.2502 (4) | 7.5424 (3) | 130.7760 (3) | 622.52 (5) |
| 773 | 10.6441 (6) | 10.2525 (5) | 7.5556 (4) | 130.7835 (4) | 624.32 (6) |

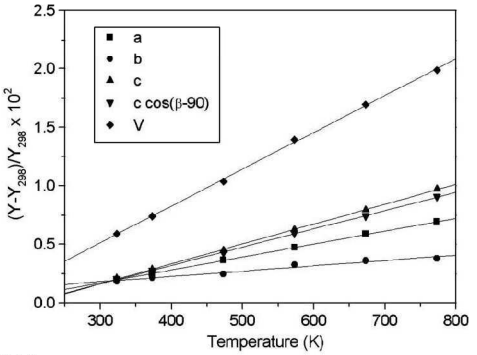


**Figure 4**
Relative thermal evolution of the cell parameters and the unit-cell volume for monoclinic KLuW.

## 5. Thermal expansion tensor

The pumping process in the laser cavity generates heat in the laser system. In spite of the cooling or refrigeration system, there will be energy losses, which transform into heat. The thermal stability of the geometry of the sample in the laser device can be improved or predicted, if the anisotropic linear thermal expansion of the laser material KREW is known. KREW materials also present anisotropy in thermal properties. A good laser cavity design must take into account this anisotropy at temperatures higher than room temperature. For these reasons, and also because linear thermal expansion is related to the thermo-optical coefficients (Biswal *et al.*, 2004), which need to be known for laser materials, the determination of the linear thermal expansion tensor is important.

As before, the unit-cell parameters of KLuW were measured as a function of temperature by X-ray powder diffraction analysis, and using a Siemens D-5000 diffractometer (Bragg–Brentano parafocusing geometry and vertical $\theta$–$\theta$ goniometer) equipped with a high-temperature chamber (Anton-Paar HTK10). The X-ray powder diffraction patterns were recorded at $2\theta$ = 10–70°, step size = 0.03°, step time = 5 s, at temperatures of 298, 323, 373, 473, 573, 673 and 773 K. The samples were placed on a platinum support. The range of temperatures chosen was large enough for the behaviour of the unit-cell parameters to be described under the conditions to which the crystal is submitted during the pumping process.

In order to obtain the cell parameters, the X-ray patterns were fitted using the *FullProf* program and the structural model was obtained for KLuW by single-crystal diffraction. Table 6 summarizes the evolution of the KLuW unit-cell parameters at different temperatures. The unit-cell parameters $a$, $b$ and $c$ increase and $\beta$ remains basically constant when the temperature rises.

The values of the linear thermal expansion coefficients are the slopes of the linear relationship between $(\Delta L/L)$ and temperature in the different crystallographic directions (Chung *et al.*, 1993). The values for the monoclinic KLuW are $\alpha_{100} = 10.6\ (2) \times 10^{-6}$, $\alpha_{010} = 3.35\ (2) \times 10^{-6}$, $\alpha_{001} = 16.3\ (2) \times 10^{-6}$, $\alpha_{c^*} = 15.1\ (1) \times 10^{-6}$, $\alpha_V = 29.2\ (3) \times 10^{-6}\ \mathrm{K}^{-1}$; see Fig. 4. From these results and the expression $\alpha_n = n_i n_j \alpha_{ij}$, where $n = (n_1, n_2, n_3)$, we obtain $\alpha_{13}$, and, in this way, the linear thermal expansion tensor at 298 K in the crystallophysical system $X_1 \| \mathbf{a}$, $X_2 \| \mathbf{b}$, $X_3 \| \mathbf{c}^*$ is

$$\alpha_{ij} = \begin{pmatrix} 10.6 & 0 & -3.15 \\ 0 & 3.35 & 0 \\ -3.15 & 0 & 15.1 \end{pmatrix} \times 10^{-6}\ \mathrm{K}^{-1}.$$

The linear thermal expansion tensor in the principal system $X_1'$, $X_2' \| \mathbf{b}$, $X_3'$ can be obtained by diagonalizing the above tensor. In monoclinic crystals with $\beta > 90°$, the $b$ principal axis always coincides with the 2 symmetry axis. In the present study, this axis corresponds to the minimum thermal expansion coefficient, $X_2'$. Therefore, the diagonalized linear thermal expansion tensor has the following values:

$$\alpha'_{ij} = \begin{pmatrix} 8.98 & 0 & 0 \\ 0 & 3.35 & 0 \\ 0 & 0 & 16.72 \end{pmatrix} \times 10^{-6}\ \mathrm{K}^{-1}.$$

The principal axis with medium thermal expansion, $X_1'$, was found at $\rho = 27.24°$ rotating clockwise from the $a$ axis with the $b$ positive axis pointing towards us. Finally, the principal axis with the maximum thermal expansion coefficient, $X_3'$, was found at $\delta = 13.51°$, with $\delta = (\beta - 90°) - \rho$ rotating anticlockwise from the $c$ axis. The thermal expansion ellipsoid with the values of these angles can be seen in Fig. 5.

The angle between $X_3'$ and $c$ of KLuW is similar to that of KREW tungstates (RE = Gd, Y, Er and Yb) (Pujol, Solé *et al.*, 2001). On the other hand, if we observe the linear thermal expansion anisotropy on face (010) (using the ratio $\alpha_{33}'/\alpha_{11}'$ to determine this anisotropy), we observe that it decreases along the KREW series. Thus, KLuW is the host in the KREW series that has the lowest thermal anisotropy in the (010) plane. This means that it has the least probability of cracking for thermal reasons during the lasing process.

## 6. Refractive index tensor

The monoclinic phase of KLuW belongs to the 2/*m* crystallographic point group and is therefore a biaxial crystal with inversion centre. The $N_p$ orthogonal principal crystallo-optic axis is parallel to the $2(C_2)$ symmetry axes. The other two principal axes are in the *ac* plane. The orientation of the principal axes $N_m$, $N_g$ to the $c$ axis was determined at $\lambda = 632.8$ nm by using two crossed Glan–Taylor polarizers. The principal axis $N_g$ is located at $\kappa = 18.5°$ clockwise to the $c$ crystallographic axis when the positive $b$ axis is pointing towards the observer. $N_m$ is rotated at 59.7° with respect to the $a$ crystallographic axis in the clockwise direction. Fig. 6 shows the optical ellipsoid of KLuW. We used the minimum-deviation method with a semiprism (see Solé *et al.*, 2001) to determine the dispersion of the three refractive indices labelled $n_g$, $n_m$ and $n_p$ in relation to the wavelength in the range 410–1200 nm at room temperature. Two prisms cut in different principal planes were used. One of the prisms provided $n_p$ and $n_m$, and the other $n_p$ and $n_g$ with an accuracy of $5 \times 10^{-4}$. Fig. 7 shows the experimental values of refractive indices and the fitted curve using the Sellmeier equation

$$n^2 = A + \frac{B}{1 - (C/\lambda)^2} - D\lambda^2.$$

Table 7 summarizes the Sellmeier coefficients, which characterize KLuW in the visible and near-IR spectral regions. Using these measurements, it is possible to localize the two optic axes. The optic axes are located in the $N_pN_g$ plane, at an angle of $V_g$ to the $N_g$ axis:

$$\sin V_g = \frac{n_g}{n_m}\left(\frac{n_m^2 - n_p^2}{n_g^2 - n_p^2}\right)^{1/2}.$$

For KLuW, at 1064 nm, the $V_g$ angle is 41.016°, which means that the angle between the two optic axes is 82.03°. Therefore, KLuW is an optically positive biaxial crystal ($V_g < 45°$).

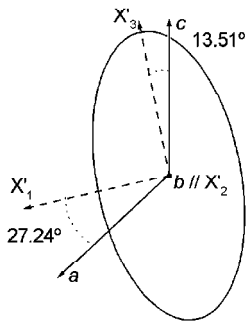


**Figure 5**
Thermal expansion ellipsoid of KLuW.

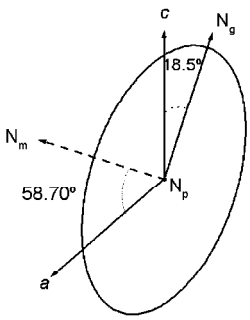


**Figure 6**
Optical ellipsoid of KLuW at room temperature.

**Table 7**
Room-temperature Sellmeier coefficients of KLuW.

| Principal refractive index | $A$ | $B$ | $C$ (μm) | $D$ (μm$^{-2}$) |
|---|---|---|---|---|
| $n_g$ | 3.58334 | 0.73512 | 0.26700 | 0.02953 |
| $n_m$ | 3.36989 | 0.74309 | 0.26193 | 0.04331 |
| $n_p$ | 3.21749 | 0.75382 | 0.25066 | 0.05076 |

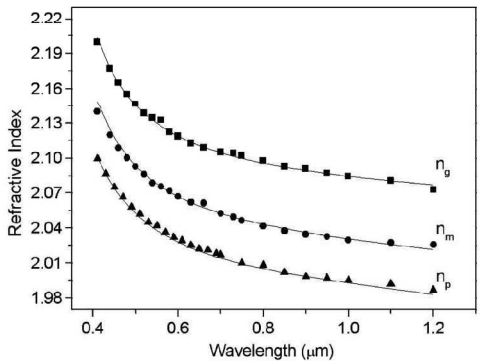


**Figure 7**
Dispersion of the principal refractive indices of KLuW at room temperature.

This work was supported by EU project DT-CRYS, NMP3-CT-2003-505580, by CICyT (Comisión Interministerial de Ciencia y Tecnologia of the Spanish Government) under the MAT-2002-04603-C05-03 and MAT-2005-06354-C03-02 projects, and by the Generalitat de Catalunya under the projects 2001SGR317 and 2005SGR658.

## References

Biswal, S. P., O'Connor, S. & Bowman, S. R. (2004). *CLEO/QELS 2004, Conference on Lasers & Electro-Optics CLEO'04*, San Francisco (CA), USA, May 16–21, 2004, paper CThT62, Technical Digest CD-ROM.

Borowiec, M. T., Majchrowski, A., Domuchowski, V., Dyakonov, V. P., Michalski, E., Zayarniuk, T., Zmija, J. & Szymczak, H. (2003). *Proc. SPIE*, **5136**, 20–25.

Borowiec, M. T., Watterich, A., Zayarnyuk, T., Dyakonov, V. P., Majchrowski, A., Zmija, J., Baranski, M. & Szymczak, H. (2003). *J. Appl. Spectrosc. (Zh. Prikladnoi Spektroskopii, Belarus)*, **70**, 7.

Boulon, G. (2003). *Opt. Mater.* **22**, 85–87.

Bourdet, G. L. (2001). *Opt. Commun.* **200**, 331–342.

Brenier, A. (2001). *J. Lumin.* **92**, 199–204.

Brenier, A. & Boulon, G. (2001). *J. Alloy. Compd.* **323–324**, 210–213.

Carvajal, J. J., García-Muñoz, J. L., Solé, R., Gavaldà, Jna., Massons, J., Solans, X., Díaz, F. & Aguiló, M. (2003). *Chem. Mater.* **15**, 2338–2345.

Chung, D. D. L., DeHaven, P. W. & Arnold, H. (1993). *X-ray Diffraction at Elevated Temperatures. A Method for in situ Process Analysis*. New York: Debashis Ghosh VCH.

Deloach, L. D., Payne, S. A., Chase, L. L., Smith, L. K., Kway, W. L.  Krupke, W. F. (1993). *IEEE J. Quantum Electron.* **29**, 1179–1191.

Grabtchikov, A. S. (2000). *J. Alloy Compd.* **300–301**, 300–302.

Griebner, U., Liu, J., Rivier, S., Aznar, A., Grunwald, R., Solé, R., Aguiló, M., Díaz, F. & Petrov, V. (2005). *IEEE J. Quantum Electron.* **41**, 408–414.

Griebner, U., Rivier, S., Petrov, V., Zorn, M., Erbert, G., Weyers, M., Mateos, X., Aguiló, M., Massons, J. & Díaz, F. (2005). *Optics Express*, **13**, 3465–3470.

Huber, D. L., Hamilton, D. S. & Barnett, B. (1977). *Phys. Rev. B*, **16**, 4642–4650.

Inokuti, M. & Hirayama, F. (1965). *J. Chem. Phys.* **43**, 1978–1989.

Kaminskii, A. A. (1996). *Crystalline Lasers: Physical Processes and Operating Schemes*. New York: CRC Press.

Kaminskii, A. A., Gruber, J. B., Bagaev, S. N., Ueda, K., Hömmerich, U., Seo, J. T., Temple, D., Zandi, B., Kornienko, A. A., Dunina, E. B., Pavlyuk, A. A., Klevtosva, R. F. & Kuznetsov, F. A. (2002). *Phys. Rev. B*, **65**, 125108(1–29).

Kaminskii, A. A., Ueda, K., Eichler, H. E., Findeisen, J., Bagayev, S. N., Kuznetsov, F., Pavlyuk, A. A., Boulon, G. & Bourgeois, F. (1998). *Jpn J. Appl. Phys.* **37**, L923–L926.

Klevtsov, P. V. & Kozeva, L. P. (1969). *Sov. Phys.* **14**, 185–187.

Klevtsov, P. V., Kozeeva, L. P. & Kharchenko, Yu. L. (1975). *Sov. Phys Crystallogr.* **20**, 732–735.

Klevtsov, P. V., Kozeeva, L. P. & Kletsova, R. F. (1968). *Izv. Akad. SSSR Ser. Neorg. Mater.* **4**, 1147–1151.

Klevtsov, P. V., Kozeeva, L. P., Kharchenko, Yu. L. & Pavlyuk, A. A. (1974). *Sov. Phys. Crystallogr.* **19**, 342–347.

Krueger, A. & Féru, P. (2004). *Photonics Spectra*, http://www.photonics.com.

Krupke, W. F. (2000). *IEEE J. Sel. Top. Quantum Electron.* **6**, 1287–1296.

Kushida, T. (1973). *J. Phys. Soc. Jpn*, **34**, 1318–1325.

Mateos, X., Petrov, V., Aguiló, M., Solé, R. M., Gavaldà, J., Massons, J., Díaz, F. & Griebner, U. (2004). *IEEE J. Quantum Electron.* **40**, 1056–1059.

Narkhova, G. I. & Ustimenko, N. S. (1998). *Quantum Electron.* **28**, 804–805.

Pujol, M. C., Bursukova, M. A., Güell, F., Mateos, X., Solé, R., Gavaldà, Jna., Aguiló, M., Massons, J., Díaz, F., Klopp, P., Griebner, U. & Petrov, V. (2001). *Phys. Rev. B*, **65**, 165121(1–11).

Pujol, M. C., Solé, R., Massons, J., Gavaldà, Jna., Solans, X., Díaz, F. & Aguiló, M. (2002). *J. Appl. Cryst.* **35**, 108–112.

Pujol, M. C., Solé, R., Massons, J., Gavaldà, Jna., Solans, X., Zaldo, C., Díaz, F. & Aguiló, M. (2001). *J. Appl. Cryst.* **34**, 1–6.

Rivier, S., Mateos, X, Petrov, V., Griebner, U., Aznar, A., Silvestre, O., Solé, R., Aguiló, M., Díaz, F., Zorn, M. & Weyers, M. (2005). *Opt. Express Lett.* **30**, 2484–2486.

Rodriguez-Carvajal, J. (2000). *Reference Guide for the Computer Program FullProf*. Laboratorie León Brillouin, CEA-CNRS, Saclay, France.

Shannon, R. D. (1976). *Acta Cryst.* A**32**, 751–767.

Sheldrick, G. M. (1997). *SHELXS97* and *SHELXL97*. University of Göttingen, Germany.

Solé, R., Nikolov, V., Ruiz, X., Gavaldà, Jna., Solans, X., Aguiló, M. & Díaz, F. (1996). *J. Cryst. Growth*, **169**, 600–603.

Solé, R., Nikolov, V., Vilalta, A., Carvajal, J. J., Massons, J., Gavaldà, Jna., Aguiló, M. & Díaz, F. (2001). *J. Mater. Res.* **17**, 563–569.

Stewen, C., Contag, K., Larinov, M., Giesen, A. & Hügel, H. (2005) *IEEE J. Select Top. Quantum Electron.* **6**, 650–657.

Ustimenko, N. S. & Gulin, A. V. (1998). *Instrum. Exp. Tech.* **41**, 386–387.

Ustimenko, N. S. & Gulin, A. V. (2002). *Quantum Electron.* **32**, 229–231.

Vander Voort, G. F. (1989). *Factors that Affect the Precision of Mechanical Tests*, ASTM STP 1025, pp. 3–39. Philadelphia: ASTM.

Yudanova, L. I., Potapova, O. G. & Pavlyuk, A. A. (1986). *Izv. Akad. Nauk SSSR Neorg. Mater.* **23**, 1884–1887.

Zou, X. & Toratani, H. (1995). *Phys. Rev. B*, **52**, 15889–15897.

CRYSTAL GROWTH & DESIGN
XXXX
VOL. 0, NO. 0
1–7

# Liquid-Phase Epitaxy Crystal Growth of Monoclinic $KLu_{1-x}Yb_x(WO_4)_2/KLu(WO_4)_2$ Layers

A. Aznar, O. Silvestre, M. C. Pujol, R. Solé, M. Aguiló, and F. Díaz*

*Física i Cristal·lografia de Materials (FiCMA), Universitat Rovira i Virgili, Campus Sescelades, 43007, Tarragona, Spain*

*Received January 18, 2006; Revised Manuscript Received May 22, 2006*

**ABSTRACT:** Epitaxial layers of $KLu_{1-x}Yb_x(WO_4)_2/KLu(WO_4)_2$ with different Yb concentrations were grown by liquid-phase epitaxy. The quality of the epitaxial layers principally depends on the Yb concentration and the crystal face. In solutions with up to 50 mol % of substitution of $Lu_2O_3$ by $Yb_2O_3$, defect-free layers can be grown and the highest quality face is (010). The layers grown on the (−111) face tend to have a higher density of morphologies. The optical spectroscopy of $Yb^{3+}$ in thin layers coincides with that obtained in doped bulk crystals.

## Introduction

In recent years, the concept of thin-disk lasers has aroused considerable interest, mainly in microchip technology. The advantages of thin-disk lasers are their high optical efficiency, high beam quality, and the possibility of high power with weak thermal lensing.[1,2]

Thin-disk lasers have mainly been based on $Nd^{3+}$ or $Yb^{3+}$ ions. Among all the lanthanides, $Yb^{3+}$ has attracted most of the attention because it has several advantages. Its electronic structure is very simple: the ground level is $^2F_{7/2}$, the unique excited level is $^2F_{5/2}$, and the difference in energy is about 10 000 $cm^{-1}$.[3] The recent development of diode lasers emitting at around 1 $\mu$m makes it possible to efficiently pump $Yb^{3+}$ with low cost. These ions also have the advantage that their quantum defect for laser emission is small, heat generation in the lasing process is very weak, and there are no upconversion processes, cross-relaxations, or excited-state absorptions, which are very common in other lanthanides with several excited levels.[4]

A promising material for $Yb^{3+}$ thin-disk lasers can be obtained from liquid-phase epitaxial (LPE) growth of monoclinic $KLu_{1-x}Yb_x(WO_4)_2$ on $KLu(WO_4)_2$ substrates, because even at high doping levels the mismatch between layer and substrate is very small. This is very favorable for reducing stress at the layer/substrate interface.

In the present paper, we discuss the conditions that are suitable for the single-crystal growth of $KLu(WO_4)_2$ (hereafter KLuW) substrates and the LPE growth of $KLu_{1-x}Yb_x(WO_4)_2$ (hereafter $KLu_{1-x}Yb_xW$) on these substrates. We analyze the growth velocity and layer quality as a function of the various growth parameters.

## Experimental Section

**Substrate Crystal Growth.** KLuW has a polymorphic phase transition at a temperature of 1298 K.[5] The interesting phase for laser systems is the low-temperature phase, which crystallizes in the monoclinic system with the *C*2/*c* spatial group and the following cell parameters: $a = 10.576(7)$ Å, $b = 10.214(7)$ Å, $c = 7.487(2)$ Å, $\beta = 130.68(4)°$ and $Z = 4$.[6] Because of this phase transition, KLuW and other crystals from this family have traditionally been grown from high-temperature solutions. The solvent $K_2W_2O_7$ has several advantages over other solvents, as we discussed previously:[7] mainly the absence of foreign ions and a sufficiently low melting temperature.

The crystal growth experiments were carried out in a cylindrical vertical furnace with a Kanthal heater. The furnace temperature was regulated with a Eurotherm 903P controller/programmer connected to a thyristor.

Before the substrate crystals were grown, the solubility curve of KLuW in $K_2W_2O_7$ was investigated to obtain information about the concentration and temperature regions of the stability of the monoclinic phase and the dependence of the saturation temperature on the solution concentration. For this purpose, solutions weighing 15−25 g were prepared in conical 25 $cm^3$ platinum crucibles and the reagents were $K_2CO_3$, $WO_3$, and $Lu_2O_3$. The experimental procedure to determine the solubility curve was as follows: the solution was homogenized and then slow-cooled to obtain crystals on a platinum rod, and finally the saturation temperature of each solution was determined. The details of this procedure have been explained in a previous study.[7]

The substrates were grown in 125 $cm^3$ cylindrical platinum crucibles. The reagents were the same as for the determination of the solubility curve. The solution composition was 12 mol % KLuW−88 mol % $K_2W_2O_7$ and weighed about 200 g. The axial temperature gradient in the solution was about 1.0 K/cm, with the bottom being hotter than the surface. Two kinds of crystal growth runs were applied. In the first case, we grew three single crystals on *b*-oriented seeds perpendicular to the surface of the solution and located at about 1 cm from the center of the surface of the solution with equal distances between the seeds. These crystals were used as substrates with no additional treatment, only cleaning, so that the differences in the epitaxial crystal growth on the various crystal faces could be studied. In the second case we grew a crystal also on a *b*-oriented seed, located at the center of the surface. This crystal was grown to be cut into plates for substrates. In both cases, after the saturation temperature had been determined by repeated seeding, the temperature of the solution was slowly decreased by 5−15 K at a rate of 0.1−0.2 K/h, depending on the crystal size required. The crystals were rotated at a constant speed of 40 rpm in all the experiments. The crystals were then removed slowly from the solution and located slightly above the solution surface, and the furnace was cooled at a rate of 25 K/h.

**Liquid-Phase Epitaxial Growth.** The LPE experiments were carried out in a special vertical furnace built with a wide zone of uniform temperature so that the temperature gradient in the solution was practically zero. The crucibles used were cylindrical, 30 mm in diameter and 40 mm in height, filled with about 70 g of solution. The reagents were the same as in the above experiments, and $Yb_2O_3$ was used for substitution. The solution composition used for epitaxial growth was 5 mol % $KLu_{1-x}Yb_xW$−95 mol % $K_2W_2O_7$ and different levels of Lu substitution by Yb. After the solution had been homogenized, its saturation temperature was accurately determined with a (010)-oriented KLuW seed rotating at 40 rpm. The kinetics of the growth/dissolution processes was also studied, because it is important in deciding the experimental conditions for growing the LPE single-crystal layers.[8]

As we have mentioned above, we used two types of substrates: tabular single crystals with dimensions of about 5 mm in every direction and plates cut perpendicular to the *b* direction. The first type was used to study how the quality and thickness of the epitaxial layer depend on the crystalline face, solution composition, and experimental conditions. The second type was used to study how the time of growth, solution

* To whom correspondence should be addressed. E-mail: f.diaz@urv.net.

10.1021/cg060032j CCC: $33.50 
Published on Web 06/30/2006 

ISBN:978-84-691-1552-7 /DL:T.151-2008

**Table 1. Experiments Carried out and Growth Conditions**

| experiment | composition of Yb in solution (mol %) | type of substrate | crystalline face | $\Delta T_{growth}$ (K)[a] | growth time (h) |
|---|---|---|---|---|---|
| 1 | 5 | plate | (010) | −2 | 2.5 |
| 2 | 10 | plate | (010) | −2 | 3 |
| 3 | 10 | plate | (010) | −2 | 4.5 |
| 4 | 10 | plate | (010) | −2 | 0.5/1/1.5/2 |
| 5 | 10 | as grown | (010) (110) (310) (−111) | −2 | 2 |
| 6 | 10 | plate | (010) | −1 | 4.5 |
| 7 | 20 | plate | (010) | 2 | 3 |
| 8 | 20 | plate | (010) | −2 | 4.5 |
| 9 | 20 | plate | (010) | −6 | 3.5 |
| 10 | 20 | plate | (010) | −6 | 2/4/20 |
| 11 | 20 | plate | (010) | −6 | 1/2/3.5/10/17/20/26 |
| 12 | 20 | as grown | (010) (110) (310) (−111) | −2 | 3 |
| 13 | 50 | plate | (010) | −2 | 3.5 |
| 14 | 50 | plate | (010) | −2 | 4.5 |
| 15 | 50 | As-grown | (010) (110) (310) (−111) | −2 | 2 |
| 16 | 50 | plate | (010) | −3 | 3.5 |
| 17 | 50 | plate | (010) | −3 | 4.5 |
| 18 | 50 | plate | (010) | −6 | 3.5 |
| 19 | 50 | plate | (010) | −6 | 1/2/3/6/20 |

[a] $\Delta T_{growth}$ is the difference between the layer growth temperature and the saturation temperature.

composition, and supersaturation affect the quality and thickness of the layers growing on the (010) face.

The plate substrates were prepared by cutting slices of 1.5 mm thickness from a single crystal with a diamond saw. These slices were cut with the *b* direction perpendicular to the plate, and they were dipped in the solution with the *c* direction perpendicular to the surface of the solution. Some plates with natural and polished (010) faces were used to evaluate how cutting and polishing processes affect the growth of the layer.

Before being placed in the furnace, the substrates were carefully cleaned, in rotation, in 1/1 $HNO_3/H_2O$ (5 min), distilled water (5 min), acetone (5 min), and ethanol (5 min). Then they were slowly placed in the furnace to prevent thermal stress and heated for about 1 h above the surface of the solution. The substrate was then placed for 5 min in the solution at a temperature 1 K above the saturation temperature so that the outer part of the crystal was dissolved. The epitaxial growth was then carried out for several hours at a temperature of 1−6 K below the saturation temperature. All the experiments were made with the crystal rotating at 40 rpm. After the epitaxial growth, the crystal was removed from the flux and cooled slowly to room temperature to prevent any thermal stress, which could produce cracks.

The experiments were carried out with different solution compositions (5, 10, 20, and 50 mol % of $Yb_2O_3$ substituting $Lu_2O_3$ in the solution) and experimental growth conditions (see Table 1). In the experiments designed to study how the velocity of growth changes as a function of the distance from the interface (thickness of the layer) (experiments 4, 10, 11, and 19), the crystals were initially dipped 5−7 mm into the solution and then pulled out in steps of 1 mm for known intervals of time. In the final step, the crystals were removed totally from the solution. Experiments 5, 12, and 15 were designed to study how the crystal face affected the layer growth. The influence of supersaturation on quality and layer thickness was studied in experiments 13, 16, and 18 for 50 mol % of $Lu_2O_3$ substituted by $Yb_2O_3$ in the solution and in experiments 8 and 10 for 20 mol % of $Lu_2O_3$ substituted by $Yb_2O_3$ in the solution.

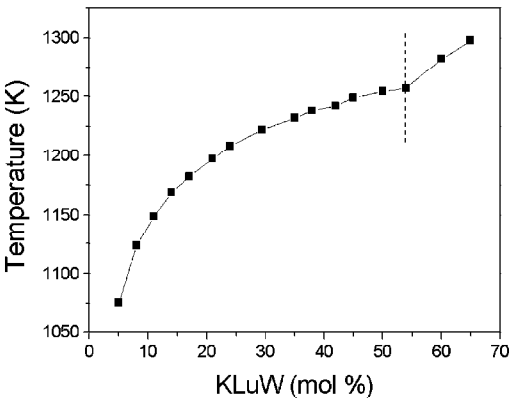


**Figure 1.** Solubility curve of KLuW in the $K_2W_2O_7$ solvent.

The composition of the crystals was measured by electron probe microanalysis with wavelength dispersive spectroscopy (EPMA-WDS) using Cameca SX 50 equipment. These measurements were also used to determine the thickness of the epitaxial layers. We detected the substrate/layer interface because the composition changes at this point.

The thicknesses of the epitaxial layers were also measured by observation with an Olympus optical microscope at magnifications of ×5, ×10, ×20, and ×50 using transmission light. In these observations the layer/substrate interface is clearly distinguishable and the layer thickness can be measured if the magnification of the microscope is known.

The epitaxial layers that were grown were observed not only by an optical microscope but also by an atomic force microscope (AFM), using a Molecular Imaging Pico Plus 2500 apparatus and a Sensofar PL$\mu$ 2300 interferometric microscope. By analyzing the AFM and interferometric images, we obtained information about the layer morphologies, spiral growths, density, and height of the growth steps in the epitaxial layers. The quality of the layers on the various crystallographic faces was also studied.

**Spectroscopic Study.** The optical $N_m$-polarized absorption at room temperature of a $KLu_{0.88}Yb_{0.12}(WO_4)_2$/KLuW epitaxial layer was measured in the 900−1050 nm range, using a Cary Variant 500 spectrophotometer, with a Glan Taylor polarizer. The fluorescence spectra were measured in 90° geometry with a laser diode, emitting at 940 nm, as an excitation source. Fluorescence was dispersed through a IIR 460 Jovin Yvon-Spex monochromator and detected by a cooled Hamamatsu R5509-72 NIR equipment. We analyzed the luminiscence signal using an EG&G 7265DPS lock-in amplifier. The sample was pumped along the *c* crystallographic axis, and the emitted light was collected parallel to the *b* direction.

## Results and Discussion

**Substrate Crystal Growth.** Figure 1 shows the solubility curve of KLuW in the $K_2W_2O_7$ solvent, which is of particular interest for the next growth experiments. In the low-concentration region, the saturation temperature increases considerably as the solute concentration increases and then increases more slightly. At approximately 55 mol % of solute, the high-temperature phase of $KLu(WO_4)_2$ begins to appear. The average degree of supersaturation for solute concentrations between 5 and 20 mol % is $0.16 \times 10^{-2}$ g/(K (g of solution)), while for concentrations above 20 mol % it is $0.80 \times 10^{-2}$ g/(K (g of solution)). To avoid problems in the crystal growth process, solutions with solute concentrations between 5 and 20 mol % are the most suitable.

The single crystals of KLuW grown by top-seeded solution growth were transparent, colorless, and free from inclusions and cracks. Figure 2 shows as an example an as-grown KLuW single

ISBN:978-84-691-1552-7 /DL:T.151-2008

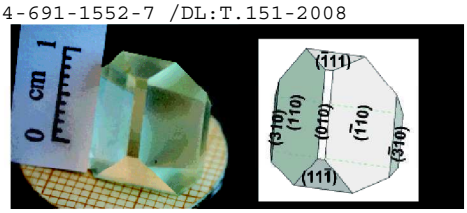


**Figure 2.** As-grown KLuW single crystal before it is cut into plates for substrates and crystal scheme carried out by the program Shape.

crystal before it is cut into plates for substrates and a crystal scheme.

**Liquid-Phase Epitaxial Growth.** Table 1 summarizes the experiments carried out with plates and as-grown crystals to study how such parameters as the crystal face, solution composition, and growth conditions influence the velocity and quality of growth.

Experiments made at different times and dissolution temperatures indicate that a time of 5 min at a temperature 1 K above saturation is enough to slightly dissolve the surface part of the substrate without introducing defects into the subsequent crystal growth.

To study the influence of the crystalline face on the velocity of growth and quality of the epitaxial layer, several experiments were made using as-grown single crystals (with different faces) as substrates. The data for these growth experiments are given in Table 1 (experiments number 5, 12, and 15). These experiments reveal that, of all the faces studied, the face with the highest velocity of epitaxial layer growth is the (010) face, independent of the level of substitution of Lu by Yb in the solution. The growth of the KLuW substrates already showed that the (010) face tended to be poorly developed, which indicates that this face also tends to grow faster than the neighboring faces. Figure 3 shows several Yb concentration

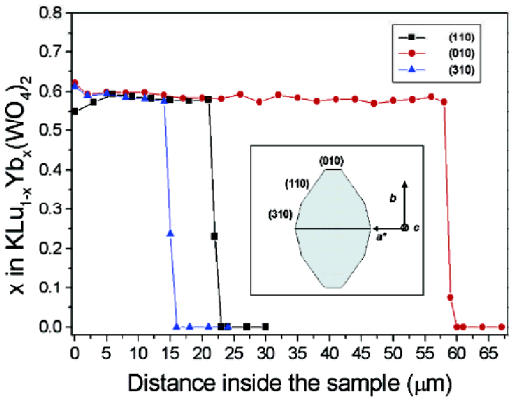


**Figure 3.** Ytterbium concentration profile for the $KLu_{0.48}Yb_{0.52}W$ layer on KLuW substrates on three different faces: (310), (110), and (010).

profiles for $KLu_{0.48}Yb_{0.52}(WO_4)_2$/KLuW (experiment 15) on three different faces of the crystal, from the outer edge of the layer to the substrate. It also shows the interface concentration gap. As can be seen in this figure, there is no appreciable diffusion of Yb from the layer to the substrate. For a fixed growth time (2 h), the layers on the (010), (110), and (310) faces have thicknesses of 59, 23, and 15 $\mu$m, respectively. This

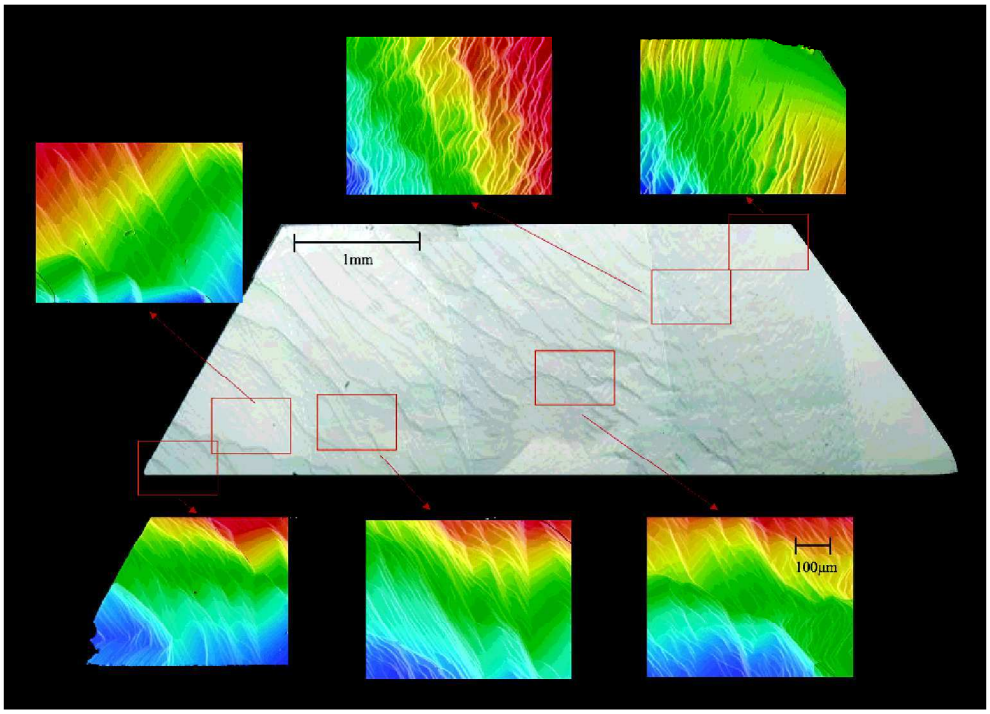


**Figure 4.** General view of the epitaxial layer grown on the (−111) crystal face and details of the micromorphologies observed by interferometry.

ISBN:978-84-691-1552-7 /DL:T.151-2008

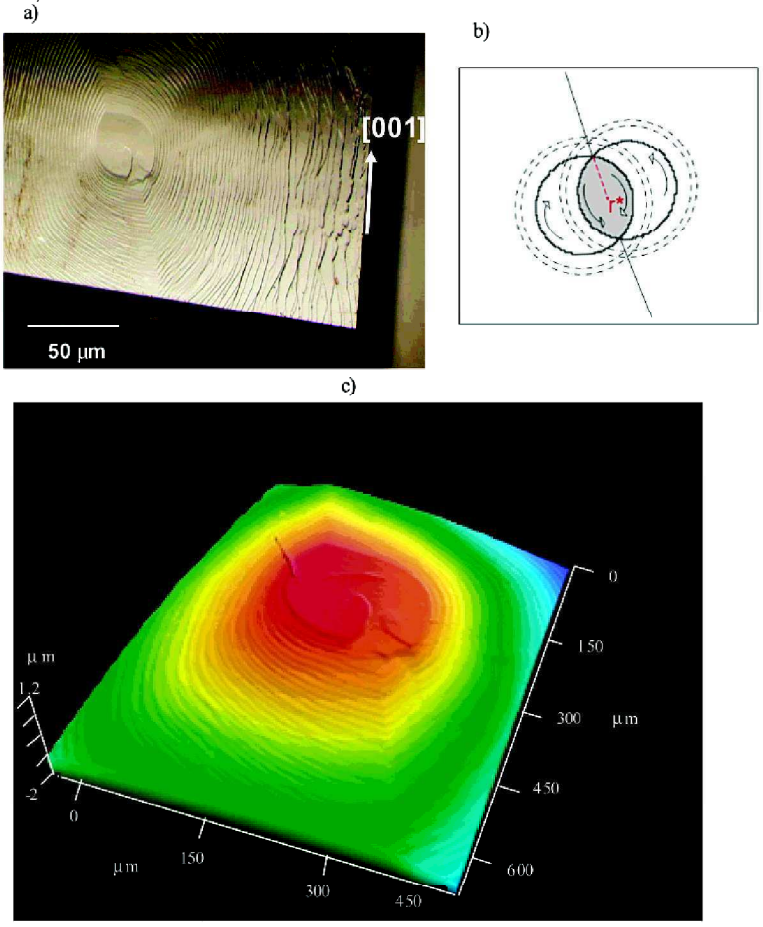


**Figure 5.** (a) Photograph of the growth of two dislocation screw spirals of opposite sign observed in a $KLu_{0.88}Yb_{0.12}(WO_4)_2$ epitaxial layer grown on a (010) face of a KLuW substrate. (b) Scheme of the origin of the screw spiral growth. (c) Interferometric microscope observation of the growth pattern.

confirms that, of all the faces studied, the (010) face is the one with the fastest growth, under the growth conditions reported.

To study the crystal quality and the micromorphologies, the grown layers were observed by optical microscopy, by atomic force microscopy (AFM), and by interferometric microscopy. The observations make it clear that the layers grown on the (−111) faces have a higher density of micromorphologies, such as growth steps, than the layers grown on the (010), (110), and (310) faces. Figure 4 shows a general view of the epitaxial layer grown on the (−111) face and details of the different surface morphologies, observed with an interferometric microscope. This epitaxial layer has a flat area on the right side of the figure. After this zone the growth fronts of the layer become unstable, and their perimeter has a scalloped shape, as can be seen in the figure. On the left, the fronts of the growth layers are grouped and have a wavy appearance. The highest quality layers are on the (010) faces, as they were for the epitaxial growth of $KY_{1-x}Yb_xW$/KYW, carried out in a previous study.

The mismatch between the substrate and the layer could be important for the quality of the layer/substrate interface. High mismatches produce stress at this interface and favor the formation of cracks that can propagate to the layer.[9] Taking into account the difference in the parameters between KLuW and $KLu_{1-x}Yb_x(WO_4)_2$ for different levels of substitution of Lu by Yb up to stoichiometric $KYb(WO_4)_2$ (KYbW),[10] we calculated the mismatch for the different faces and substitutions, using the expression

$$f_{(hkl)} = (S_{(hkl)}(\text{subst}) - S_{(hkl)}(\text{layer}))/S_{(hkl)}(\text{layer})$$

where $S_{(hkl)}$(subst) and $S_{(hkl)}$(layer) are the areas obtained from the (*hkl*) periodicity vectors of the substrate and the layer, respectively. Table 2 summarizes the mismatches obtained for the different faces and substitutions studied. From this table, we can see that the mismatches are lower on the (010) face,

**Table 2. Mismatch between KLuW Substrates and $KLu_{1-x}Yb_xW$ Layers**

| epitaxial layer | $f_{(010)}$ | $f_{(110)}$ | $f_{(310)}$ | $f_{(-111)}$ |
|---|---|---|---|---|
| $KLu_{0.88}Yb_{0.12}W$/KLuW | −0.074 | −0.081 | −0.085 | −0.089 |
| $KLu_{0.78}Yb_{0.22}W$/KLuW | −0.107 | −0.130 | −0.142 | −0.135 |
| $KLu_{0.48}Yb_{0.52}W$/KLuW | −0.143 | −0.220 | −0.259 | −0.211 |
| KYbW/KLuW | −0.215 | −0.354 | −0.425 | −0.324 |

ISBN:978-84-691-1552-7 /DL:T.151-2008

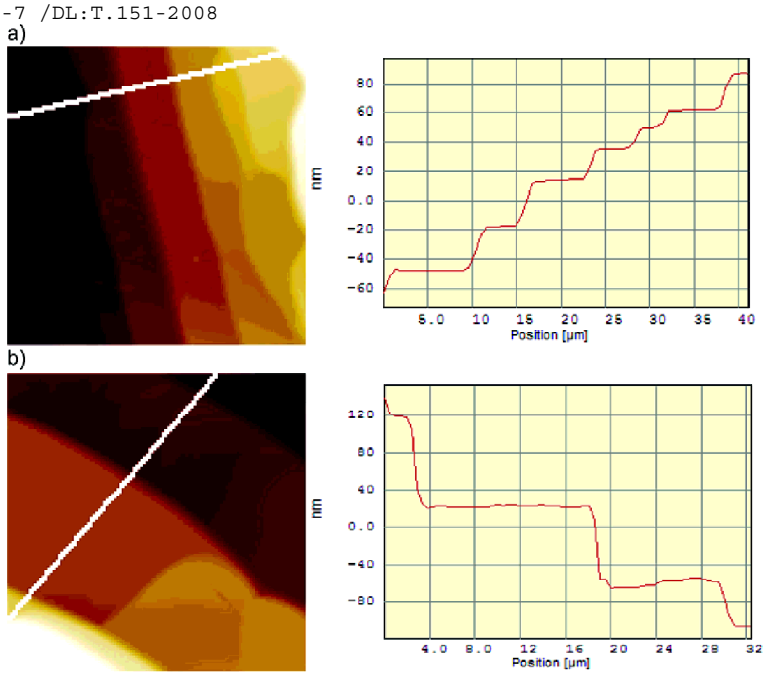


**Figure 6.** AFM images of growth steps in a $KLu_{0.88}Yb_{0.12}(WO_4)_2$ epitaxial layer on a (010)-oriented KLuW substrate and layer roughness: (a) near the central zone of the spiral growth, at about $1.5 \times r^*$, with $r^*$ being the characteristic distance of the top of the hillock of the screw spirals; (b) near the peripheral zone of a spiral growth, at approximately $8 \times r^*$.

where the layer/substrate interface has good quality, even for high substitutions. On the other hand, during the epitaxial growth of $KY_{1-x}Yb_xW/KYW$ on the same crystalline face (010), which was studied in a previous paper, some cracks tend to appear in the layer/substrate interface even at substitutions of 10 mol % of $Y_2O_3$ by $Yb_2O_3$ in solution. This difference can be explained by the fact that the mismatch between the periodicity vectors of KYbW and KYW is greater than that between KYbW and KLuW, because the ionic radii of Lu and Yb are closer than the ionic radii of Y and Yb.[6]

On the (010) faces the epitaxial growth shows mainly a flat surface, which indicates a layer-by-layer growth mechanism. On the same face, there are small areas with morphologies such as those shown in Figure 5. Figure 5a shows a photograph of growth spirals in an epitaxial layer of $KLu_{0.88}Yb_{0.12}(WO_4)_2/KLuW$ on a (010) face. A scheme of the nuclear area of the growth spirals and an observation by interferometric microscopy are shown in Figure 5b,c, respectively. These structures are formed by the superposition of two dislocation screw spirals of opposite sign, leading to a complex growth pattern of hillocks, which generates typical lines on the growth surface related to the interaction of the two opposite spirals (see Figure 5b). We have observed that, at the origin of the spirals, approximately at $1.5 \times r^*$, with $r^*$ being a characteristic distance of the top of the hillock of the screw spirals, the steps are close to one another (1−5 $\mu$m) but the further we go from the center, at $8 \times r^*$, the more the steps are separated (30−40 $\mu$m). In addition, the height of the steps at $1.5 \times r^*$ is about 20−30 nm, while in the peripheral zone, at approximately $8 \times r^*$, it is 80−100 nm, calculated by observation with AFM and interferometry. Figure 6 shows AFM images of these two zones. It also shows the roughness of this layer in these two zones.

The epitaxial layers grown on the (010) substrates showed similar characteristics, even for Yb concentrations of 50 atom % substituting Lu. It seems that there is a slight tendency for the density of steps to increase and the height of the steps also tends to increase for high Yb concentrations and growth times. For example, in a (010) epitaxial layer of $KLu_{0.48}Yb_{0.52}(WO_4)_2/KLuW$, the morphologies of the growth steps and spirals are similar to those obtained with lower substitutions, but the steps are higher, about 300−400 nm near the central zone, 500−600 nm at $1200 \times r^*$ and 700 nm at $2000 \times r^*$. The horizontal distance between growth steps increases as the distance from the center of the dislocations increases. The height of the steps also increases as the distance from the center increases. In this case, the horizontal step distances are about 10, 45−50, and 60 $\mu$m at zones near the center, at $1200 \times r^*$ and at $2000 \times r^*$, respectively.

On (010) natural faces the layer tends to grow with fewer macrosteps and other morphologies such as microsteps, hillocks, etc. and a little more slowly than on polished substrates with the same orientation. This may be due to small deviations from the (010) crystallographic direction in the process of cutting and polishing the substrate.

The thickness of the layers was also measured by observation with an optical microscope using transmission light. Figure 7 shows the thickness of the epitaxial layer of $KLu_{0.78}Yb_{0.22}(WO_4)_2$ grown on a (010)-oriented KLuW substrate as a function of the time of growth (experiment 11 in Table 1). For short growth times (about 6 h), the growth velocity is around 14.0 $\mu$m/h, while at longer times (about 22 h) it decreases to 7.1 $\mu$m/h, almost half the growth velocity at short times. Layers

ISBN:978-84-691-1552-7 /DL:T.151-2008

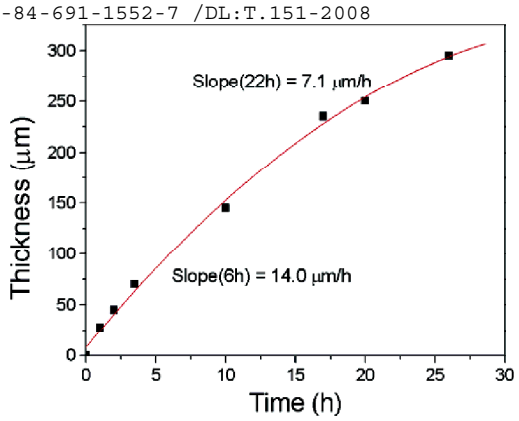


**Figure 7.** Thickness of the $KLu_{0.78}Yb_{0.22}(WO_4)_2$/KLuW epitaxial layer grown on the (010) face as a function of the growth time.

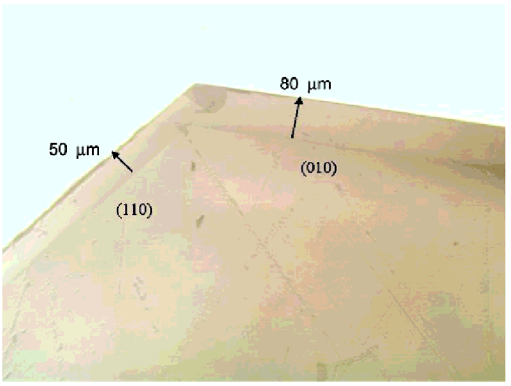


**Figure 8.** Optical microscope photograph of a section of $KLu_{0.78}Yb_{0.22}(WO_4)_2$/KLuW, perpendicular to the [001] direction.

grown with other Yb concentrations (see experiments 4 and 19) and lower supersaturations (see experiment 4) behaved in a similar way.

To determine how supersaturation affects the epitaxial growth process, experiments with different supersaturations were carried out. In the experiments in which the growth temperature of the layer was 6 K below saturation, the growth velocity increased only slightly with respect to the experiments made at 2 K below the saturation temperature. No significant differences were observed in the quality of the epitaxial layers grown on equivalent faces at 6 and 2 K below the saturation temperature.

The growth velocities obtained with an optical microscope using transmission light are similar to those obtained by EPMA. Figure 8 shows a photograph taken with this microscope of a sample of $KLu_{0.78}Yb_{0.22}(WO_4)_2$/KLuW where the layer/substrate interface is clearly observable and there is no diffusion of Yb from the layer to the substrate. The same figure indicates the thickness of the epitaxial layer.

As has been mentioned above, the change in the ytterbium concentration at the $KLu_{1-x}Yb_x(WO_4)_2$/KLuW interface was measured by EPMA. From these results, we calculated the

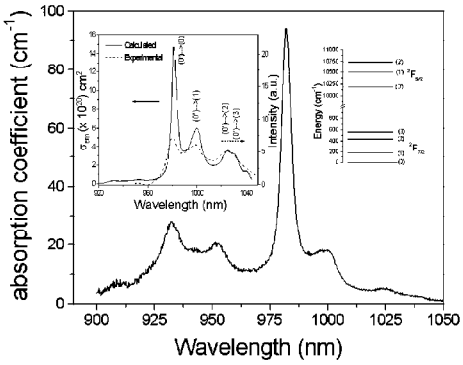


**Figure 9.** Absorption coefficient of $KLu_{0.88}Yb_{0.12}(WO_4)_2$/KLuW with $N_m$ polarization. The inset gives an emission cross section spectrum of the same sample calculated by the reciprocity method and an experimental emission spectrum.

**Table 3. Distribution Coefficient of Yb ($K_{Yb}$) and Chemical Formula of the Layer in $KLu_{1-x}Yb_xW$/KLuW, as a Function of the Yb Concentration in the Solution**

| [Yb]/([Yb] + [Lu]) in solution (atom %) | $K_{Yb}$ | chemical formula of the layer |
|---|---|---|
| 5 | 1.24 | $KLu_{0.94}Yb_{0.06}(WO_4)_2$ |
| 10 | 1.23 | $KLu_{0.88}Yb_{0.12}(WO_4)_2$ |
| 20 | 1.11 | $KLu_{0.78}Yb_{0.22}(WO_4)_2$ |
| 50 | 1.04 | $KLu_{0.48}Yb_{0.52}(WO_4)_2$ |

coefficient of distribution of Yb in the epitaxial layers, according to the formula

$$K_{Yb} = \frac{\{[Yb]/([Yb] + [Lu])\}_{crystal}}{\{[Yb]/([Yb] + [Lu])\}_{solution}}$$

where [Yb] and [Lu] are the Yb and Lu concentrations in mole percent.

Table 3 shows the distribution coefficient of Yb in the layer for different concentrations of Yb in the solution. In all cases, the distribution coefficient is slightly higher than unity and tends to decrease when the Yb concentration in the solution increases.

**Spectroscopic Study.** Figure 9 shows the polarized optical absorption, at room temperature, of a $KLu_{0.88}Yb_{0.12}(WO_4)_2$/KLuW (010)-oriented epitaxial layer. The light was polarized parallel to the principal optical direction $N_m$. In this family of materials, the optical absorption of $Yb^{3+}$ strongly depends on the light polarization, and the absorption values are highest when $E \| N_m$.[11] As can be observed from the spectrum, the $^2F_{7/2} \rightarrow {}^2F_{5/2}$ transition has three main peaks centered at 982.0, 951.8, and 932.6 nm and two less intense peaks centered at 999.5 and 1024.6 nm. The maximum absorption cross-section $\sigma_a$ at 982.0 nm, calculated with the $Yb^{3+}$ concentration of $7.83 \times 10^{20}$ ions/cm$^3$, amounts to $1.18 \times 10^{-19}$cm$^2$. These results agree well with those previously published for bulk crystals.[11]

The emission cross-section spectrum was calculated by the reciprocity method, using the absorption cross-section spectrum at room temperature and the splitting determined at low temperature in ref 11. The results are included in the inset of Figure 9 and compared with the experimental unpolarized emission spectrum obtained in the present paper. The peaks correspond to the transition from the excited $^2F_{5/2}$ level to the four sublevels of the ground state $^2F_{7/2}$. It is worth mentioning that the relative intensity of the peak (0′) → (0) shows a significant decrease in the experimental spectrum in comparison

ISBN:978-84-691-1552-7 /DL:T.151-2008

with the calculated spectrum. The experimental emission spectrum is an average of $N_g$ and $N_m$ polarized emission spectra, as a result of the aforementioned experimental configuration. There is a significant overlap between the absorption and emission spectra around 982 nm, which can produce reabsorption during lasing experiments. Thin layers make it possible to minimize this effect.[12] The maximum calculated emission cross-section is $1.48 \times 10^{-19}$ atm/cm$^2$ at 981.2 nm.

Efficient continuous-wave laser emission was achieved around 1030 nm from KLuW:Yb/KLuW samples obtained and described in the present paper. The lasing slope efficiency in the epitaxial layer exceeds that recently reported for Yb-doped bulk KLuW crystals in a similar pump and laser configuration. This is attributed to the fact that the reabsorption is considerably lower. More details of the laser operation can be found in ref 12.

## Conclusions

High-quality epitaxial layers of $KLu_{1-x}Yb_x(WO_4)_2$ have been obtained on KLuW substrates for Yb concentrations of 5, 10, 20, and 50 mol % of $Lu_2O_3$ substituted by $Yb_2O_3$ in the solution. At these levels of substitution the quality of the layers is high. Of all the faces studied, the face with the highest quality of epitaxial growth is (010), although the (110) face generally has very high quality. The layers on faces (310) and (−111) generally have a greater density of micromorphologies, such as growth steps. No diffusion of Yb from the layer to the substrate is observed. The growth rate is higher for the (010) face than for the other faces studied, and it is practically constant for short growth times (up to several hours).

**Acknowledgment.** This work was supported by the EU project DT-CRYS, NMP3-CT-2003-505580, by the Ministerio de Educación y Ciencia projects MAT2004-20471-E, MAT-2005-06354-C03-02, and CIT-020400-2005-14, and by the Generalitat de Catalunya project 2005SGR658.

## References

(1) Giesen, A.; Hügel, H.; Voss, A.; Witting, K.; Brauch, U.; Opower, H. *Appl. Phys. B* **1994**, *58*, 365.
(2) Innerhofer, E.; Südmeyer, T.; Brunner, F.; Häring, R.; Aschwanden, A.; Paschotta, R.; Hönninger, C.; Kumkar, M.; Keller, U. *Opt. Lett.* **2003**, *28*(5), 367.
(3) Zou, X.; Toratani, H. *Phys. Rev. B* **1995**, *52*, 15889.
(4) Brunner, F.; Südmeyer, T.; Innerhofer, E.; Morier-Genoud, F.; Paschotta, R.; Kisel, V. E.; Shcherbitski, V. G.; Kuleshov, N. V.; Gao, J.; Contag, K.; Giesen, A.; Keller, U. *Opt. Lett.* **2002**, *27*(13), 1162.
(5) Kletsov, P. V.; Kozeeva, L. P.; Kharchenko, L. Yu.; Pavlyuk, A. A. *Sov. Phys. Crystallogr.* **1974**, *19*(3), 342.
(6) Pujol, M. C.; Mateos, X.; Aznar, A.; Solans, X.; Suriñac, S.; Massons, J.; Díaz, F.; Aguiló, M. Submitted for publication in *J. Appl. Crystallogr*.
(7) Solé, R.; Nikolov, V.; Ruiz, X.; Gavaldà, J.; Solans, X.; Aguiló, M.; Díaz, F. *J. Cryst. Growth* **1996**, *169*, 600.
(8) Aznar, A.; Solé, R.; Aguiló, M.; Díaz, F.; Griebner, U.; Grunwald, R.; Petrov, V. *Appl. Phys. Lett.* **2004**, *85*(19), 4313.
(9) Solé, R.; Nikolov, V.; Vilalta, A.; Carvajal, J. J.; Massons, J.; Gavaldà, J.; Aguiló, M.; Díaz, F. *J. Cryst. Growth* **2002**, *237*, 602.
(10) Pujol, M. C.; Bursukova, M. A.; Güell, F.; Mateos, X.; Solé, R.; Gavaldà, J.; Aguiló, M.; Massons, J.; Díaz, F.; Klopp, P.; Griebner, U.; Petrov, V. *Phys. Rev. B* **2002**, *65*, 165121.
(11) Mateos, X.; Solé, R.; Gavaldà, J.; Aguiló, M.; Massons, J.; Díaz, F.; Petrov, V.; Griebner, U. *Opt. Mater.*, in press.
(12) Griebner, U.; Liu, J.; Rivier, S.; Aznar, A.; Grunwald, R.; Solé, R.; Aguiló, M.; Díaz, F.; Petrov, V. *IEEE J. Quantum Electron.* **2005**, *41*(3), 408.

CG060032J

UNIVERSITAT ROVIRA I VIRGILI
CRECIMIENTO Y CARACTERIZACIÓN DE CAPAS EPITAXIALES DE KRE 1-X 4BX (WO4)2 / KRE (WO4)2 (RE=Y,LU) PARA APLICACIONES LÁSER
Ana Isabel Aznar Écija

ISBN:978-84-691-1552-7 /DL:T.151-2008

Available online at www.sciencedirect.com
SCIENCE DIRECT®
ELSEVIER
Journal of Non-Crystalline Solids 352 (2006) 2367–2370
JOURNAL OF NON-CRYSTALLINE SOLIDS
www.elsevier.com/locate/jnoncrysol

# Epitaxially grown Yb:$KLu(WO_4)_2$ composites for continuous-wave and mode-locked lasers in the 1 μm spectral range

V. Petrov [a,*], S. Rivier [a], U. Griebner [a], J. Liu [a], X. Mateos [a], A. Aznar [b], R. Sole [b], M. Aguilo [b], F. Diaz [b]

[a] *Max-Born-Institute for Nonlinear Optics and Ultrafast Spectroscopy, A3 Dept., 2A Max-Born-Str., D-12489 Berlin, Germany*
[b] *Física i Cristal·lografia de Materials (FiCMA), Universitat Rovira i Virgili (URV), Campus Sescelades, C/Marcel.lí Domingo, S/N, 43007-Tarragona, Spain*

Available online 30 May 2006

**Abstract**

Epitaxial layers of up to 50% Yb-doped monoclinic $KLu(WO_4)_2$ could be successfully grown on passive $KLu(WO_4)_2$ substrates. These composite samples were characterized and continuous-wave and mode-locked laser operation was achieved with Ti:sapphire and diode-laser pumping. A 10% Yb-doped epitaxy provided an output power exceeding 500 mW at 1030 nm and a maximum slope efficiency of 66% with Ti:sapphire laser pumping. A 50% Yb-doped epitaxy exhibited serious thermal problems without special cooling and rather limited cw performance. Quasi-cw operation provided in this case an average output power of 43 mW at 1032 nm for a 10% duty cycle. More than 100 mW cw could be generated at 1030 nm also with diode-pumping of the 10% Yb-doped $KLu(WO_4)_2$ epitaxy. Pulses as short as 114 fs were generated at 1030 nm with this same sample under Ti:sapphire laser pumping in a laser mode-locked by a saturable absorber mirror.


*PACS:* 42.55.Rz; 42.55.Xi; 42.60.Fc

*Keywords:* Crystal growth; Lasers

## 1. Introduction

$Yb^{3+}$ is a very promising activating ion possessing a number of advantages over $Nd^{3+}$ for laser operation in the 1 μm spectral range [1]. These include (1) the relatively simple two-level energy scheme for which disturbing up-conversion and excited-state absorption processes are absent, (2) the lower quantum defect which means also lower thermal load and more possibilities for power scaling, (3) the longer energy storage time, and (4) the broader spectral linewidths which means on the one hand reduced requirements to the pump source and in particular the laser diodes and on the other hand higher potential to achieve tunable generation and short (femtosecond) pulses.

Concerning crystalline hosts, the monoclinic potassium double tungstates, to which the title compound $KLu(WO_4)_2$ (KLuW) belongs, have several additional advantages [2]: (1) for any rare earth dopant they allow very high doping levels to be achieved without concentration quenching because the relevant ion separation is relatively large, (2) for any rare earth ion the absorption and emission cross sections are one of the largest, partly due to the strong anisotropy, and (3) for Yb-doping the main absorption peak near 980 nm is very suitable for InGaAs pumping diodes.

In the case of KLuW specific advantages come from the smallest difference in the ionic radii of the 'passive' Lu-ion and the 'active' Yb-ion, which additionally facilitates high doping levels reaching 100% for the stoichiometric $KYb(WO_4)_2$ (KYbW) [3]. The extremely high absorption cross section peak for polarization parallel to the $N_m$ opti-

* Corresponding author. Tel.: +49 30 63921272; fax: +49 30 63921289.
*E-mail address:* petrov@mbi-berlin.de (V. Petrov).

0022-3093/$ - see front matter © 2006 Elsevier B.V. All rights reserved.
doi:10.1016/j.jnoncrysol.2006.02.077

cal axis ($1.18 \times 10^{-19}$ cm$^2$ at 981.1 nm with a FWHM $\sim$ 3.6 nm [4]) results in absorption lengths as low as 13.3 μm for the stoichiometric KYbW. Such thin layers are very interesting for implementation in high power thin-disk lasers [5] because they can ensure more efficient heat removal and greatly simplified single-pass pump geometries but since their practical realization is impossible, growing them on passive isostructural substrates seems a very promising solution. This was our main motivation for the development and laser studies of Yb-doped monoclinic epitaxies. The very initial results based on $KY(WO_4)_2$ or KYW (20% doped Yb:KYW on a KYW substrate) were published in [6]. Here we report on our most recent and superior results achieved with Yb:KLuW epitaxies both in the continuous-wave (cw) and the mode-locked regime.

## 2. Experimental

Yb-doped KLuW layers were grown on KLuW substrates by liquid phase epitaxy (LPE) with 10, 20 and 50 at.% doping in the melt. We used a vertical furnace in which the axial gradient is negligible so that the layer grows homogeneously as described in [6,7]. The 10% and 50% samples used in the present work had an Yb-ion density of $7.89 \times 10^{20}$ and $3.45 \times 20^{21}$ ions/cm$^3$, respectively, determined by electron probe microanalysis. The thickness of the activated layer was 100 and 38 μm, and the thickness of the whole sample including the substrate was 1.2 and 2.4 mm, respectively. The crystals were grown along the ***b*** crystallographic direction (parallel to the $N_p$ optical axis) because of the better crystalline quality. In such monoclinic crystals the other two principal optical axes $N_m$ and $N_g$ lie in the ***a***–***c*** plane. The samples were cut and used for propagation along the ***b*** ($N_p$) axis and polarization of the electric field parallel to the $N_m$ axis which results in maximum absorption and emission cross sections [4]. The high crystalline quality of the samples was confirmed by a ZYGO$^{TM}$ interferometer. No cracks at the interface layer-substrate were found. The epitaxial surfaces had radius of curvature RC = 0.71 and 0.42 m for the 10% and 50% Yb-doped layers, respectively. The corresponding surface roughness had a rms value of <0.8 and 0.9 nm. Fig. 1 shows the surface profile of the 50% Yb-doped KLuW epitaxy.

The Yb-fluorescence lifetime was measured for both doping levels with the pinhole method (Fig. 2) and compared to bulk Yb(10%):KLuW. This method helps to avoid reabsorption effects. The lifetime was only slightly lower for the 50% Yb-doped epitaxy (224.3 ± 2.3 μs) than for the 10% Yb-doped epitaxy (241.1 ± 25 μs) and both values were in reasonable agreement with the 254 ± 9 μs measured for the bulk sample.

For pumping we used a tunable Ti:sapphire laser (960–1025 nm, linewidth < 1 nm, max. 3 W) and a diode laser. The Gaussian beam of the Ti:sapphire laser could be used also for pumping in a second pass, after reflection at one of the cavity mirrors. The tapered diode laser delivered up to 2 W at $M^2 < 3$ for the slow axis emission. It was tunable by the temperature from 975 to 982 nm and its spectral linewidth was about 1 nm. A standard astigmatically compensated V-shaped cavity was used for the cw laser experiments and a similar Z-shaped cavity was employed for the mode-locked experiments (see Fig. 3). The pump beam was focused by means of an anti-reflection coated lens L with a focal length of 62.8 mm. The folding mirror ($M_2$, RC = −100 mm) was highly transmitting at the pump wavelength (near 980 nm). The end mirror for the cw experiments ($M_1$, RC = −50 mm), see Fig. 3(a), was highly transmitting (for single pass pumping) or highly reflecting (for double pass pumping) at the pump wavelength. The transmission of the output coupler, $M_3$, could be varied between 0.1% and 10%.

For mode-locking experiments (Fig. 3(b)), the end mirror $M_1$ was substituted by an analogous folding mirror with RC = −100 mm in the Z-shaped cavity. The intensity on the saturable absorber mirror (SAM) which terminated the resonator was increased by the additional focusing mirror $M_3$ (RC = −100 mm). The output couplers, $M_4$ (for the picosecond regime) or $M_5$ (for the femtosecond regime), terminated the second cavity arm. The dispersion compensated cavity configuration contained two Brewster angle SF10 prisms, $P_1$ and $P_2$, separated by 31 cm (Fig. 3(b)). The SAM was grown by metal organic vapor-phase epitaxy (Ferdinand-Braun-Institute, Berlin, Germany) and con-

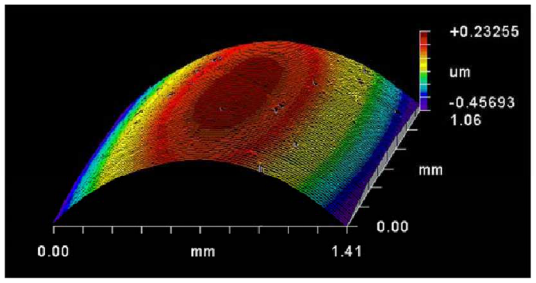


Fig. 1. Surface profile of the 50% Yb-doped KLuW composite measured with a ZYGO interferometer.

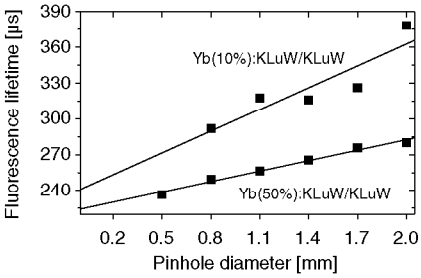


Fig. 2. Fluorescence lifetime measurement of the epitaxial Yb:KLuW/KLuW samples with different doping by the pinhole method.

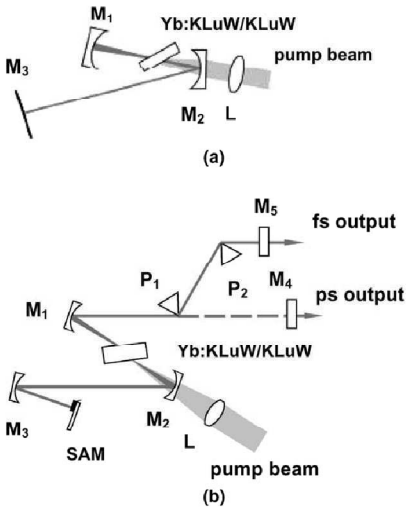


Fig. 3. Experimental set-up of the V-shaped (a) and Z-shaped (b) cavities used for cw and mode-locked operation with the intracavity prisms and SAM.

sisted of a bottom Bragg mirror comprising 25 pairs of AlAs/GaAs quarterwave layers. The reflection band extended from 980 to 1070 nm. The absorber was a 10-nm-thick InGaAs surface quantum well structure with a saturable absorption of ≈1%. Its relaxation time, measured by the pump-probe technique, amounted to less than 5 ps.

The uncoated epitaxial samples were positioned at Brewster angle and mounted on a copper base without special measures for heat removal. The estimated pump waist in the position of the samples was roughly 30 μm in the case of Ti:sapphire laser pumping and slightly larger for the diode laser.

## 3. Results and discussion

### 3.1. Continuous-wave operation

Limiting the pump power of the Ti:sapphire laser to 1.85 W (incident on the epitaxy) a maximum output power of 415 mW was achieved with single pass pumping of the 100 μm thick 10% Yb-doped epitaxy using an output coupler of 3% transmission. The resulting pump efficiency was 55% calculated with respect to the absorbed power. The maximum slope efficiency of 66% was achieved with higher output coupling (10%). Both the pump and slope efficiencies were higher in comparison to our previous results with 10% Yb-doped bulk KLuW crystals [8]. Moreover, the decreased thresholds (of the order of 70 mW absorbed power) and the shorter oscillation wavelength (decreasing from 1040 nm for 1% output coupler to 1026 nm for 10% output coupler) indicate strongly reduced reabsorption of the epitaxy in comparison to the bulk crystals. Even without cooling no damage of this epitaxial crystal occurred regardless of the high power levels (intracavity intensity exceeding 1 MW/cm$^2$) applied.

Since strong bleaching of the single pass absorption was observed we implemented also double pass pumping, exchanging mirror $M_1$ in Fig. 3(a). This really improved the overall absorption and we achieved a maximum output power of 515 mW at 1030 nm with a 3% output coupler.

Pumping with the diode laser in a single pass produced a maximum output power of 105 mW at 1030 nm for a maximum incident pump power of 1.25 W and 3% output coupler. This gives a pump efficiency of 20% with respect to the absorbed power. The highest slope efficiency with respect to the absorbed power was 37.1% using an output coupler of 5% transmission. Thresholds as low as 120 mW (absorbed power) were measured with the 1% output coupler.

We obtained lasing with the 38 μm thick 50% Yb-doped epitaxy at 1032 nm using at first double pass pumping with the Ti:sapphire laser in the cavity shown in Fig. 3(a) with 1% output coupler. This was possible, however, only applying a chopper with a duty cycle of 10%. The average laser power reached 43 mW for an average incident pump power of 125 mW. There were strong indications of thermal effects when we tried to increase the duty cycle. We also observed strong feedback to the Ti:sapphire pump laser which makes it difficult to accurately estimate the actual efficiencies with respect to the absorbed powers and also the thresholds.

Therefore we had to employ the single-pass pumping configuration, again exchanging mirror $M_1$ in Fig. 3(a). An output power of 20 mW was reached for 1% output coupler at an incident pump power of 97 mW (both average values with the 10% duty cycle chopper). The corresponding slope efficiency was 42% (Fig. 4). The laser threshold was 18 mW of incident power (9 mW of absorbed power). The laser wavelength was 1032 nm independent of the output coupler (1%, 2%, or 3%).

The estimated small signal absorption of this sample was 78% at 981 nm. The actual absorption in the single-pass pump configuration was about 64% in lasing conditions at higher pump power levels. This indicates that the

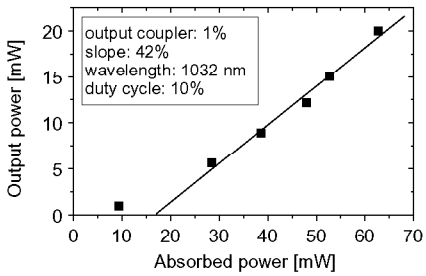


Fig. 4. Quasi-cw laser performance of the Yb(50%):KLuW/KLuW epitaxial composite with a 10% pump duty cycle. The average powers are presented: experimental points (squares) and linear fit for the slope (line).

absorption bleaching effect (reduction of the absorption down to 42% was observed in non-lasing conditions) was partially compensated at higher pump levels by the recycling effect.

It was also possible to achieve pure cw oscillation with single pass pumping in the absorption maximum and 0.1% output coupler, however, the efficiency was very low. The output power was 17 mW at 1046.1 nm for an incident power of 400 mW (absorbed power of 250 mW). The laser threshold was 76 mW of incident power (absorbed power of 46 mW). The output power quickly dropped to zero at incident pump levels above 400 mW. Pump powers exceeding 500 mW obviously damaged this epitaxial sample because strong scattering of the transmitted pump beam was observed behind the sample. This damage was confirmed later by simple observation with a microscope. It was located at the upper surface of the epitaxial layer.

Finally, we tested an analogous 50% Yb-doped KLuW epitaxy with a larger thickness (67% μm) but the results could not be improved. We achieved lasing only under quasi-cw pumping and the strong thermal problems persisted.

### 3.2. Mode-locked operation

Mode-locked operation was achieved with the 10% Yb-doped KLuW epitaxy using the Ti:sapphire laser as a pump source. The cavity configuration without the intracavity prisms (Fig. 3(b)) produced pulses of 1.8 ps duration (FWHM assuming $sech^2$ pulse shape) at a pulse repetition frequency of 100 MHz. The emission spectrum was centered at 1030 nm. The maximum output power obtained was 119 mW for an output coupler of 3% corresponding to a pump efficiency of 17% and a slope efficiency of 27% with respect to the absorbed power. The time-bandwidth product in this case was 1.78 (far exceeding the Fourier limit of 0.315).

The insertion of the two prisms into the cavity (see Fig. 3(b)) allowed to produce pulses as short as 114 fs at the same wavelength and a repetition rate of 101 MHz. The average output power was 31 mW for an absorbed power of 632 mW and output coupler of 1%. The time-bandwidth product of 0.43 in this case is only slightly above the Fourier limit. The output power could be increased using the 3% output coupler and 94 mW were obtained, again at 1030 nm, for an absorbed pump power of 671 mW. The FWHM increased to 200 fs but the pulses were almost bandwidth-limited (time-bandwidth product: 0.32).

We believe that the lower limit for the obtained pulse duration was partially due to the reflection characteristics of the folding mirrors which are restricted by the close separation of the laser and pump wavelengths and this was evidenced by the shape of the recorded pulse spectra on the low-wavelength side. In a very similar laser configuration we previously achieved shorter (81 fs) pulse durations at 1046 nm under the same experimental conditions using a 2.8 mm thick bulk Yb(5%):KLuW crystal [9]. Although the present results with the epitaxial sample are not superior in terms of pulse duration, the strongly reduced reabsorption of the 10% Yb-doped KLuW epitaxy in comparison with the analogous bulk crystals, which is manifested in the shorter oscillation wavelengths, is expected to provide potentially broader gain bandwidths and consequently shorter (below 80 fs) output pulses if specially designed dichroic coatings for the folding mirror $M_2$ are used.

## 4. Conclusion

The results obtained so far with Yb-doped monoclinic KLuW epitaxies make us confident that better management of the heat dissipation as well as better adjustment of the layer thickness to the Yb concentration will further increase the output powers in the cw regime allowing operation of 100% doped epitaxies, and shorten the pulse duration in the mode-locked regime.

## Acknowledgements

This work was supported by the European Commission under Project DT-CRYS (STRP-505580-1). X. Mateos acknowledges financial support from the Secretaria de Estado de Educacion y Universidades of Spain and from the Fondo Social Europeo. We thank Ch. Kränkel and K. Petermann (University of Hamburg, Hamburg, Germany) for the pinhole measurements of the lifetime in Fig. 2, R. Grunwald (Max-Born-Institute, Berlin, Germany) for the ZYGO measurements, and M. Zorn and M. Weyers (Ferdinand-Braun-Institute, Berlin, Germany) for fabricating the SAM devices.

## References

[1] W.F. Krupke, IEEE J. Select. Topics Quantum Electron. 6 (2000) 1287.
[2] A.A. Lagatsky, N.V. Kuleshov, V.P. Mikhailov, Opt. Commun. 165 (1999) 71.
[3] M.C. Pujol, M.A. Bursukova, F. Güell, X. Mateos, R. Sole, J. Gavalda, M. Aguilo, J. Massons, F. Diaz, P. Klopp, U. Griebner, V. Petrov, Phys. Rev. B 65 (2002) 165121.
[4] X. Mateos, R. Solé, Jna. Gavaldà, M. Aguiló, J. Massons, F. Díaz, V. Petrov, U. Griebner, Opt. Mat. 28 (2006) 519.
[5] S. Erhard, J. Gao, A. Giesen, K. Contag, A.A. Lagatski, A. Abdolvand, N.V. Kuleshov, J. Aus der Au, G.J. Spühler, F. Brunner, R. Paschotta, U. Keller, OSA Trends in Optics and Photonics (TOPS), vol. 56, Conf. Lasers and Electro-Optics, Techn. Digest., Washington, DC, 2001, p. 333.
[6] A. Aznar, R. Solé, M. Aguiló, F. Díaz, U. Griebner, R. Grunwald, V. Petrov, Appl. Phys. Lett. 85 (2004) 4313.
[7] U. Griebner, J. Liu, S. Rivier, A. Aznar, R. Grunwald, R.M. Solé, M. Aguiló, F. Díaz, V. Petrov, IEEE J. Quantum Electron. 41 (2005) 408.
[8] X. Mateos, V. Petrov, M. Aguiló, R.M. Solé, Jna. Gavaldà, J. Massons, F. Díaz, U. Griebner, IEEE J. Quantum Electron. 40 (2004) 1056.
[9] U. Griebner, S. Rivier, V. Petrov, M. Zorn, G. Erbert, M. Weyers, X. Mateos, M. Aguiló, J. Massons, F. Díaz, Opt. Exp. 13 (2005) 3465.

UNIVERSITAT ROVIRA I VIRGILI
CRECIMIENTO Y CARACTERIZACIÓN DE CAPAS EPITAXIALES DE KRE 1-X 4BX (WO4)2 / KRE (WO4)2 (RE=Y,LU)
PARA APLICACIONES LÁSER
Ana Isabel Aznar Écija

ISBN:978-84-691-1552-7 /DL:T.151-2008

**Crystal growth of monoclinic $KY_{1-x}Yb_x(WO_4)_2$ /$KY(WO_4)_2$ layers by Liquid Phase Epitaxy**

O. Silvestre, A. Aznar, R. Solé, M.C. Pujol, F. Díaz and M. Aguiló*
* Corresponding author. E-mail: magdalena.aguilo@urv.cat.

Física i Cristal·lografia de Materials (FiCMA), Universitat Rovira i Virgili (URV), Campus Sescelades
c/ Marcel·lí Domingo, s/n, E-43007-Tarragona, Spain

Monoclinic layers of $KY_{1-x}Yb_x(WO_4)_2$ with a thickness of up to 330 μm were grown on $KY(WO_4)_2$ substrates by Liquid Phase Epitaxy (LPE) using $K_2W_2O_7$ solvent. The layers grown from solutions of up to 7.5 atomic % substitution of Y by Yb, were generally with flat surfaces on {010} and {110} crystal faces with no macroscopic defects at the layer/substrate interface. At an already 10 atomic % of Yb substituting Y, some defects at the interface tend to begin to appear and increase for higher concentrations. The layers grown on {310} and {-111} faces were with more growth instabilities even at low Yb concentrations. The thermal evolution of the lattice mismatches between the epilayer and the substrate for {010}, {110}, {310} and {-111} faces were calculated ranging from 0.55% at 1273 K to -0.31% at 298 K. The optical spectroscopic studies carried out with these samples agree well with that already published for Yb-doped KYW bulk crystals, being the measured absorption and calculated by the reciprocity method emission cross sections at 981nm with $E//N_m$, $\sigma_{abs}$= 12.5 x $10^{-20}$ $cm^2$ and $\sigma_{em}$= 15.8 x $10^{-20}$ $cm^2$, respectively.

## Introduction

The lasers based on thin films have the advantage of high beam quality with high efficiency, making it possible to obtain high power with low thermal lensing[1].

The interest for laser crystals containing $Yb^{3+}$ as an active ion has been increasing in the last few years. This is due to the small quantum defect and the absence of excited state absorption and upconversion processes as a consequence of its simple electronic level structure. $Yb^{3+}$ has a unique excited level, $^2F_{5/2}$, with an energy difference of about 10000 $cm^{-1}$ with the $^2F_{7/2}$ ground level. In addition, its large absorption band at around 980 nm permits pumping with high power InGaAs laser diodes [2,3].

The crystals of the family of monoclinic double tungstates, such as $KGd(WO_4)_2$, $KY(WO_4)_2$ (hereafter KYW) and $KLu(WO_4)_2$ are excellent hosts for $Yb^{3+}$ ions[4, 5, 6]. It is also possible to obtain thin layers of these crystals doped with rare earth metals by liquid phase epitaxial growth on substrates of the same family. Among all the crystals of this family, the KYW has been probed to be a suitable crystal host for $Yb^{3+}$ doping, at least up to concentrations needed for lasing experiments with high efficiency [7].

Monoclinic KYW crystallizes with a *C2/c* space group and cell parameters $a$ = 10.6313(4) Å, $b$ = 10.3452(6) Å, $c$ = 7.5547(2) Å, β = 130.752(2)º and Z=4[8].

In the present paper, we discuss the suitable conditions to obtain $KY_{1-x}Yb_x(WO_4)_2/KY(WO_4)_2$ (hereafter $KY_{1-x}Yb_xW$/KYW) by liquid phase epitaxy (LPE). The evolution of lattice mismatch has also been calculated from room temperature to 1273K. Spectroscopic studies of these crystals, such as optical absorption and emission are also carried out as a previous study to laser experiments.

UNIVERSITAT ROVIRA I VIRGILI
CRECIMIENTO Y CARACTERIZACIÓN DE CAPAS EPITAXIALES DE KRE 1-X 4BX (WO4)2 / KRE (WO4)2 (RE=Y,LU) PARA APLICACIONES LÁSER
Ana Isabel Aznar Écija

ISBN:978-84-691-1552-7 /DL:T.151-2008

## Experimental Section

**Solubility curves.** The knowledge of the solubility curve of the solute in a suitable solvent is very important for choosing the composition of the solution from which the crystal growth will take place. The $K_2W_2O_7$ solvent has been proved as the best known option to grow KREW bulk tungstates by TSSG because, in relation with other solvents, it has several advantages such as low melting temperature and the absence of foreign ions that could be incorporated into the crystal [9]. Other solvents as $K_2WO_4$ [10] were used as well, but they introduce a rather high viscosity into the solution as well as creeping problems. In a previous work of some authors of this paper, $K_2W_2O_7$ was proved to be a suitable solvent for the growth of epitaxial layers of KLuW [11]. In literature, it can be found that Yb:KYW epitaxial layers were grown using a ternary NaCl-KCl-CsCl solvent but use of this solvent leads to a precipitation of yttrium and tungsten containing oxides[12]. Before the LPE experiments, we determined the solubility curve of $KY_{0.8}Yb_{0.2}(WO_4)_2$ in the solvent $K_2W_2O_7$.

The solubility experiments were made in 25 $cm^3$ platinum crucibles located inside a vertical cylindrical furnace with a Kanthal heater. The temperature was controlled with a controller/programmer 818 P connected to a tyristor. The reagents used were $K_2CO_3$ (99% purity), $Y_2O_3$ (99.9% purity), $Yb_2O_3$ (99.9% purity) and $WO_3$ (99.9% purity). The solution weights were 15-25 g. After homogenizing the solution, the temperature of the furnace was decreased at a rate of 10 K every 30 minutes until crystals on a platinum rod were observed. After that, the temperature of saturation of the solution was determined more accurately by increasing/decreasing the temperature of the furnace and observing if there was dissolution or growth of the crystals nucleated on the platinum rod. The crystals obtained were identified by observation with an optical microscope and by X-ray powder diffraction [8].

**Substrate crystal growth.** In order to obtain substrates with a structure as close as possible to the structure of the epitaxial layers, monoclinic crystals of KYW were grown by the Top Seeded Solution Growth-Slow Cooling (TSSG-SC) method. Supersaturation was obtained by slow cooling of the solution from the saturation temperature. The crystal growth was carried out using $K_2W_2O_7$ as solvent.

The experiments were carried out in a cylindrical vertical furnace. The temperature control was made with a Eurotherm 903 P controller/programmer connected to a tyristor.

The substrates were grown from about 200 g of solution prepared in 125 $cm^3$ cylindrical platinum crucibles and the reagents were $K_2CO_3$, $Y_2O_3$ and $WO_3$ with the same purity of the ones used for the solubility curves. The solution composition was 12 mol % KYW/88 mol % $K_2W_2O_7$ and was chosen taking into account the solubility curve of KYW in this solvent [13].The axial temperature gradient in the solution was 1.5 K/cm, with the surface cooler than the bottom to avoid the nucleation of crystals at the bottom of the crucible.

Two kinds of crystal growth experiments were made. First, we simultaneously grew three crystals located at the surface of the solution about 1 cm from the center and equally spaced. The orientation of these crystals was with the ***b*** direction perpendicular to the surface of the solution. The aim of these crystal growth runs was to obtain small crystals (about 5 mm as maximum dimension) to be used as-grown as substrates and to study the epitaxial growth on different crystal faces. In the second kind of runs, we grew a unique single crystal in every experiment with ***b*** crystallographic direction perpendicular to the surface of the solution and located at the center of the solution surface. The crystals obtained in these last experiments were big enough to be cut into plates perpendicular to ***b*** direction to use as substrates in the epitaxial growth. In both cases, the solution temperature was decreased at a rate of 0.1-0.2 K/h for 20-28 K from the saturation temperature. The crystal rotation was 40 rpm in all the experiments. After the growth process, they were removed from the solution and maintained just above the surface of the solution, while the furnace was cooled at a rate of 25-30 K/h to avoid thermal stresses.

ISBN:978-84-691-1552-7 /DL:T.151-2008

**Unit Cell parameters.** The unit cell parameters of $KY_{1-x}Yb_xW$ for different levels of substitution of Y by Yb (different values of x) were refined from the X-ray powder diffraction data. The crystals needed were obtained with the same procedure than the ones of the solubility curve. For these measurements, we used a Siemens D-5000 powder diffractometer, with Bragg-Brentano parafocusing geometry and vertical θ-θ goniometer. The X-ray powder diffraction patterns were recorded at $2\theta = 10 – 70^o$ with a step size of 0.02º and a step time of 16 s. The cell parameters were refined using the Fullprof program[14].

The change of the cell parameters of undoped KYW and $KY_{0.8}Yb_{0.2}W$ with the temperature was obtained from the X-ray powder diffraction data obtained using the same diffractometer, equipped with a high temperature chamber Anton-Paar HTK10, over the range between room temperature and 1273 K. The X-ray powder diffraction patterns were recorded at $2\theta = 10 – 70^o$, with a step size of 0.03º and a step time of 5 s. The X-ray patterns were recorded at 298 K, 323 K, 373 K. After that, the time interval between measurements was of 100 K up to 1273 K. The cell parameters were also refined with the Fullprof program.

**Liquid Phase Epitaxy.** The liquid phase epitaxy experiments were made in a special furnace with a wide isothermal zone to achieve a thermal gradient in the solution of practically zero. This thermally stable zone contributes to the homogeneous growth over the entire surface of the substrate where the growth process occurs. The LPE experiments were carried out using cylindrical platinum crucibles 30 mm in diameter and 40 mm high. The solution weighed about 70 g. The reagents were the same as in the growth of the substrates and $Yb_2O_3$ (99.9% purity) for substitution. Different solution compositions were used in these experiments, ranging from 5 mol % $KY_{1-x}Yb_xW$ / 95 mol % $K_2W_2O_7$ to 12 mol % $KY_{1-x}Yb_xW$ / 88 mol % $K_2W_2O_7$ in order to study the influence of the solute concentration in the epitaxial growth. Different solution compositions lead to a difference in the slope of the solubility curve. The chosen solute/solvent composition has to compromise between the rate of growth and the macrodefect density in the epilayer/substrate interface. A small slope in the solubility curve lead to a high solute deposition with small temperature fluctuations and this fact could involve the appearance of defects in the interface. On the contrary, a high slope in the solubility curve involves a low growth rate and the crystal growth is less affected by temperature fluctuations.

The saturation temperature of the solution as well as the kinetics of growth/dissolution at temperatures slightly below/above the temperature of saturation were determined accurately with a KYW seed in contact with the surface of the solution rotating at 40 rpm. These measurements were important to decide the growth conditions of the epitaxial layers [15].

In order to study the influence of the crystalline face on the quality and thickness of the epitaxial layer, LPE experiments on as-grown KYW substrates were carried out. A second kind of experiment, made with (010) oriented plates, were carried out in order to study how the time of growth, solution composition and supersaturation affected the quality and thickness of the epitaxial growth. These plates were obtained by cutting a KYW single crystal in slices of 2 mm thick. After that, these plates were polished to optical grade quality and were mounted in a vertical position with platinum wires on an alumina rod.

Before being introduced to the furnace, the substrates were carefully cleaned by dipping them for 5 minutes in $HNO_3$/distilled $H_2O$ = 1/1. After that, they were dipped for 5 minutes in distilled water and 5 minutes in $C_2H_5$-OH. The entire cleaning process of was made with the crystal in rotation.

The first LPE experiments were carried out using the same solution composition as the growth of the substrates, only substituting part of the $Y_2O_3$ by $Yb_2O_3$ in different proportions. After that, we decreased the solute concentration in the solution in order to study its influence on the quality of the layers. The experiments carried out are summarized in tables 1 and 2. The solute concentration and Yb contents in the solution are shown in these tables. Also, there are temperatures below the saturation temperature where the LPE crystal growth was made and the time of growth. In all the experiments, the surface of the substrates was first dissolved slightly by maintaining the temperature of the solution 1 degree above the saturation temperature for 5 minutes. After that the temperature was decreased to the growth temperature. In addition, all the LPE crystal growth experiments were carried out with the

ISBN:978-84-691-1552-7 /DL:T.151-2008

substrate rotating at 40 rpm. Finally, the crystals were removed from the solution and taken out of the furnace slowly in order to avoid thermal shocks that could produce cracks in the crystal.

Experiments 1-5, 9 and 12 in as-grown substrates (table 1) and experiments 23 and 27 in (010) slices (table 2) were designed to study the influence of the Yb concentration in the solution in the LPE crystal growth. Experiments 5-11 and 20-22 in as-grown substrates (table 1) and experiments 23-26 and 28 in (010) slices (table 2) were designed for studying the influence of the time of growth on the quality and the thickness of the epitaxial growth. Experiments 9-10, 14-16 and 17-19 in as-grown crystals (table 1) were made for studying the influence of the growth temperature, and consequently supersaturation, on the epitaxial crystal growth.

The composition of the layers obtained by LPE were measured by electron probe microanalysis (EPMA) using a Cameca SX 50. These measurements also allowed us to detect the layer/substrate interface by a compositional change and to measure the thickness of the layer. But because the use of this method to measure the layer thickness requires a lot of EPMA measurements, we only used it in a few cases. The thickness of the epitaxial layers was also measured with an Olympus Optical Microscope (magnification x5, x10, x20 and x50) using transmission light and by scanning electron microscope (SEM), using backscattered electrons.

The quality of the layer on every crystal face as a function of the solution composition and growth conditions was studied by observing the crystals first with the optical microscope mentioned above and after that with confocal and interferometric microscopy to obtain information of the growth morphologies.

**Spectroscopic study.** The optical polarized absorption with $E//N_m$ at a room temperature of a $KY_{0.81}Yb_{0.19}W$/KYW(010) epitaxial layer was measured in the 900-1050 nm range, using a Cary Variant 500 spectrophotometer, with a Glan-Taylor polarizer. Fluorescence was dispersed through a HR 460 Jovin Yvon-Spex monochromator and detected by a cooled Hamamatsu R5509-72 NIR. The fluorescence spectra were measured in 90º geometry with a laser diode, emitting at 940 nm, as the excitation source. We analyzed the luminescence signal using an EG&G 7265DPS lock-in amplifier. The sample was pumped along the ***c*** crystallographic axis, and the emitted light was collected parallel to the ***b*** direction.

Lasing experiments were made using a $KY_{0.81}Yb_{0.19}W$/KYW with a layer of 48 μm grown from a solution with 20 mol % of Y substituted by Yb. Continuous-wave lasing at 1030 nm with an output power of 40mW was obtained at room temperature. More details of laser experiments can be seen in reference[16].

## Results and Discussion

**Solubility curves.** Figure 1 shows the solubility curve of $KY_{0.8}Yb_{0.2}W$ in the solvent $K_2W_2O_7$. Compared with those of the KYW and KYbW, published elsewhere[13,17], it can be said that there was no significant difference in their solubility. At around 54% solute composition and 1273 K, there appears a drastic change in the slope of the solubility curve. After this point, the $C_{2/c}$ monoclinic morphology leads to layered crystals corresponding to orthorhombic high temperature phase isostructural to $KY(MoO_4)_2$[18,19,20]. The insets in Figure 1 show a photograph of both crystal habits that appeared: the monoclinic and the layered one. The solidus line is located at 884 K and indicates the temperature below what the solution turns solid for any composition.

In the solubility curve shown in Figure 1, we can observe two regions with very different slopes. From 5 to about 15 mol % solute, the solubility curve has a higher slope than for solute concentrations above 15 mol %. From these results, we concluded that solutions with solute concentration lower than 15 mol % are, a priori, the most suitable for single crystal and epitaxial growth since the supersaturation of the solution would be less affected by temperature fluctuations.

ISBN:978-84-691-1552-7 /DL:T.151-2008

**Substrates crystal growth.** As it has been mentioned in the experimental details, two kinds of substrates were used: as-grown substrates and slices perpendicular to (010) direction cut from bulk crystals and polished. The crystals obtained in the two kinds of crystal growth runs were transparent, colorless and free from inclusions and other macroscopic defects.

The crystals with dimensions less than 5 mm were used for substrates without any other treatment, only careful cleaning. These KYW single crystals are formed by the {110},{010}, {-111} and {310} faces as can be seen in figure 2, where it is shown a photograph of a crystal and a morphological scheme made with the Shape program [21].

The bulk crystals to be cut in slices weighted between 3.0 and 6.3 g and their dimensions were in the range 7-9.1 mm x 6.9-9.2 mm x 13.6-19.8 mm in $\boldsymbol{a^*}$ x $\boldsymbol{b}$ x $\boldsymbol{c}$ directions. These crystals were cut with a diamond saw and polished to obtain (010) slices with minimum deviation from this direction and a roughness less than 3 μm.

**Unit Cell parameters**. Before carrying out the LPE experiments, the change of the cell parameters with the Yb contents in the crystal was determined because of its relation with the defect generation in the film/substrate interphase of the composite.

Table 3 shows the unit cell parameters of KYW and $KY_{1-x}Yb_xW$ for different levels of substitution of Y by Yb. As a consequence of the minor ionic radius of $Yb^{3+}$ (0.985 Å) with respect to the ionic radius of $Y^{3+}$ (1.019 Å)[22], the cell parameters decrease when the Yb concentration increases, except for the angle $\boldsymbol{\beta}$ that within experimental error is practically constant. The change in $\boldsymbol{b}$ parameter is more significant than the change in $\boldsymbol{a}$ and $\boldsymbol{c}$ parameters. Consequently the cell volume also decreases with the increasing of Yb.

A bidimensional lattice mismatch can be defined by the expression $f_{(hkl)} = [(S_{L\,(hkl)} - S_{S\,(hkl)})/ S_{S\,(hkl)}] \times 100$, where $S_{S\,(hkl)}$ and $S_{L\,(hkl)}$ are the areas of the (hkl) periodicity vectors of the substrate and the layer, respectively. Table 4 summarizes the lattice mismatches for the {010}, {110}, {310} and {-111} faces at room temperature. High mismatches between the layer and the substrate will lead to a high stress in the interface that could produce cracks[14]. It can be said that, up to 10 atomic % of Yb substituting Y in the layer, the face with the lowest mismatch between the layer and the substrate is the (-111) face, while for higher Yb concentrations, the face with the lowest mismatch is the (010) face. The layer on the (110) face has a higher mismatch than the layer on the (010) face, but lower than the one on the (310) face. In addition to having a low mismatch, the (010) face also has a low rate of growth, which could be the reason because the epitaxies on this face are generally with a high level of flatness and few defects. Moreover, the (010) face is the most interesting one for optical applications due to the fact that the principal optical axes $\boldsymbol{N_g}$ and $\boldsymbol{N_m}$ are contained in the *a-c* plane perpendicular to (010) direction.

**Lattice mismatch variation with temperature**. Since the thermal expansion of the epilayer and the substrate are not equal, (Figures 3.a and 3.b), the lattice mismatch is not constant as the temperature varies. The thermal evolution of the lattice mismatch between the substrate and the epilayer, KYW and $KY_{0.8}Yb_{0.2}W$, respectively, are presented in Figure 3.c.

ISBN:978-84-691-1552-7 /DL:T.151-2008

The linear thermal expansion coefficients in a given crystallographic direction are $\alpha=(\partial L/\partial T)/L$, where L is the initial parameter at 298K and $\Delta L$ is the change in this parameter when the temperature is changed by $\Delta T$. The $\alpha_{ij}$ are the slopes and conform the linear thermal expansion tensor in the crystallophysical frame. Using the experimental data of figure 3a), the linear thermal expansion values for $KY_{0.8}Yb_{0.2}W$ are: are $\alpha_{100}=10.5 \times 10^{-6}(K)^{-1}$, $\alpha_{010}=2.77 \times 10^{-6}(K)^{-1}$, $\alpha_{001}=18.3 \times 10^{-6}(K)^{-1}$, $\alpha_{c*}=20.7 \times 10^{-6}(K)^{-1}$, $\alpha_V=30.0 \times 10^{-6}(K)^{-1}$. By diagonalising this tensor , we obtained a linear thermal expansion tensor in the principal system $X'_1$, $X'_2$, $X'_3$. The linear thermal expansion tensor values in the principal system are: $\alpha'_{33}=21.1 \times 10^{-6} K^{-1}$, $X'_3$ found at 30.2º rotating anti-clockwise from ***c*** axis with the ***b*** positive axis pointing us; $\alpha'_{11}=10.1 \times 10^{-6} K^{-1}$ for $X'_1$ principal direction and $\alpha'_{22}=20.7 \times 10^{-6} K^{-1}$, for $X'_2$ (***b*** crystallographic direction) principal axis. Comparing these values to the previously published ones for KYW in [8], it can be observed that these values are higher and this fact implies a greater dilatation of the epilayer than the substrate when increasing the temperature.

A $f_{(hkl)}>0$ indicates a tensile strain while a $f_{(hkl)}<0$ implies a compressive strain in the composite interface. Figure 3.c shows the evolution of the lattice mismatch from room temperature to 1273 K. As can be seen, the values of $f_{(hkl)}$ are around 0.6% at higher temperature where the growth process occurs and it decreases as the temperature does. So, a very slow cooling ramp once the epitaxial sample is grown and extracted from the solution will be needed until around 773 K to avoid interface defects due to the high difference between the epitaxial and substrate lattice parameters. Below this temperature, the cooling ramp rate can be faster because the lattice mismatch difference is rather low. As can be seen, the thermal evolution of lattice mismatch is very similar for all the faces studied.

**Liquid Phase Epitaxy**. The experiments of LPE using as-grown substrates to study the quality of the epitaxies grown on the different crystal faces and LPE on (010) plates are summarized in tables 1 and 2, respectively. The dissolution of the surface of the substrates at 1 degree above the saturation temperature over five minutes has proven that there is no contribution to the increase of the defects in the interface since only it only dissolves the outer part of the crystal in order to eliminate possible surface defects.

For a 5 atomic % Yb substitution, the mismatch between the layer and the substrate on the (010) face is small enough to permit the growth of the layer on the substrate with a high flatness. For substitutions of Y by Yb higher than 10 atomic %, the tendency for defects to appear in the interface is increased. The layer/substrate mismatch on (-111) face is of the same order as on the (010) face but the layers on (-111) face were generally of poor quality. One possible explanation is that this face has a growth rate higher than its neighbor faces and this can contribute to the occurrence of more defects in the layer. The layers grown on the (110) face generally have a high quality of up to 10 mol % of substitution of Y by Yb because the mismatch is also small in this case. Finally the layers obtained on the (310) faces generally have more defects than the layers grown on (010) and (110) faces but less than the layers grown on (-111) faces. So, for the following studies, only (010) oriented slices were used. As an example, Figure 4 shows photographs of LPE layers grown on different crystal faces, where we can observe the typical growth defects on these faces.

The Yb concentration in the growth solution has a significant influence on the quality of the layers. Thus, using the growth conditions of this work, we have observed that in some of the experiments, there is a tendency for some cracks to begin appearing in the layer/substrate interface of the crystal when the substitution of $Y_2O_3$ by $Yb_2O_3$ in the solution is 10 mol %. By increasing the substitution to 20 mol %, even with low solute concentration in the solution, the cracks are present in equal distribution in the layer/substrate interface (see Figure 5). In the epitaxial growth of KYbW/KYW, the interface defects are so important that it does not make the samples transparent (experiments 12 and 13), probably due to the high lattice mismatch between the layer and the substrate.

The most commonly observed morphologies in the layers are growth steps and were first observed by optical microscope and after that by confocal and interferometric microscopy. Figure 6 shows, as an example, a confocal image of representative $KY_{0.95}Yb_{0.05}W$/KYW and $KY_{0.80}Yb_{0.20}W$/KYW layers grown on (010) faces with the same z-axis scale. As can be seen in the figure, the rms (root mean square) roughness of the $KY_{0.80}Yb_{0.20}W$/KYW sample is clearly higher than that of the

ISBN:978-84-691-1552-7 /DL:T.151-2008

$KY_{0.95}Yb_{0.05}W$/KYW one, 490 and 160 nm respectively. In the profiles, there can also be observed a higher height in the growth steps. In the case of the $KY_{0.80}Yb_{0.20}W$/KYW epitaxial sample, there can be observed a high number of growth centers in the form of growth hillocks which were more active than centers which had dominated the growth process over the whole face. These growth centers can be mainly due to solution remains in the surface of the crystal. Surface cracks are a source for solution which leads to the structures shown in the inset of the Figure 6b).

The increase of the thickness of the epitaxial growth on the (010) face as a function of the growth time was studied (experiments number 26 and 28). First, we dipped the crystal into the solution several millimeters, followed by pulling the crystal in steps of 1 mm at known intervals of time (30 minutes in experiment 26 and longer times in exp 28). In the final pull, we entirely took out the crystal from the solution. Figure 7 shows the evolution of the layer thickness on (010) crystal face with the time of growth and the average growth rates at 6 and 22 hours. The growth rate increases almost linear until around 10 hours at 19.5 µm/h and then it decreases to 2.4 µm/h at 22 hours. Comparing these growth rates with these previously published for $KLu_{0.8}Yb_{0.2}W$/KLuW[11], it can be observed that the growth rates for $KY_{0.80}Yb_{0.20}W$/KYW are much higher. This effect can be due to the higher value of lattice mismatch between the epilayer and the substrate, which induces a higher number of defects in the interface leading to an increase in the number of kinks where the growth units can attach.

Table 5 shows the layer thickness of $KY_{1-x}Yb_xW$/KYW grown from 12 mol % solute and a 10 atomic % of Y substituted by Yb in solution, two different levels of supersaturation and different times of growth. The thicknesses of the faces were evaluated by the observation by SEM of the epitaxy cut perpendicular to **b** crystallographic direction and measuring the distance from the substrate-epilayer interface. This is the reason why the values of (-111) thickness are not present in table 5. Of all the faces studied, the face with higher velocity of layer growth is the (010), followed by the (110). The layers grown on (010) and (110) faces are generally of higher quality than the layers obtained on the (310) and (-111) faces.

The solute/solvent ratio in the growth solution slightly influences the growth velocity, but the quality of the layer/substrate is practically unchanged (experiments number 9 and 17).

The influence of the growth temperature of the epitaxial layers is studied in experiments number 9-10, 14-16 and 17-19. From these experiments, we conclude that at low levels of supersaturation (growing from 2 to 6 degrees below the saturation temperature, using about 70 g of solution), no significant changes in the quality of the epitaxial growth nor in the velocity of growth are observed.

The layer composition was measured by EPMA with Wavelength Dispersive Spectroscopy (WDS) and the distribution coefficient of Yb was calculated according to the expression: $K_{Yb} = \{[Yb] / ([Yb] + [Y])\}_{layer} / \{[Yb] / ([Yb] + [Y])\}_{solution}$, where [Yb] and [Y] are the concentrations of Yb and Y, respectively. Table 6 summarizes the composition of the layers and the distribution coefficient of Yb for different levels of substitution of Y by Yb. We have observed that in the distribution coefficient of Yb, there was practically no change with the solute/solvent ratio with the ratios studied in this work. For all the levels of substitution studied, the distribution coefficient of Yb is close to unity.

**Spectroscopic Study.** Figure 8 shows the polarized optical absorption of a oriented $KY_{0.81}Yb_{0.19}(WO_4)_2$/KYW (010) epitaxial layer at room temperature. The light was polarized parallel to the principal optical direction $N_m$. In this family of materials, the optical absorption of $Yb^{+3}$ strongly depends on the light polarization; in previous studies, the highest absorption values reported are by Mateos *et al.* [23] at 980.6 nm with $E//N_m$ $\sigma_{abs}$= 11.7 x $10^{-20}$ $cm^2$ and by Kuleshov *et al.* [24], at 981.2 nm with *E//a'* ( where *a'* is the unit cell parameter expressed in the spatial group *I2/c*; a' = (a + c), ***a*** and ***c*** are the unit cell parameters in *C2*/c), the cross section value is $\sigma_{abs}$= 13.3 x $10^{-20}$ $cm^2$.

As can be observed from the spectrum, the $^2F_{7/2} \rightarrow {}^2F_{5/2}$ transition has three main peaks centered at 933.6, 981.8 and 1000.0 nm.

The maximum absorption cross section $\sigma_{abs}$ at 981.8nm, calculated with the $Yb^{+3}$ concentration of 1.992 x $10^{21}$ ions/$cm^3$, amounts to 12.5 x $10^{-20}$$cm^2$. The emission cross section spectrum was calculated with the reciprocity method using the absorption cross section spectrum at room temperature and the splitting determined at low temperature in the reference[16]. The results are included in the inset of

ISBN:978-84-691-1552-7 /DL:T.151-2008

Figure 9 and compared with the experimental unpolarized emission spectrum obtained in the present paper. The peaks correspond to the transition from the excited $^2F_{5/2}$ level to the four sublevels of the ground state $^2F_{7/2}$.

It is worth mentioning that the relative intensity of the peak at 981.8 nm, corresponding to the $^2F_{5/2}(0') \rightarrow {}^2F_{7/2}(0)$ sublevels transition, shows a slight decrease in the experimental spectrum in comparison with the calculated spectrum. The experimental emission spectrum is an average of $N_g$ and $N_m$ polarized emission spectra as a result of the above described experimental configuration. There is a significant overlap between the absorption and emission spectrum around 982 nm, which can produce reabsorption during lasing experiments. Thin layers minimize this effect [24].The maximum calculated emission cross section is 15.8 x $10^{-20}$ atm/cm$^2$ at 982.6 nm.

Efficient continuous-wave laser emission was achieved at around 1030 nm with an output of 40 mW from a sample $KY_{0.81}Yb_{0.19}(WO_4)_2$/KYW (010) epitaxial layer obtained and described in the present paper. More details of the laser operation can be found in references [16].

## Conclusions

Epitaxial layers of $KY_{1-x}Yb_x(WO_4)_2/KY(WO_4)_2$ were grown by liquid phase epitaxy on bulk substrates and (010) slices. Up to 10 atomic % of Y layers substituted by Yb are generally of high quality, principally on faces (010) and (110). For substitutions higher than that, some cracks at the layer/substrate interface began to appear. The layers grown on (310) and (-111) are generally of worse quality than the layers on the (010) and (110) faces. The face with higher velocity of growth is the (010) face. No significant increase in the growth velocity of the layer with the level of supersaturation, for the low levels of supersaturation studied in this work, was observed.

The optical absorption with $E // N_m$ polarization shows three main absorption peaks corresponding to the $^2F_{7/2} \rightarrow {}^2F_{5/2}$ transition centered at 933.8 nm, 981.8 nm and 998.4 nm and a maximum absorption cross section of 1.22 x $10^{-19}$ atm/cm$^3$.

**Acknowledgements.** This work was supported by the EU project DT-CRYS, NMP3-CT-2003-505580, by the Ministerio de Educación y Ciencia projects MAT2004-20471-E, MAT-2005-06354-C03-02, and CIT-020400-2005-14, and by the Generalitat de Catalunya project 2005SGR658.

UNIVERSITAT ROVIRA I VIRGILI
CRECIMIENTO Y CARACTERIZACIÓN DE CAPAS EPITAXIALES DE KRE 1-X 4BX (WO4)2 / KRE (WO4)2 (RE=Y,LU) PARA APLICACIONES LÁSER
Ana Isabel Aznar Écija

ISBN:978-84-691-1552-7 /DL:T.151-2008

Table 1: Experiments of LPE growth on as-grown substrates and growth conditions

| **Experiment number** | **Solute/solvent (molar ratio)** | **Yb contents in solution (mol %)** | **$\Delta T_{growth}$ (K)** | **Growth time (h)** |
|---|---|---|---|---|
| **1** | 12/88 | 0 | -2 | 2 |
| **2** | 12/88 | 1 | -2 | 2 |
| **3** | 12/88 | 2.5 | -2 | 2 |
| **4** | 12/88 | 5 | -2 | 2 |
| **5** | 12/88 | 7.5 | -2 | 2 |
| **6** | 12/88 | 7.5 | -2 | 3 |
| **7** | 12/88 | 7.5 | -2 | 4 |
| **8** | 12/88 | 10 | -2 | 1 |
| **9** | 12/88 | 10 | -2 | 2 |
| **10** | 12/88 | 10 | -1 | 2 |
| **11** | 12/88 | 10 | -1 | 4 |
| **12** | 12/88 | 100 | -2 | 2 |
| **13** | 12/88 | 100 | -1 | 2 |
| **14** | 7/93 | 20 | -1 | 4 |
| **15** | 7/93 | 5 | -3 | 4 |
| **16** | 7/93 | 5 | -6 | 4 |
| **17** | 5/95 | 10 | -2 | 2 |
| **18** | 5/95 | 10 | -3 | 2 |
| **19** | 5/95 | 10 | -4 | 2 |
| **20** | 5/95 | 20 | -2 | 2 |
| **21** | 5/95 | 20 | -2 | 3 |
| **22** | 5/95 | 20 | -2 | 4 |

Table 2: Experiments of LPE growth on (010) plates and growth conditions

| **Experiment number** | **Solute/solvent (molar ratio)** | **Yb contents in solution (mol %)** | **$\Delta T_{growth}$ (K)** | **Growth time (h)** |
|---|---|---|---|---|
| **23** | 5/95 | 10 | -2 | 2 |
| **24** | 5/95 | 10 | -2 | 3 |
| **25** | 5/95 | 10 | 0/-2 | Ramp 0.5ºC/h during 2 h |
| **26** | 5/95 | 10 | -2 | 0.5/1/1.5/2 |
| **27** | 5/95 | 20 | -2 | 2 |
| **28** | 7/93 | 20 | -6 | 2/3/4/5/8/12/20/22/24 |

UNIVERSITAT ROVIRA I VIRGILI
CRECIMIENTO Y CARACTERIZACIÓN DE CAPAS EPITAXIALES DE KRE 1-X 4BX (WO4)2 / KRE (WO4)2 (RE=Y,LU) PARA APLICACIONES LÁSER
Ana Isabel Aznar Écija

ISBN:978-84-691-1552-7 /DL:T.151-2008

Table 3: Cell parameters of KYW and $KY_{1-x}Yb_xW$

| $[Yb]_{solution}$at. % | a (Å) | b (Å) | c (Å) | β (º) | Volume ($Å^3$) |
|---|---|---|---|---|---|
| **0** | 10.6313(4) | 10.3452(6) | 7.5547(3) | 130.752(2) | 629.44(5) |
| **5** | 10.6250(5) | 10.3380(5) | 7.5475(3) | 130.745(2) | 628.09(5) |
| **10** | 10.6239(5) | 10.3326(5) | 7.5448(3) | 130.745(3) | 627.48(5) |
| **20** | 10.6200(6) | 10.3213(6) | 7.5382(4) | 130.744(3) | 625.98(6) |
| **50** | 10.6098(5) | 10.2952(5) | 7.5223(4) | 130.751(3) | 622.45(5) |
| **100** | 10.6003(12) | 10.2673(12) | 7.5066(8) | 130.766(6) | 618.78(12) |

Table 4: Mismatch between $KY_{1-x}Yb_xW$ layers and KYW substrate

| Composition | $f_{(010)}$ | $f_{(110)}$ | $f_{(310)}$ | $f_{(-111)}$ |
|---|---|---|---|---|
| **$KY_{0.95}Yb_{0.05}W$/KYW** | -0.1440 | -0.1570 | -0.1635 | -0.1283 |
| **$KY_{0.9}Yb_{0.1}W$/KYW** | -0.1901 | -0.2290 | -0.2487 | -0.1863 |
| **$KY_{0.8}Yb_{0.2}W$/KYW** | -0.3125 | -0.3974 | -0.4403 | -0.3252 |
| **$KY_{0.5}Yb_{0.5}W$/KYW** | -0.6287 | -0.8038 | -0.8923 | -0.6745 |
| **KYbW/KYW** | -0.9473 | -1.2195 | -1.3572 | -1.0397 |

Table 5: Layer thicknesses of $KY_{1-x}Yb_xW$/KYW grown from 12 mol % solute a 10 mol % of Y substituted by Yb in solution

| Experiment number | Growth time (h) | $\Delta T_{growth}$ (K) | (010) face Thickness (μm) | (110) face Thickness (μm) | (310) face Thickness (μm) |
|---|---|---|---|---|---|
| **8** | 1 | -2 | 63 | 32 | 14 |
| **9** | 2 | -2 | 77 | 50 | 20 |
| **10** | 2 | -1 | 68 | 46 | 16 |
| **11** | 4 | -1 | 103 | 48 | 25 |

Table 6: Crystal composition and distribution coefficient of Yb for different levels of substitution.

| Solute/solvent (molar ratio) | $K_{Yb}$ | Stoichiometric formula |
|---|---|---|
| **5** | 1.03 | $KY_{0.95}Yb_{0.05}(WO_4)_2$ |
| **10** | 1.02 | $KY_{0.90}Yb_{0.10}(WO_4)_2$ |
| **20** | 0.95 | $KY_{0.81}Yb_{0.19}(WO_4)_2$ |

UNIVERSITAT ROVIRA I VIRGILI
CRECIMIENTO Y CARACTERIZACIÓN DE CAPAS EPITAXIALES DE KRE 1-X 4BX (WO4)2 / KRE (WO4)2 (RE=Y,LU) PARA APLICACIONES LÁSER
Ana Isabel Aznar Écija

ISBN:978-84-691-1552-7 /DL:T.151-2008

**Figure captions:**

**Figure 1.** Solubility curve of $KY_{0.8}Yb_{0.2}W$ in the solvent $K_2W_2O_7$.

**Figure 2.** KYW single crystal before being cut in slices for substrates and a crystal scheme made with the Shape program.

**Figure 3.** (a) Thermal evolution of unit cell parameters of $KY_{0.8}Yb_{0.2}W$, (b) KYW and (c) lattice mismatch.

**Figure 4.** Typical growth defects on several crystal faces.

**Figure 5.** Morphologies in the layer/substrate interface that appeared for a sample with 20 mol % of Y substituted by Yb in the epitaxial layer.

**Figure 6.** (a) Confocal image of a $KY_{0.95}Yb_{0.05}W$/KYW layers grown on a (010) face and (b) $KY_{0.8}Yb_{0.2}W$/KYW layers grown on a (010) face.

**Figure 7.** Epitaxial layer thickness in front of the time of growth on a (010) slice (experiment number 28) with image and scheme view of the sample.

**Figure 8.** Optical absorption with $N_m$ polarization of a $KY_{0.81}Yb_{0.19}(WO_4)_2$/KYW crystal at room temperature.

**Figure 9.** Emission cross section spectrum of a $KY_{0.81}Yb_{0.19}(WO_4)_2$/KYW crystal. Inset: Emission cross section calculated using the reciprocity method and absorption cross section spectrum used for the calculations.

UNIVERSITAT ROVIRA I VIRGILI
CRECIMIENTO Y CARACTERIZACIÓN DE CAPAS EPITAXIALES DE KRE 1-X 4BX (WO4)2 / KRE (WO4)2 (RE=Y,LU) PARA APLICACIONES LÁSER
Ana Isabel Aznar Écija

ISBN:978-84-691-1552-7 /DL:T.151-2008

Figure 1

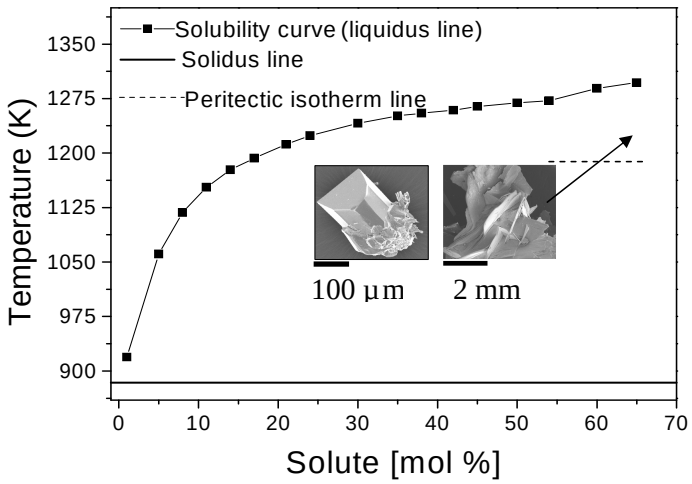


Figure 2

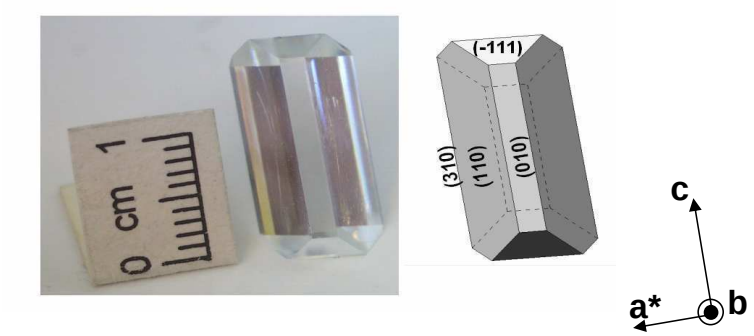

UNIVERSITAT ROVIRA I VIRGILI
CRECIMIENTO Y CARACTERIZACIÓN DE CAPAS EPITAXIALES DE KRE 1-X 4BX (WO4)2 / KRE (WO4)2 (RE=Y,LU) PARA APLICACIONES LÁSER
Ana Isabel Aznar Écija

ISBN:978-84-691-1552-7 /DL:T.151-2008

Figure 3

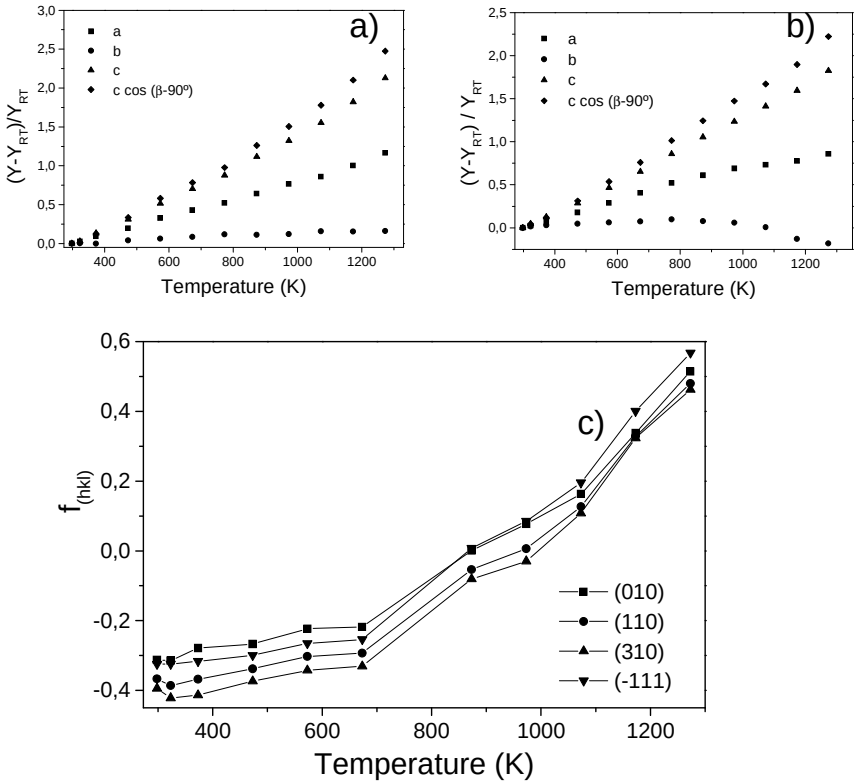

UNIVERSITAT ROVIRA I VIRGILI
CRECIMIENTO Y CARACTERIZACIÓN DE CAPAS EPITAXIALES DE KRE 1-X 4BX (WO4)2 / KRE (WO4)2 (RE=Y,LU)
PARA APLICACIONES LÁSER
Ana Isabel Aznar Écija

ISBN:978-84-691-1552-7 /DL:T.151-2008

Figure 4

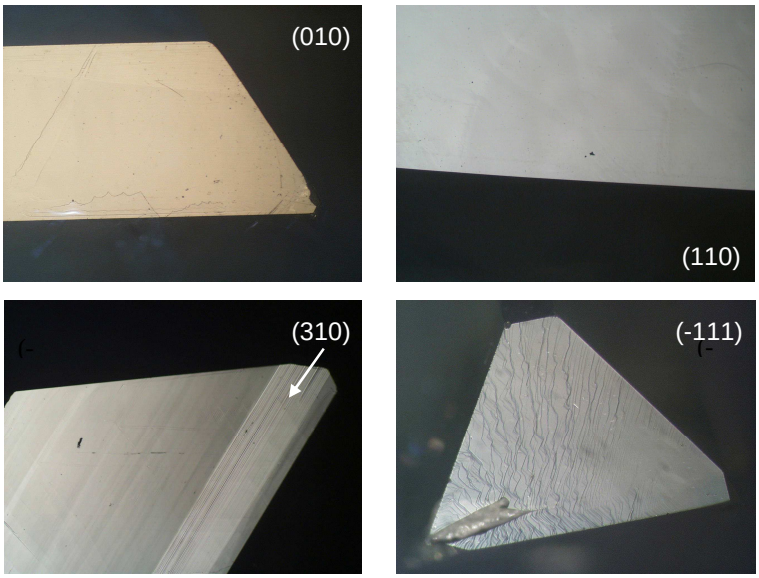


Figure 5

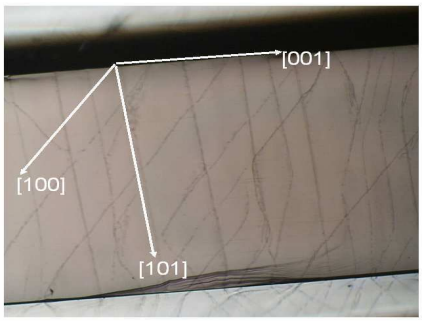

UNIVERSITAT ROVIRA I VIRGILI
CRECIMIENTO Y CARACTERIZACIÓN DE CAPAS EPITAXIALES DE KRE 1-X 4BX (WO4)2 / KRE (WO4)2 (RE=Y,LU) PARA APLICACIONES LÁSER
Ana Isabel Aznar Écija

ISBN:978-84-691-1552-7 /DL:T.151-2008

Figure 6

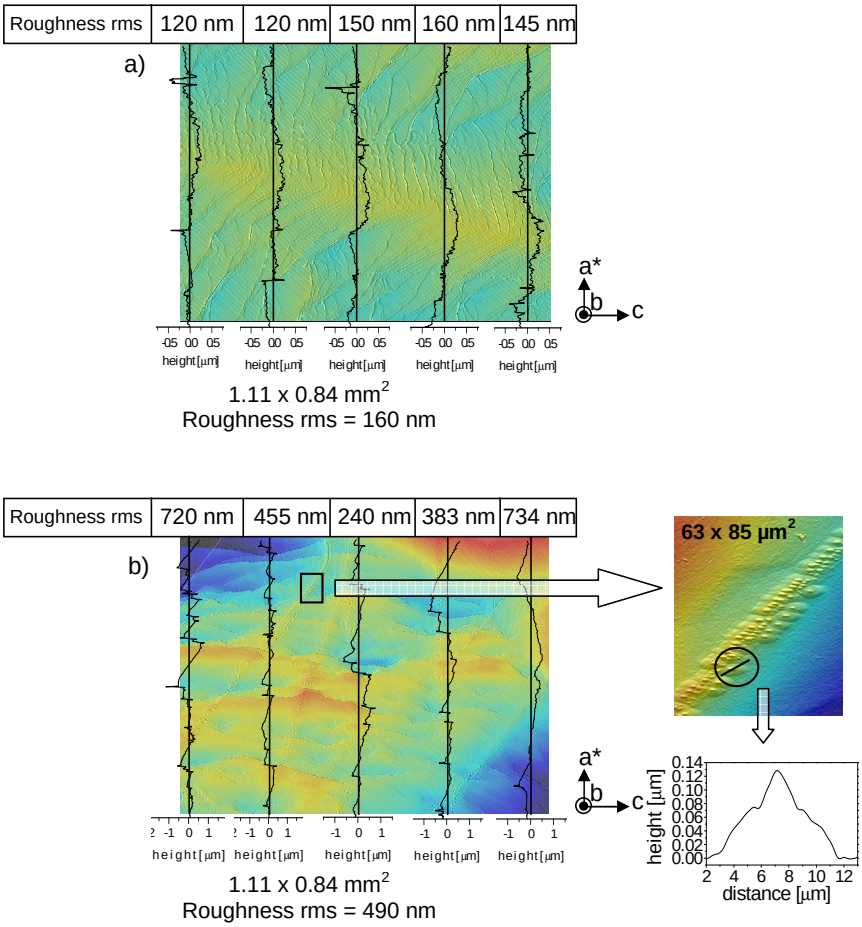

UNIVERSITAT ROVIRA I VIRGILI
CRECIMIENTO Y CARACTERIZACIÓN DE CAPAS EPITAXIALES DE KRE 1-X 4BX (WO4)2 / KRE (WO4)2 (RE=Y,LU)
PARA APLICACIONES LÁSER
Ana Isabel Aznar Écija

ISBN:978-84-691-1552-7 /DL:T.151-2008

Figure 7

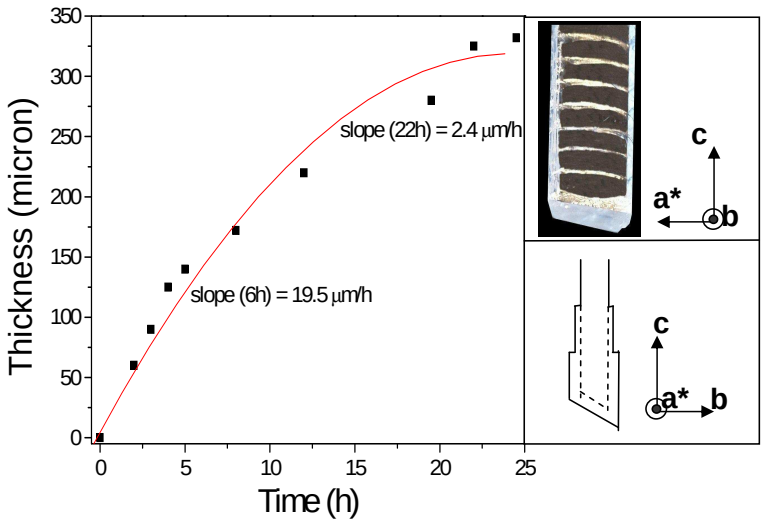

UNIVERSITAT ROVIRA I VIRGILI
CRECIMIENTO Y CARACTERIZACIÓN DE CAPAS EPITAXIALES DE KRE 1-X 4BX (WO4)2 / KRE (WO4)2 (RE=Y,LU)
PARA APLICACIONES LÁSER
Ana Isabel Aznar Écija

ISBN:978-84-691-1552-7 /DL:T.151-2008

Figure 8

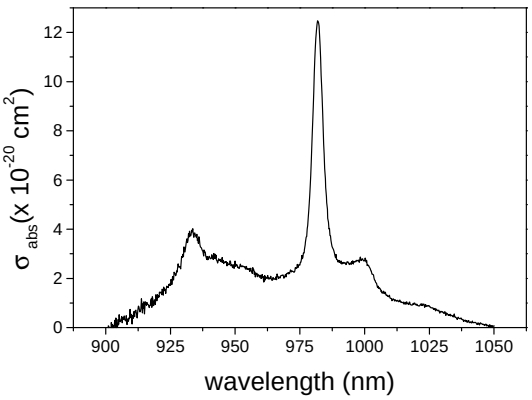


Figure 9

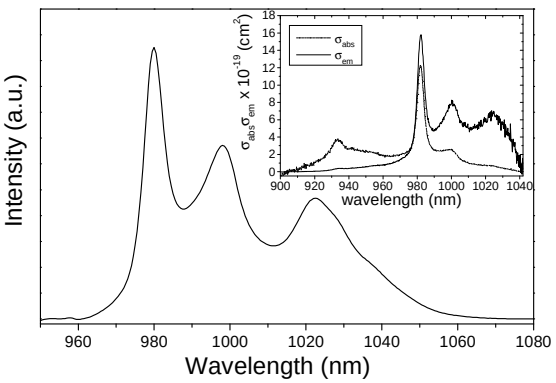

ISBN:978-84-691-1552-7 /DL:T.151-2008

**References**

[1] Innerhofer, E.; Südmeyer, T.; Brunner, F.; Häring, R.; Aschwanden, A.; Paschotta, R.; Hönninger, C.; Kumkar, M.; Keller, U. *Opt. Lett.* **2003,** *28*, 367.
[2] Zou, X.; Tortani, H. *Phys. Rev. B* **1995**, *52*, 15889.
[3] Brunner, F.; Südmeyer, T.; Innerhofer, E.; Morier-Genoud, F.; Paschotta, R.; Kisel, V.E.; Shcherbitski, V.G.; Kuleshov, N.V.; Gao, J.; Contag, K.; Giesen, A.; Keller, U. *Opt. Lett.* **2002,** *27*, 1162.
[4] Pujol, M.C.; Solé, R.; Nikolov, V.; Gavaldà, Jna.; Massons, J.; Zaldo, C.; Aguiló, M.; Díaz, F. *J. Mater. Res.*, **1999**, *14*, 3739.
[5] Griebner, U.; Liu, J.; Rivier, S.; Aznar, A.; Grunwald, R.; Solé, R.; Aguiló, M.; Díaz, F.; Petrov, V. *IEEE J. Quantum Electron.*, **2005**, *41*, 408.
[6] Mateos, X.; Solé, R.; Gavaldà, Jna.; Aguiló, M.; Díaz, F., *J. Lumin*., **2005**, *115*, 131.
[7] Lagatsky, A. A.; Kuleshov, N. V.; Mikhailov, V. P. *Opt. Comunn.* **1999**, 65, 71.
[8] Pujol, M.C.; Mateos, X.; Solé, R.; Gavaldà, Jna.; Massons, J.; Aguiló, M.; Díaz, F. *Mater. Science Forum*, **2001**, *378-381*, 710.
[9] Solé, R.; Nikolov, V.; Ruiz, X.; Gavaldà, Jna.; Solans, X.; Aguiló, M.; Díaz, F. *J. Cryst. Growth*, **1996**, *169*, 600.
[10] Kletsov, P.V.; Kozeeva, L.P. *Sov. Phys.- Dokl.* **1969**,*14*, 185.
[11] Aznar, A.; Silvestre, O.; Pujol, M.C.; Solé, R.; Aguiló, M.; Díaz, F. *Cryst. Growth & Design*, **2006**, *6*, 1781.
[12] Romanyuk, Y.E.; Utke, I.; Ehrentraut, D.; Apostolopoulos, V.; Pollnau, M.; García-Revilla, S.; Valiente, R. *J. Cryst. Growth*, **2004**, *269*, 377.
[13] Tu, C.; Huang, Y.; Luo, Z.; Chen, G. *J. Cryst. Growth*, **1994**, *135*, 636.
[14] Rodríquez-Carvajal, J. *Reference Guide for the Computer Program Fullprof*. Laboratorie León Brillouin, CEA-CNRS: Saclay, France, 1996.
[15] Solé, R.; Nikolov, V.; Vilalta, A.; Carvajal, J. J.; Massons, J.; Gavaldà, Jna.; Aguiló, M.; Díaz, F. *J. Crystal Growth*, **2002**, *237-239*, 602.
[16] Aznar, A.; Solé, R.; Aguiló, M., Díaz, F.; Griebner, U.; Grunwald, R.; Petrov, V. *Appl. Phys. Lett.*, **2004**, *85*, 4313.
[17] Pujol, M.C.; Solé, R.; Massons, J.; Gavaldà, Jna.; Solans, X.; Díaz, F.; Aguiló, M. *J. Appl. Crystallogr*. **2002**, *35*, 108.
[18] Kletsov, P.V.; Kozeeva, L.P.; Kharchenko, L.Y.; Pavlyuk, A.A. *Sov. Phys. Crystallogr.* **1974**, *19*, 342.
[19] Kletsov, P. V.; Kozeeva, L. P. *J. Struct. Chem.* **1977**, *18*, 339.
[20] Kletsov, P. V.; Kozeeva, L. P.; Kharchenko, L. Y. *Sov. Phys. Crystallogr*. **1974**, *20*, 732.
[21] Dowty, E. *Shape for windows*, *version 5.0.1*; 1995.
[22] Shannon, R. D. *Acta Crystallogr. A* **1976**, *32*, 751.
[23] Mateos, X.; Solé, R.; Gavaldà, Jna.; Aguiló, M.; Massons, J.; Díaz, F. *Opt. Mater.* **2006**, *28* 423.
[24] Kuleshov, N. V.; Lagatsky, A. A.; Podlipensky, A. V.; Mikhailov, V. P. *Opt. Lett.* **1997**, *22*, 1317.